Science
AAAS

Supplementary Materials for

Recording physiological history of cells with chemical labeling

Magnus-Carsten Huppertz *et al*.

Corresponding authors: Julien Hiblot, julien.hiblot@mr.mpg.de; Kai Johnsson, johnsson@mr.mpg.de

Science **383**, 890 (2024)
DOI: 10.1126/science.adg0812

The PDF file includes:

Other Supplementary Material for this manuscript includes the following:

Materials and Methods

Chemical procedures

General information

All chemical reagents and solvents for synthesis and purification were purchased from commercial suppliers (Merck KGaA, Honeywell International Inc., Fisher Scientific International, Inc., Carl Roth GmbH & Co. KG, VWR International, Acros Organics B.V.B.A.). Preparative HPLC-MS was performed on a Shimadzu prominence preparative HPLC system equipped with a LCMS-2020 mass spectrometer. A Shimazu shim-pack GIS column (5 µm, C18, 50 × 250 mm) was used with a flow rate of 50 mL·min^{-1}. Analytical HPLC-MS was performed on a Shimadzu Nexera X2 analytical HPLC system equipped with a LCMS-2020 mass spectrometer. A Supleco Titan column (5 µm, C18, 50 × 1.9 mm) was used with a flow rate of 1 mL·min^{-1}. High resolution mass spectrometry (HRMS) was measured by the MS-facility of the Max Planck Institute for Medical Research on a Bruker maXis IITM ETD.

HaloTag substrates

Fluorescent substrates for HaloTag were synthesized according to published procedures (*44, 45*). JF dyes were kind gifts from Dr. L. D. Lavis (Janelia research campus):

- https://www.janelia.org/open-science/janelia-fluor-dyes and
- https://www.janelia.org/open-science/jfx-dyes.

HaloTag substrates JF_{525}, JF_{549}, TMR, and JF_{646} can also be obtained from Promega Corporation:

- https://www.promega.de/en/products/protein-detection/protein-labeling/halotag-fluorescent-ligands/?catNum=G8251 and
- https://www.promega.de/en/products/protein-detection/protein-labeling/janelia-fluor-halotag-ligands/?catNum=GA1110,

For samples of CPY-CA and SiR-CA, please contact the corresponding authors.
The chemical structure and photophysical properties of the fluorescent substrates are reported in fig. S32.

Solid phase peptide synthesis

Solid phase peptide synthesis was done with standard Fmoc chemistry on an automated microwave peptide synthesizer (Liberty Blue, CEM Corp.). *N,N'*-diisopropylcarbodiimide (DIC) was used as coupling reagent, ethyl cyano(hydroxyimino)acetate (oxyma) as activating base, 20% piperidine in DMF as deprotecting reagent and DMF as a solvent. Preloaded wang-resin (0.25 mmol loading) was swollen in DMF for 5 min, followed by cycles of deprotection, washing, and coupling: deprotection: 10 mL 20% piperidine, 100 s, 90 ºC; wash: 4 × 10 mL DMF; coupling: 2.5 mL 1 M DIC, 1.25 mL 0.5 M oxyma and 6.25 mL 0.2 M protected amino acid, 265 s. For arginine the coupling step was repeated twice. After a final deprotection and washing step, resins were washed with dichloromethane (DCM) and dried under reduced pressure. Peptides were deprotected and cleaved from the resin with 5 mL of 95% TFA, 2.5% H_2O and 2.5% TIS (RT, 4 h). The volume of cleavage mixture was reduced under a stream of air to ~1 mL and peptides were precipitated by pouring the mixture into 50 mL -20 ºC diethyl ether. The precipitated peptides were separated from the supernatant by centrifugation (15 min, 4000 g, -10 ºC) and dried under reduced pressure. Crude products were dissolved in 10% MeCN, 0.1% formic acid in H_2O, purified via preparative HPLC (0% to 60% MeCN in H_2O, 0.1% formic acid, 60 min) and lyophilized. Purity and correct mass were confirmed via analytical HPLC-MS and HRMS.

Biochemistry and molecular biology

General information

DNA and protein concentrations were determined by measuring absorption at 260 nm and 280 nm with a NanoDrop 2000c spectrometer (Thermo Fisher Scientific), respectively. DNA solutions were kept at -20 °C and proteins were either stored at -80 ºC after flash freezing in liquid nitrogen or mixed 1:1 with 90% (w/v) glycerol in activity buffer (table S4) and stored at -20 ºC. All microplate reader experiments were performed using a microplate reader Spark20M instrument (Tecan Group). Data analyses of *in vitro* experiments were performed using custom R scripts (*46, 47*) if not specified otherwise. All buffer compositions are summarized in table S4.

Molecular cloning

Molecular cloning was performed using either Gibson assembly (*48*) or the Q5 site-directed mutagenesis kit (NEB) according to the manufacturer's protocol. Polymerase chain reactions were done using the KOD hot-start DNA polymerase master mix (Sigma-Aldrich) according to the manufacturer's protocol. Plasmids generated by Gibson assembly were electroporated in *E. coli* strains E.cloni 10G (Lucigen) or NEB stable (NEB) for pAAV-hSyn1 vectors and pTol2-*elavl3*(HuC) vectors. Sequences were verified by Sanger sequencing (Eurofins) with particular attention to the ITR integrity on the pAAV-hSyn1 vectors and the Tol2 recombination sites on pTol2-elavl3 vectors. All plasmids, building blocks and backbones used in this study are listed in table S5.

Protein expression and purification

Proteins were expressed in *E. coli* strain BL21(DE3) (Novagen). Lysogenic broth (LB) cultures were grown at 37 °C until they reached an optical density at 600 nm (OD_{600}) of 0.8. Transgene expression was induced by the addition of 0.5 mM isopropyl-β-D-thiogalactopyranoside (IPTG) and cells were grown at 16 °C overnight in the presence of 1 mM $MgCl_2$. Cells were harvested by centrifugation (10 min, 4 000 g, 4 ºC), resuspended in IMAC lysis buffer (table S4) and lysed by sonication on ice. Lysates were cleared by centrifugation (75 000 g, 4 ºC, 10 min) and proteins were purified via IMAC using a HisTrap FF crude column (Cytiva) on an ÄktaPure FPLC system (Cytiva). Strep-tagged proteins were further purified using a StrepTrap HP column (Cytiva) on the ÄktaPure FPLC system (Cytiva). Buffer was exchanged using a HiPrep 26/10 desalting column (Cytiva) to activity buffer (table S4).

For N-terminally His_{10}-TEV tagged HaloTag, cpHaloTag141-145, cpHaloTag154-156 and cpHaloΔ, the purification tag was removed by overnight cleavage with TEVp at 30 ºC as previously described (*49*). Cleaved proteins were purified with a HisTrap FF crude column (Cytiva) on the ÄktaPure FPLC system (Cytiva) by collecting the flow-through. These proteins were further purified by size exclusion chromatography (HiLoad 26/600 Superdex 75, Cytiva) using activity buffer (table S4).

All proteins were concentrated using Amicon Ultra-15 centrifugal filter devices (Merck) with a molecular weight cut-off (MWCO) smaller than the protein size to a final concentration of 100-500 µM. Correct size and purity of proteins were assessed by SDS-PAGE and liquid chromatography-mass spectrometry (LC-MS) analysis. Protein sequences are listed at the dedicated section 4 of the supplementary information.

Protein crystallization and X-ray diffraction data collection

The proteins were concentrated to 17.0-40.0 mg/mL in activity buffer (table S4). Crystallization was performed at 20 °C using the vapor-diffusion method. Crystals of cpHaloΔ were grown by mixing equal volumes of protein solution, reservoir solution

containing 0.1 M CHES pH 9.5, 1.0 M trisodium citrate and additive solution of 40% (v/v) polypropylene glycol P400. Crystals of cpHaloTag154-156 were grown by mixing protein solution and precipitant solution composed of 0.1 M Bicine pH 9.0, 1.6 M ammonium sulfate. Crystals of cpHaloΔ were briefly washed in cryoprotectant solution consisting of the reservoir solution saturated with polypropylene glycol P400 and supplemented with 20% (v/v) ethylene glycol before flash-cooling in liquid nitrogen. Crystals of cpHaloTag154-156 were rinsed in the reservoir solution supplemented with 20% (v/v) ethylene glycol, prior to flash-cooling in liquid nitrogen.

Single crystal X-ray diffraction data were collected at 100 K on the X10SA beamline at the SLS (PSI, Villigen, Switzerland). All data were processed with XDS (*50*). The structures of cpHaloΔ and cpHaloTag154-156 were determined by molecular replacement (MR) using Phaser (*51*) and HaloTag coordinates (PDB code 5Y2X) as a search model. The final models were optimized in iterative cycles of manual rebuilding using Coot (*52*) and refinement using Refmac5 (*53*) and phenix.refine (*54*). Data collection and refinement statistics are summarized in table S6, model quality was validated with MolProbity (*55*) as implemented in PHENIX. Atomic coordinates and structure factors have been deposited in the Protein Data Bank under accession codes: 8B6N (cpHaloTagΔ) and 8B6P (cpHaloTag154-156).

Isothermal titration calorimetry (ITC) measurement of cpHaloΔ - Hpep1 affinities

To measure the affinity between cpHaloΔ and Hpep1, cpHaloΔ protein was dialyzed overnight at 4 ºC using Slide-A-Lyzer dialysis cassettes (10K MWCO, Thermo Scientific) against 400 mL activity buffer (table S4). Potential protein aggregates were removed by centrifugation (21,000 g, 10 min, 4 ºC) and the protein concentration was adjusted to 200 µM. Lyophilized Hpep1 was dissolved in the dialysis buffer by incubation at 50 ºC for 5 min and regular vortexing to reach a concentration in the range of 10 mM. The peptide was quantified using the Pierce quantitative fluorometric peptide assay kit (Thermo Fisher Scientific) according to the manufacturer's protocol. The protein solution was loaded into the cell of the MicroCal PEAQ-ITC (Malvern Panalytical) instrument, the syringe was loaded with peptide solution. Measurements consisted of two series of 12x 3 µL injections with syringe re-loading in between the injection series. Data from both series were concatenated (ConCat32 software, Malvern Panalytical). Control measurements were performed with dialysis buffer in the cell and peptide solution in the syringe. Data were analyzed with the MicroCal PEAQ-ITC analysis software (version 1.30) using point-to-point subtraction of the control to fit K_D, ΔH and ΔH offset. The final K_D value was determined by averaging three independent measurements and uncertainties were estimated by calculating the standard deviation.

To determine the affinity between TMR-labeled cpHaloΔ (cpHaloΔ-TMR) and Hpep1, cpHaloΔ protein (5 µM) was labeled in presence of Hpep1 (1 mM) and TMR-CA substrate (10 µM) in activity buffer (table S4) overnight at 4 ºC. The labeled protein was concentrated with an Amicon Ultra-15 centrifugal filter device (Merck) and purified by size exclusion chromatography (HiLoad 26/600 Superdex 75, Cytiva) using activity buffer (table S4). The successful removal of Hpep1 and cpHaloΔ labeling was confirmed by mass spectrometry analysis. ITC measurements and analysis were performed as described above with an Hpep1 concentration in the range of 7 mM, performing only a single series of 12 injections per measurement.

Protein thermostability measurement via nanoDSF

Thermostabilities of HaloTag, cpHaloTag141-145, cpHaloTag154-156 and cpHaloΔ were measured with 20 µM protein solution in activity buffer (table S4) on a Prometheus NT 48 nanoscale differential scanning fluorimeter (NanoTemper) over a temperature range from

20 ºC to 95 ºC with a heating rate of 1 ºC.min^{-1} by monitoring changes in the ratio of the fluorescence intensities at 350 nm and 330 nm. The indicated melting temperature (mean of 2 samples) corresponds to the inflection point (maximum of the first derivative).

Stopped flow labeling kinetics

Labeling kinetics of cpHaloTag141-145 and cpHaloTag154-156 were measured by recording fluorescence anisotropy changes over time using a BioLogic SFM-400 stopped-flow instrument (BioLogic Science Instruments, Claix, France) in a single-mixing configuration at 37 °C. Excitation wavelength was set to 555 nm (monochromator) and a 570 nm longpass emission filter was used. Technical triplicates were recorded with protein concentrations varying from 0.5 µM to 20 µM and a constant TMR-CA concentration of 0.5 µM in activity buffer (table S4). The anisotropy of the free TMR-CA was measured to obtain a baseline. The dead time of the instrument was measured according to the manufacturer's protocol (BioLogic Technical Note 53) by recording the fluorescence decay during the pseudo-first-order reaction of N-acetyl-L-tryptophanamide with a large excess of N-bromosuccinimide and fitting a first-order reaction model to this data. Data were analyzed as previously described for HaloTag (*21*). In short, data were processed to adjust time values, average data and determine baseline anisotropy. A two-step reaction model (equations 1-2) was fit to all data (global fit) using the DynaFit software (*56*) to obtain estimates for the kinetic rate constants k_1, k_{-1} and k_2. The apparent second-order labeling rate constant k_{app} was calculated according to equation 3. Uncertainties and confidence intervals of fitted parameters were estimated using the Monte Carlo method (*57*) (N = 1000, 5% worst fits discarded).

(1) $$P + S \underset{k_{-1}}{\overset{k_1}{\leftrightarrow}} PS^*$$

(2) $$PS^* \xrightarrow{k_2} PS$$

(3) $$k_{app} = k_1 \frac{k_2}{k_2 + k_{-1}}$$

Background labeling kinetics of cpHaloΔ

Labeling kinetics of cpHaloΔ in absence of the Hpep were measured by recording fluorescence polarization over time in a microplate reader using black, non-binding, flat bottom, low volume, 384-well polystyrene plates (Corning) at 37 ºC with a final volume of 40 µL activity buffer (table S4). A humidity cassette was used to limit evaporation over extended periods of time and all measurements were performed in technical triplicates. Final concentration of cpHaloΔ was varied from 2 to 250 µM while TMR-CA substrate concentration was kept constant at 50 nM. The fluorescence polarization of the free TMR-CA was measured to obtain a baseline. Data were analyzed as described above for stopped flow kinetic data. However, during model fitting concentrations of the cpHaloΔ dilutions (except for the 250 µM starting solution) were allowed to vary up to 30% to account for inaccuracies in the dilution series and instead of fitting k_1 and k_{-1} individually only the ratio (*i.e.*, $K_D = k_{-1}/k_1$) was fit.

Labeling kinetics of complemented split-HaloTag

Labeling kinetics of complemented split-HaloTag were measured by recording fluorescence polarization over time in a microplate reader using black, non-binding, flat bottom, low volume, 384-well polystyrene plates (Corning) at 37 ºC with a final volume of

40 µL activity buffer (table S4). A humidity cassette was used to limit evaporation over extended periods of time and all measurements were performed in technical triplicates. Final concentrations were 500 nM cpHaloΔ protein, 50 nM TMR-CA substrate and 0 µM to 250 µM Hpep1. The fluorescence polarization of the free TMR-CA was measured to obtain a baseline. Data were processed to adjust time values, average data and determine baseline fluorescence polarization. A simplified model describing the reaction mechanism (equations 4-5) was fit to the data using the DynaFit software (*56*) to obtain estimates for the kinetic rate constants k_1, k_{-1} and k_{app}. As the K_D of the cpHaloΔ - Hpep1 interaction was known from ITC experiments, the ratio of k_1/k_{-1} was fixed to 4.64 mM. Uncertainties and confidence intervals of fitted parameters were estimated using the Monte Carlo method (*57*) (N = 1000, 5% worst fits discarded).

(4) $$cpHalo\Delta + Hpep \underset{k_{-1}}{\overset{k_1}{\leftrightarrow}} P$$

(5) $$P + S \xrightarrow{k_2} PS$$

Labeling kinetics of complemented split-HaloTag with different HaloTag substrates

Labeling kinetics of complemented split-HaloTag were measured by recording fluorescence polarization over time in a microplate reader using black, non-binding, flat bottom, low volume, 384-well polystyrene plates (Corning) at 37 ºC with a final volume of 40 µL activity buffer (table S4). A humidity cassette was used to limit evaporation over extended periods of time and all measurements were performed in technical triplicates. Final concentrations were 500 nM cpHaloΔ protein, 50 nM HaloTag substrate (TMR-CA, CPY-CA, JF_{669}-CA, JF_{552}-CA or JF_{525}-CA) and 1 mM Hpep3. Reactions were started by addition of HaloTag substrate. A second-order reaction rate equation (equation 6) was fit to the data to obtain estimates for the apparent second-order rate constant k_{app}. FP_{free} was fixed to the FP of the free dye in buffer. Uncertainties and confidence intervals of fitted parameters were estimated using the Monte Carlo method (*57*) (N = 1000).

(6) $$FP(t) = FP_{bound} + \frac{FP_{free} - FP_{bound}}{[A]_0} \cdot \frac{[A]_0([A]_0 - [B]_0)e^{([A]_0 - [B]_0)k_{app} \cdot t}}{[A]_0 e^{([A]_0 - [B]_0)k_{app} \cdot t} - [B]_0}$$

with:

t:	time
FP(t):	FP at time t
FP_{bound}:	FP of the bound dye
FP_{free}:	FP of the free dye
$[A]_0$:	dye concentration at t = 0
$[B]_0$:	protein concentration at t = 0
k_{app}:	apparent second-order rate constant

Split-HaloTag labeling by SDS-PAGE

cpHaloΔ (1 µM) was incubated with an excess of TMR-CA (2 µM) at different Hpep1 concentrations (0 µM to 1000 µM) in activity buffer (table S4) for 1 h at 37 ºC. Reactions were stopped by adding 4x Laemmli buffer (Bio-Rad) and heat denaturated at 95 ºC for 10 min. 11.25 pmol of the samples were loaded on precasted SDS gels (Mini-PROTEAN TGX stain-free 4-20%, Bio-Rad) and run for 20 min at 300 V. Gels were imaged on a Typhoon fluorescence laser-scanner (532 nm excitation laser, 570 nm emission filter, 20 nm bandpass).

Labeling kinetics of circularly permuted HaloTag variants

Labeling kinetics of circularly permuted HaloTag variants were measured by recording fluorescence polarization over time in a microplate reader equipped with an injector module (Tecan Group) using black, non-binding, flat bottom, low volume, 96-well polystyrene plates (Corning) at 37 ºC with a final volume of 200 µL FP buffer (table S4). All measurements were performed in technical triplicates with final concentrations of 50 nM protein and 10 nM TMR-CA substrate. Reactions were started by injection of 100 µL TMR-CA substrate. A second-order reaction rate equation (equation 6) was fit to the data to obtain estimates for the apparent second-order rate constant k_{app}. FP_{free} was fixed to the FP of the free dye in buffer. Uncertainties and confidence intervals of fitted parameters were estimated using the Monte Carlo method (*57*) (N = 1000).

Labeling kinetics of split-HaloTag - FKBP/FRB fusions

Labeling kinetics of split-HaloTag - FKBP/FRB fusions were measured by recording fluorescence polarization over time in a microplate reader using black, non-binding, flat bottom, low volume, 384-well polystyrene plates (Corning) at 37 ºC with a final volume of 40 µL FP buffer (table S4). All measurements were performed in technical triplicates. Final concentrations were 250 nM of each protein, 50 nM HaloTag substrate (TMR-CA, CPY-CA, JF_{669}-CA, JF_{552}-CA or JF_{525}-CA) and 500 nM rapamycin. Reactions were started by addition of rapamycin. A second-order reaction rate equation (equation 6) was fit to the data to obtain estimates for the apparent second-order rate constant k_{app}. FP_{free} was fixed to the FP of the free dye in buffer. Uncertainties and confidence intervals of fitted parameters were estimated using the Monte Carlo method (*57*) (N = 1000).

Hpep library screening

The Hpep library consisting of 384 synthetic peptides was screened for the ability to activate the labeling reaction of cpHaloΔ. To dissolve the peptides, 0.5 mL MQ water were added to each tube and tubes were shaken for 1 h at 1800 rpm and 45 ºC. Tubes were centrifuged for 10 min, 4000 g, at room temperature to sediment any undissolved peptide. 20 µL of the supernatants were transferred into a black, non-binding, flat bottom, low volume, 384-well polystyrene plate (Corning). 10 µL of 2 µM cpHaloΔ protein (0.5 µM final) in activity buffer (table S4) was added and the labeling reaction was started by addition of 10 µL of 0.4 µM TMR-CA substrate (0.1 µM final) in activity buffer (table S4). Labeling kinetics were measured by recording fluorescence polarization over time in a microplate reader at 37 ºC. A humidity cassette was used to limit evaporation over extended periods of time. A second-order reaction rate equation (equation 6) was fit to the data in conditions where at least 200 mFP were reached to obtain estimates for the apparent second-order rate constant k_{app}. The initial slope at time 0 ($s_{t=0}$) was calculated using the derivative of equation 6 at t=0 (equation 7).

(7) $$s_{t=0} = \frac{dFP}{dt}(t=0) = [B]_0 \cdot k_{app}(FP_{free} - FP_{bound})$$

with:

t:	time
$s_{t=0}$:	initial slope at t = 0
FP_{bound}:	FP of the bound dye
FP_{free}:	FP of the free dye
$[B]_0$:	protein concentration at t = 0
k_{app}:	apparent second-order rate constant

In conditions where 200 mFP were not reached, due to the reaction being too slow, a linear model (equation 8) was fit to the data to determine the initial slope $s_{t=0}$.

(8) $$FP(t) = FP_{free} + t \cdot s_{t=0}$$

with:

t:	time
$s_{t=0}$:	initial slope at t = 0
FP_{free}:	FP of the free dye

Initial slopes relative to the parental Hpep1 were calculated to obtain relative labeling speeds and negative slopes were arbitrarily set to 10^{-2} for plotting on logarithmic scale.

Half maximal effective concentration (EC_{50}) of Hpep variants

To determine the EC_{50} of purified Hpep variants for split-HaloTag activation, labeling kinetics of cpHaloΔ were measured as a function of peptide concentration by recording fluorescence polarization over time in a microplate reader using black, non-binding, flat bottom, low volume, 384-well polystyrene plates (Corning) at 37 ºC with a final volume of 40 µL FP buffer (table S4). A humidity cassette was used to limit evaporation over extended periods of time. For peptides with high EC_{50} (> 1 µM) final concentrations of 500 nM cpHaloΔ protein and 100 nM TMR-CA substrate were used, for peptides with low EC_{50} (< 1 µM) final concentrations of 20 nM cpHaloΔ protein and 4 nM TMR-CA substrate were used. The Hpep was titrated in concentrations from 0 mM to 5 mM, depending on the EC_{50} of the respective peptide. Peptides were quantified via the Pierce quantitative fluorometric peptide assay kit (Thermo Fisher Scientific) according to the manufacturers protocol. Reactions were started by addition of TMR-CA substrate. Kinetics were analyzed as described above for the Hpep library screen. Initial slopes ($s_{t=0}$) were plotted against the Hpep concentration and a sigmoidal dose response model (equation 9) was fit to this data to estimate EC_{50} values. Uncertainties and confidence intervals of fitted parameters were estimated using the Monte Carlo method (*57*) (N = 1000).

(9) $$s_{t=0}([Hpep]) = \frac{s_{max}}{1 + 10^{(LogEC50 - log10([Hpep]))}}$$

with:

$s_{t=0}$:	initial slope at t = 0
s_{max}:	maximal initial slope at t = 0
[Hpep]:	Hpep concentration
LogEC50:	log_{10} of the half maximal effective concentration (EC_{50})

Caprola labeling kinetics

Labeling kinetics of Caprola variants were measured by recording fluorescence polarization over time in a microplate reader at 37 ºC using black, non-binding, flat bottom, 96-well, polystyrene plates (OptiPlate, PerkinElmer) with a final reaction volume of 200 µL. Measurements were performed in FP buffer (table S4) supplemented with 100 µM EGTA and with or without 5 mM $CaCl_2$ in technical triplicates. Final concentrations of 200 nM Caprola protein and 50 nM HaloTag substrate (TMR-CA, CPY-CA, JF_{669}-CA, JF_{552}-CA or JF_{525}-CA) were used. Caprola protein and substrate were prepared in 100 µL and the reactions were started by adding 100 µL 10 mM $CaCl_2$ in FP buffer (table S4) (5 mM final concentration). Control experiments were conducted where 100 µL of buffer without $CaCl_2$ was added. Data analysis was performed as described above for split-HaloTag - FKBP/FRB

fusions. To measure the reaction speed of the background labeling reaction in absence of $CaCl_2$ which is orders of magnitudes slower, fluorescence polarization assays were conducted as described above for the control experiments with TMR-CA. However, a humidity cassette and a much lower sampling rate (1/300s) were used to limit evaporation and enable measurements over 24 h. Data analysis was performed as described above, but since FP did not plateau after 24 h FP_{bound} was fixed to 371 mFP which is the average plateau reached after full labeling of Caprola in presence of Ca^{2+}.

Caprola reversibility assay

Caprola labeling kinetics with TMR-CA were performed as described above in a plate reader equipped with an injector module (Tecan Group). To start or pause the reaction, 15 µL of $CaCl_2$ or EGTA in FP buffer (table S4) were injected to reach the following final concentrations:

- 150 µM $CaCl_2$
- 300 µM EGTA (when FP reached 185 mFP)
- 450 µM $CaCl_2$
- 2250 µM EGTA (when FP reached 260 mFP)
- 3375 µM $CaCl_2$

pH dependence of Caprola labeling

The pH dependence of Caprola labeling was determined by performing labeling kinetics as described above using FP buffer (table S4) with adjusted pH ranging from 6.8 to 8.

Ca^{2+}-dependence of Caprola labeling

The responsiveness of Caprola variants for calcium (EC_{50}) was determine by measuring labeling kinetics at different free Ca^{2+} concentrations. Kinetics were recorded by measuring fluorescence polarization over time in a microplate reader at 37 ºC using black, non-binding, flat bottom, 96-well, polystyrene plates (OptiPlate, PerkinElmer) with a final reaction volume of 200 µL. To obtain buffers with precise and buffered free Ca^{2+} concentrations from 0 µM to 39 µM a calcium calibration kit (Thermo Fisher Scientific) was used (100 mM KCl, 30 mM MOPS, pH 7.2 and K_2EGTA / CaEGTA in different ratios). Reactions were started by mixing equal volumes of Caprola protein (200 nM) and TMR-CA (50 nM) substrate in the respective buffers. Data from replicates were averaged and a second-order reaction rate equation (equation 6) was fit to the data when at least 200 mFP were reached to obtain estimates for the apparent second-order rate constant k_{app}. The initial slope at time 0 ($s_{t=0}$) was calculated using the derivative of equation 6 at t = 0 (equation 7). In conditions where 200 mFP were not reached, due to the reaction being too slow, a linear model (equation 8) was fit to the data to determine the initial slope $s_{t=0}$. The initial slopes $s_{t=0}$ were plotted against the free Ca^{2+} concentration and a sigmoidal dose response model (equation 10) was fit to this data to estimate EC_{50} values. Uncertainties and confidence intervals of fitted parameters were estimated using the Monte Carlo method (*57*) (N = 1000).

$$s_{t=0}([Ca^{2+}_{free}]) = \frac{s_{max}}{1 + 10^{(LogEC50 - log10([Ca^{2+}_{free}])) * HillSlope}} \quad (10)$$

with:

$s_{t=0}$: initial slope at t = 0
s_{max}: maximal initial slope at t = 0
$[Ca^{2+}_{free}]$: free Ca^{2+} concentration
LogEC50: log_{10} of the half maximal effective concentration (EC_{50})
HillSlope: Hill coefficient

Multi-color sequential Caprola labeling

His10-tagged Caprola9 protein (5 nmol) in activity buffer (table S4) was immobilized on a 5 mL HisTrap FF crude column (Cytiva) on an ÄktaPure FPLC system (Cytiva). The column was washed with 5 column volumes of EGTA buffer (50 mM HEPES, 50 mM NaCl, 100 µM EGTA, pH 7.3). Then two rounds of substrate incubation each with 2 column volumes of different fluorophore substrates (1 nmol) in either EGTA or Ca^{2+} buffer (50 mM HEPES, 50 mM NaCl, 5 mM CaCl2, pH 7.3) were applied with a constant flow of 5 mL·min-1. The column was washed with 5 column volumes of EGTA buffer in between incubation rounds. JF_{552}-CA and CPY-CA were used as substrates. Labeled Caprola protein was eluted with 3 column volumes of IMAC elution buffer (table S4) and concentrated using Amicon Ultra-15 centrifugal filter devices (Merck). Labeling was revealed by SDS-PAGE followed by in-gel fluorescence scanning as described above for split-HaloTag labeling (JF_{552}: 532 nm excitation laser, 570 nm emission filter, 20 nm bandpass; CPY: 635 nm excitation laser, 670 nm emission filter, 30 nm bandpass).

Computational methods

Design of C-terminal Hpep extensions

The crystal structure of HaloTag labeled with TMR-CA (PDB-ID: 6Y7A) was downloaded from the PDB. Water, glycerol, chloride ion and covalently bound TMR-CA ("OEH") residues were deleted and the file was modified by changing the "ASP A 106" residue to "ASX A 106". The oxygen connecting the aspartate with the covalently bound HaloTag ligand ("OD2") was removed. Residue numbering was adjusted to start at 1 and residues 140, 141, 142 and 153 which are not in split-HaloTag were removed. The numbering was adjusted to resemble the circularly permuted cpHaloΔ with Hpep1 (ARETFQAFRT) at the end of the sequence (C-terminal fragment -> N-terminal fragment -> Hpep1). A Rosetta remodel blueprint file was generated with the getBluePrintFromCoords.pl script.

```
~/Rosetta/main/tools/remodel/getBluePrintFromCoords.pl -pdbfile split_halo.pdb -chain
A > resfile
```

The first lines of the file were modified to extend the protein by two glycine residues in order to limit potential bias by the charged terminus of cpHaloΔ in direct proximity to the Hpep1 extension:

```
1 x L PIKAA G
1 x L PIKAA G
1 D L PIKAA D
2 V H PIKAA V
3 G H PIKAA G
4 R H PIKAA R
5 K H PIKAA K
6 L .
7 I .
[...]
```

The last lines of the file were modified to extend Hpep1 by four residues:

```
[...]
286 A .
287 F .
288 R H PIKAA R
289 T L PIKAA T
0 X L ALLAAxc
0 X L ALLAAxc
0 X L ALLAAxc
0 X L ALLAAxc
```

RosettaRemodel (*58*) was run with the following flags:

```
-nstruct 10000
-run:chain A
-use_clusters false
-hb_srbb 1.0
-find_neighbors
-packing:linmem_ig 10
-use_input_sc
-no_optH false
-flip_HNQ
-ex1
-ex2
-packing:extrachi_cutoff 3
-packing:ex1aro
-packing:ex2aro
-renumber_pdb true
-in:file:fullatom
-in:file:s in/split_halo.pdb
-remodel:blueprint in/resfile
--out:path:all out
```

Command:

```
~/Rosetta/main/source/bin/remodel.mpi.linuxgccrelease @flags
```

Design of new 10mer and N-terminally extended 14mer Hpeps

Preparation of the split-HaloTag structure. The crystal structure of HaloTag labeled with TMR-CA (PDB-ID: 6Y7A) was downloaded from the PDB. Water, glycerol, chloride ion and covalently bound TMR-CA ("OEH") residues were deleted and the file was modified by changing the "ASP A 106" residue to "ASX A 106". The oxygen connecting the aspartate with the covalently bound HaloTag ligand ("OD2") was removed. Residue numbering was adjusted to start at 1 and residues 140, 141, 142 and 153 which are not in split-HaloTag were removed. The Hpep1 10mer (ARETFQAFRT) was moved to the start of the sequence and a Rosetta remodel blueprint file was generated with the getBluePrintFromCoords.pl script.

```
~/Rosetta/main/tools/remodel/getBluePrintFromCoords.pl -pdbfile split_halo.pdb -chain
A > resfile
```

The first lines of the file were modified to extend Hpep1 by four glycine residues:

```
1 x H PIKAA G
1 x H PIKAA G
1 x H PIKAA G
1 x H PIKAA G
1 A H PIKAA A
2 R .
3 E .
[...]
```

RosettaRemodel (*58*) was run with the following flags:

```
-nstruct 1
-run:chain A
-use_clusters false
-hb_srbb 1.0
-find_neighbors
-packing:linmem_ig 10
-use_input_sc
-no_optH false
-renumber_pdb true
-auto_setup_metals true
-in:file:fullatom
-in:file:s in/split_halo.pdb
-remodel:blueprint in/resfile
--out:path:all out
```

Command:

```
~/Rosetta/main/source/bin/remodel.mpi.linuxgccrelease @flags
```

The output structure was used for the subsequent steps.

In order to limit potential bias by the charged termini of cpHaloΔ in direct proximity to Hpep1, glycine-glycine spacers were attached to the termini. For N-terminal spacers residue numbering was adjusted to resemble the circularly permuted cpHaloΔ with Hpep1 (ARETFQAFRT) at the end of the sequence (C-terminal fragment -> N-terminal fragment -> Hpep1) and a Rosetta remodel blueprint file was generated with the getBluePrintFromCoords.pl script. The first lines of the file were modified to extend the protein by two glycine residues:

```
1 x L PIKAA G
1 x L PIKAA G
1 D L PIKAA D
2 V H PIKAA V
3 G H PIKAA G
4 R H PIKAA R
5 K H PIKAA K
6 L .
7 I .
[...]
```

RosettaRemodel (*58*) was run with the following flags:

```
-nstruct 100
-run:chain A
-use_clusters false
-hb_srbb 1.0
-find_neighbors
-packing:linmem_ig 10
-use_input_sc
-no_optH false
-flip_HNQ
-ex1
-ex2
-packing:extrachi_cutoff 3
-packing:ex1aro
-packing:ex2aro
-renumber_pdb true
-in:file:fullatom
-in:file:s in/split_halo.pdb
-remodel:blueprint in/resfile
--out:path:all out
```

Command:

```
~/Rosetta/main/source/bin/remodel.mpi.linuxgccrelease @flags
```

The best scoring structure was used for the subsequent steps. For C-terminal spacers residue numbering was adjusted to place Hpep1 at the start of the sequence and a Rosetta remodel blueprint file was generated with the getBluePrintFromCoords.pl script. The last lines of the file were modified to extend the protein by two glycine residues:

```
[...]
293 D .
294 E .
295 W L PIKAA W
0 X L PIKAA G
0 X L PIKAA G
```

RosettaRemodel (*58*) was run with the same flags and commands as for the N-terminal spacers. The best scoring structure was modified by moving Hpep1 to chain B and renumbering all residues.

Preparation of the covalent ligand and relaxing the split-HaloTag-TMR structure. In order to parameterize the covalently bound TMR-CA ligand for usage in Rosetta, the ligand including the ester oxygen was extracted from the 6Y7A structure. Hydrogen atoms were added in PyMOL and the hydrogen on the former ester oxygen was removed. The molecule was saved as a pdb file and converted to a mol file with Avogadro. The mol file was edited manually, changing the bond types to “4” (aromatic) for all aromatic bonds in the molecule. The ligand was parameterized using the molfile_to_params.py script.

```
~/rosetta.source.release-314/main/source/scripts/python/public/molfile_to_params.py
-n TMR -p HTL-TMR 04_TMR.mol
```

The resulting params file was modified:

- adding a “CONNECT O1” line between the “BOND_TYPE” and “CHI” lines
- removing the “CHARGE O1 FORMAL -1” line

- adding last “ICOOR_INTERNAL” line with the internal coordinates of the gamma carbon atom of ASP106 seen from O1, C21, C20 of the ligand to build the connection between ligand and protein

```
ICOOR_INTERNAL  CONN1 -142.171000   63.592000    1.396000   O1    C21   C20
```

The content of HTL-TMR_0001.pdb was copied into the previously prepared split-HaloTag pdb file (as residue number 284, chain A). The chloride ion atom from the 6Y7A structure was added (as residue 285, chain A).

The “ASX.params” file from the Rosetta database was copied and modified by removing the virtual atom “V1” (including “BOND” and “CHI” record). (rosetta.source.release-314/main/database/chemical/residue_type_sets/fa_standard/-residue_types/sidechain_conjugation/ASX.params)

A constraints file was set up to fix the bond geometry between the ASX and the covalently bound TMR-CA residue:

```
AtomPair CG 104 O1 294               HARMONIC 1.265      0.001
Angle    CB 104 CG 104 O1 294        HARMONIC 2.05034299 0.034906585
Angle    CG 104 O1 294 C21 294       HARMONIC 2.0356822  0.034906585
Dihedral CA 104 CB 104 CG 104 O1 294 HARMONIC 1.32936493 0.034906585
```

The structure was relaxed with the following flags:

```
-nstruct 10000
-cst_fa_file in/chemical_bond.cst
-constraints:cst_fa_weight 1
-relax:ramp_constraints false
-relax:constrain_relax_to_start_coords
-ex1
-ex2
-use_input_sc
-flip_HNQ
-packing:extrachi_cutoff 16
-packing:ex1aro
-packing:ex2aro
-no_optH false
-renumber_pdb true
-auto_setup_metals true
-in:file:extra_res_path in/params
-in:file:fullatom
-in:file:s in/gg_split_halo_gg.pdb
--out:path:all out
```

Command:

```
~/Rosetta/main/source/bin/relax.mpi.linuxgccrelease @flags
```

The best scoring structure was used for the subsequent steps.

Design of new 10mer Hpeps. To design new 10mer Hpeps the relaxed split-HaloTag-TMR structure from the previous steps was used. The four glycine residues extending Hpep1 were removed and a RosettaScripts (*58*) protocol was set up with the following steps:

- setting up constraints and custom fold tree
- perturbing the N- and C-terminal glycine-glycine spacers
- minimizing the spacers with FastRelax
- docking the Hpep to cpHaloΔ

- designing all Hpep residues using conservative design based on the BLOSUM80 matrix with FastDesign (using a custom relax script)

The XML script is available at https://github.com/johnsson-lab/splitHaloTag_Hpep_design (DOI: 10.5281/zenodo.8113621). The same params and bond constraints files as described above for relaxing the structure were used.

Fold tree:

```
FOLD_TREE  EDGE 246 1 -1  EDGE 246 283 -1 EDGE 246 284 1  EDGE 246 285 2
EDGE 246 291 3  EDGE 291 286 -1  EDGE 291 295 -1
```

Custom relax script:

```
repeat %%nrepeats%%
coord_cst_weight 1.0
scale:fa_rep 0.8
repack
scale:fa_rep 0.805
min 0.01
coord_cst_weight 0.5
scale:fa_rep 0.847
repack
scale:fa_rep 0.853
min 0.01
coord_cst_weight 0.0
scale:fa_rep 0.908
repack
scale:fa_rep 0.917
min 0.01
coord_cst_weight 0.0
scale:fa_rep 1
repack
min 0.00001
accept_to_best
endrepeat
```

Resfile:

```
NATAA
START

286 B ALLAAxc
287 B ALLAAxc
288 B ALLAAxc
289 B ALLAAxc
290 B ALLAAxc
291 B ALLAAxc
292 B ALLAAxc
293 B ALLAAxc
294 B ALLAAxc
295 B ALLAAxc
```

Flags:

```
-nstruct 10000
-parser:protocol in/design_Hpep.xml
-in:file:extra_res_path in/par
-in:file:fullatom
-in:file:s in/gg_split_halo_gg_relaxed.pdb
-out:path:all out
```

Command

```
~/Rosetta/main/source/bin/rosetta_scripts.mpi.linuxgccrelease @flags
```

Design of N-terminally extended 14mer Hpeps. To design new N-terminally extended 14mer Hpeps the relaxed split-HaloTag-TMR structure from the previous steps was used. Three different RosettaScripts (*58*) protocol were set up with the following overall structure:

- setting up constraints and custom fold tree
- perturbing the N- and C-terminal glycine-glycine spacers
- minimizing the spacers with FastRelax
- docking the Hpep to cpHaloΔ
- designing all Hpep residues with FastDesign (using a custom relax script).

In the first run the script was set up as described above, in the second run the FastDesign step was conducted with more repeats and in a third run the backbone of cpHaloΔ was completely fixed. The XML scripts are available at https://github.com/johnsson-lab/splitHaloTag_Hpep_design. The same params and bond constraints files as described above for relaxing the structure were used.

Fold tree:

```
FOLD_TREE  EDGE 246 1 -1  EDGE 246 283 -1 EDGE 246 284 1  EDGE 246 285 2
EDGE 246 293 3  EDGE 293 286 -1  EDGE 293 299 -1
```

Custom relax script:

```
repeat %%nrepeats%%
coord_cst_weight 1.0
scale:fa_rep 0.8
repack
scale:fa_rep 0.805
min 0.01
coord_cst_weight 0.5
scale:fa_rep 0.847
repack
scale:fa_rep 0.853
min 0.01
coord_cst_weight 0.0
scale:fa_rep 0.908
repack
scale:fa_rep 0.917
min 0.01
coord_cst_weight 0.0
scale:fa_rep 1
repack
min 0.00001
accept_to_best
endrepeat
```

Resfile:

```
NATAA
START

286 B ALLAAxc
287 B ALLAAxc
288 B ALLAAxc
289 B ALLAAxc
290 B ALLAAxc
291 B ALLAAxc
292 B ALLAAxc
293 B ALLAAxc
294 B ALLAAxc
295 B ALLAAxc
296 B ALLAAxc
297 B ALLAAxc
298 B ALLAAxc
299 B ALLAAxc
```

Flags:

```
-nstruct 10000
-parser:protocol in/design_Hpep.xml
-in:file:extra_res_path in/params
-in:file:fullatom
-in:file:s in/gg_split_halo_gg_relaxed.pdb
-out:path:all out
```

Command

```
~/Rosetta/main/source/bin/rosetta_scripts.mpi.linuxgccrelease @flags
```

Analysis of computational Hpep design and Hpep library compilation

For each Rosetta generated design of 10mer and N-terminally extended 14mer Hpeps sequences were extracted and associated to their total scores and ΔΔG values. A final score was calculated by addition of total scores and ΔΔG values to rank the structures. The top 20% designs by final score of each run were analyzed for the most beneficial Hpep mutations relative to the parental sequence. All occurring mutations were identified and ranked by the sum of the final scores subtracted by the median final score of all designs this mutation appeared in. The top 20% designs with the N-terminally extended 14mer Hpeps were analyzed for the most beneficial four amino acid extensions similarly as described above for mutations. Extensions were ranked by the sum of the final scores subtracted by the median final total score of all designs this extension appeared in. Designs of C-terminally extended Hpeps were also ranked by final score.

To compile a library of 384 Hpep candidates, top ranked sequences from the different runs were pooled and complemented with parental sequences having the top scoring mutations as single point mutations and parental sequences extended by the top scoring extensions. This resulted in 1039 sequences in total out of which 402 were unique. Control sequences were added to the list: parental peptide (ARETFQAFRT), shortened parental peptide (ARETFQAFR, known to have some residual activity) and negative control peptide (ARETAQAFRT, F->A mutation known to kill activity). All sequences were analyzed with the ThermoFisher Scientific peptide synthesis and proteotypic peptide analyzing tool. Peptides were ranked by hydrophobicity and the 384 least hydrophobic peptides were chosen for the final Hpep library. The Hpep library was ordered as synthetic peptides in 1-4 mg scale in crude quality from GenScript (Piscataway, New Jersey, U.S.).

Cell biology

General information

Mammalian cells were cultured in high-glucose (4.5 $g.L^{-1}$) and pyruvate (110 $mg.L^{-1}$) containing Dulbecco's MEM+GlutaMax™ (Gibco) medium supplemented with 10% FBS and phenol-red (herein termed DMEM) at 37 °C in a humidified incubator with 5% CO_2 atmosphere. Primary rat hippocampal neurons were cultured in NeuroBasal medium supplemented with 1x GlutaMax™ , 1x B-27™, 1x Pen/Strep™ and phenol-red (all Gibco) at 37 °C in a humidified incubator with 5% CO_2 atmosphere. The patient-derived glioblastoma cell line (PDGCL) S24 (*59*) was cultured as non-adherent neurospheres in PDGCL media, consisting of DMEM/F-12 (Life Technologies), 1x B-27 supplement (Life Technologies), 5 µg/mL insulin (Sigma), 5 µg/mL heparin (Sigma) 20 ng/mL epidermal growth factor (EGF; Life Technologie) and 20 ng/mL fibroblast growth factor (FGF; Life Technologies).

Generation of stable cell lines

Stable cell lines were prepared using the Flp-In™ T-REx™ System (Thermo Fisher) with HEK293 Flp-In™ T-REx™ cells (Thermo Fisher) or HeLa Kyoto Flp-In™ cells, which are a kind gift of Dr. Amparo Andres-Pons (EMBL, Heidelberg). Cells were transiently transfected at 80% confluency in T-25 flasks using Lipofectamine™ 3000 (Thermo Scientific) according to manufacturer's instructions using a mix of 440 ng pDNA5/FRT/TO plasmid of interest mixed with 3560 ng pOG44 plasmid (encoding the FlpIn recombinase). Cells were selected for 72 h at 37 ºC in a humidified 5% CO_2 incubator using DMEM supplemented with 100 $\mu g.mL^{-1}$ Hygromycin B (Gibco). Surviving cells were recovered in DMEM without selection agent in a T-25 dish until cell confluency of 80% was reached. Next, highly expressing cells (top 10%) according to mEGFP fluorescence intensity were sorted using a FACS Melody (Becton Dickinson, excitation 488 nm, filter 530/30 nm). Stably expressing cells were maintained as previously explained or stored in freezing medium (DMEM + 10% DMSO) at -80 °C or in the liquid nitrogen tank (vapor phase). Cell lines were regularly tested for mycoplasma contamination and were mycoplasma-free.

Chemical fixation of mammalian cells

After experimental treatment, cells were rinsed twice with pre-warmed 1x PBS (Gibco) prior to fixation. Freshly prepared 4% Paraformaldehyde or 2% Glyceraldehyde dissolved in 1x PBS without Mg^{2+}/Ca^{2+} were applied for 15 min at room temperature, while 10% Methanol (dissolved in 1x PBS without Mg^{2+}/Ca^{2+}) fixation was carried out at -20 C for 60 min. Prior to imaging cells were washed three times for 5 min with 1x PBS.

Recording of rapamycin-dependent FKPB-FRB interactions in HeLa cells

Split-HaloTag-FKBP/FRB co-expression constructs were transiently transfected into HeLa cells using Lipofectamine 3000 (ThermoFisher Scientific) according to the manufacturer's protocol. After 8 h incubation, the medium was replaced and cells were grown for additional 24 h. Cells were treated with 100 nM CPY-CA in the presence or absence of 100 nM rapamycin for 1 h. Cells were washed 3 times with fresh medium containing 1 µM HaloTag protein to scavenge the substrate before analysis via flow cytometry or confocal fluorescence microscopy.

For flow cytometry cells were detached using TrypLE™-Express (Gibco) for 5 min at 37 °C. Detached cells were suspended in 1x PBS containing 2% FBS. Cells were analyzed with a BD Fortessa X-20 flow cytometer (mEGFP: 488 nm excitation, 530/30 nm emission, CPY: 648 nm excitation, 660/20 nm emission). Data were analyzed using FlowJo (BD). Live (SSC-A/FSC-A), single (SSC-H/SSC-A) and mEGFP positive cells were gated and fluorescence intensity ratios (CPY-CA/mEGFP) were calculated.

For confocal microscopy cells were washed with PBS, fixed with 4% PFA in PBS for 15 min and washed again with PBS. Confocal microscopy was performed on a Stellaris 5 inverted microscope (Leica) equipped with a white line laser and hybrid photodetectors at 37 °C in 5% CO_2 atmosphere in a humidified chamber. A 40x/1.10 water immersion objective was used at to image a single plane at 1024x1024 pixel (194x194 µm) resolution (1.5 x zoom, 600 Hz scan speed, 68.8 µm pinhole, 32-fold line average, mEGFP 488 nm ex., 494 nm – 556 nm em., CPY 610 nm ex., 618 nm – 750 nm em.). Images were used without further processing. Additional imaging acquisition parameters are summarized in the table S7.

Recording of GPCR activation in HEK293 cells

HEK293 Flp-In™ T-Rex™ cells were plated at 10k cells/well in fibronectin-coated 96-well Ibidi µPlates. 48 h after plating, cells were co-transfected with the appropriate GPCR and β-Arrestin 2 plasmids using Lipofectamine 3000 (Invitrogen) as per the manufacturer's protocol. 24 h after transfection cells were treated with the appropriate agonist (D2R: 100 µM quinpirole; M3 mAchR: 1 mM carbachol; β2AR: 100 µM isoproterenol; mGluR2: 1 mM glutamate; GABAβ1R: 100 µM baclofen) in the presence of 200 nM CPY-CA for 1 h, washed once in complete DMEM and fixed using 4% PFA. To mitigate the effects of glutamate naturally present in fetal bovine serum, experiments with class C receptors mGluR2 and GABAβ1R included a 4 h pre-incubation in dialyzed FBS prior to addition of agonist and dye.

Confocal microscopy was performed on a Stellaris 5 inverted microscope (Leica) equipped with a white line laser, 405 nm laser diode, and hybrid photodetectors at 37 °C in 5% CO_2 atmosphere in a humidified chamber. A 20x/0.75 air objective was used to image a single plane at 1024x1024 pixel (596x596 µm) resolution (400 Hz scan speed, 2 airy units, pinhole, 4-fold line averaging, mTagBFP2 405 nm ex., 430-494 nm em., mEGFP 488 nm ex., 494-590 nm em., CPY-CA 608 nm ex., 617-730 nm em.).

For the analysis of images, the mTagBFP2 and mEGFP channels were first denoised (despeckle) and a global threshold (Otsu method) was independently applied to the mTagBFP2 and mEGFP channels. The two binary masks were merged (AND) to exclude cells which showed minimal or no expression of one of the two expressed constructs. The resulting binary mask was eroded and segmented using the watershed algorithm in FIJI (*60*). Size (100-700 µm^2) and circularity (0.2-1.00) cutoffs were applied to limit the presence of punctate debris and difficult-to-segment large clusters of cells from the quantitative data set. This final, segmented binary mask was used to extract fluorescence intensity values from the CPY-CA and mEGFP channels. Background was measured by generating an inverse mask for the mTagBFP2 and mEGFP channels, and subtracted from the extracted dataset. Ratiometric images in Figure 2B were generated by dividing the CPY-CA channel by the mEGFP channel, after background subtraction. Results are pooled from 6 wells across three technical replicates and two biological duplicates (*i.e.* three wells per condition in a single experiment, repeated at a later date with cells of a different passage number), with the exception of the titration curves in Fig. 2E which are drawn from six technical replicates.

Recording intracellular calcium levels in mammalian cells with Caprola

Chemical activation of HeLa cells. Stable HeLa Kyoto cells expressing Caprola variants were seeded onto 24-well or 96-well culture dishes and grown to 80% confluency. Ca^{2+} activators (100 µM ATP or 100 nM thapsigargin) and fluorophore substrates in DMEM were simultaneously applied and cells were incubated at 37 °C in a humidified incubator with 5% CO_2 atmosphere for 0.5 min – 4 h. Cells were then washed with DMEM supplemented with HaloTag protein (5 µM) for 10 min, followed by two washes with DMEM for 10 min

each at at 37 °C in a humidified incubator with 5% CO_2 atmosphere. Cells were subsequently analyzed by either fluorescence microcopy or flow cytometry.

Successive recordings using chemical activation in HeLa cells. Recording of successive periods of Ca^{2+}-activity in HeLa cells using spectrally distinguishable fluorophore substrates was performed as explained above with a recovery time of 120 min in between treatment/labeling periods at 37 °C in a humidified incubator with 5% CO_2 atmosphere. JF_{552}-CA (300 nM), CPY-CA (25 nM) and JF_{669}-CA (300 nM) were mixed with Ca^{2+} activators and individually applied for 60 min. In order to stop recording, cells were rinsed once with HaloTag-containing medium for 10 min, followed by two DMEM exchanges for each 10 min. Prior to imaging, cells were fixed with 4% PFA in PBS at room temperature for 20 min.

Recombinant adeno-associated virus (rAAV) preparation. rAAVs were prepared as previously described (*61*). In brief, plasmids pRV1 (AAV2 Rep and Cap sequences), pH21 (AAV1 Rep and Cap sequences), pFD6 (adenovirus helper plasmid) and the AAV plasmid containing the recombinant expression cassette driven by hSyn1 promoter and flanked by AAV2 inverted terminal repeats (ITRs) were transfected via Polyethylenimine 25000 (PEI25000) into HEK293 cells. 5 days post transfection, the medium and cells were harvested. The cells were lysed using TNT extraction buffer (20 mM Tris pH 7.5, 150 mM NaCl, 1% TX-100, 10 mM $MgCl_2$). Cell debris was removed by centrifugation and supernatants were subsequently treated with Benzonase. rAAVs were purified from excess medium and cell supernatant via FPLC using AVB Sepharose columns and subsequently concentrated using centrifugal filter devices (Amicon, Merck KgaA, Darmstadt, Germany) with a MWCO of 100 kDa. Buffer was exchanged to PBS pH 7.3 and titers of rAAVs were quantified by qPCR as previously described (*62*).

Preparation of primary rat hippocampal neuron cultures and rAAV transduction. Neurons were obtained from isolated hippocampi from new born rats (WISTAR) as described previously (*63*). Procedures were performed in accordance with the Animal Welfare Act of the Federal Republic of Germany (Tierschutzgesetz der Bundesrepublik Deutschland, TierSchG) and the Animal Welfare Laboratory Animal Regulations (Tierschutzversuchsverordnung). According to the TierSchG and the Tierschutzversuchsverordnung, no ethical approval from the ethics committee is required for the procedure of euthanizing rodents for subsequent extraction of tissues. The procedure for euthanizing rats performed in this study was supervised by animal welfare officers of the Max Planck Institute for Medical Research (MPImF) and conducted and documented according to the guidelines of the TierSchG (permit number assigned by the MPImF: MPI/T-35/18). Neurons were dissociated by tryptic digestion and seeded in 24-well or 96-well glass bottom plates coated with poly-L-ornithine (100 µg/mL in ddH_2O) and laminin (1 µg/mL in 1x HBSS). Neurons were cultured for 7 days until rAAV-mediated transduction. Equivalents of 10^9 –10^{10} GC/mL of purified rAAVs (serotype 2/1) were administered to individual samples and cultures were allowed to express transgenes for 5-7 days.

Effect of Caprola expression on the physiology of primary rat hippocampal neurons. On the day of recording, a coverslip containing mouse hippocampal neurons expressing $Caprola_6$ or non-infected controls was placed in a RC-27 chamber (Sutter Instruments), mounted under BX51 upright microscope (Olympus) equipped with differential-interference contrast (DIC) and fluorescence capabilities. $Caprola_6$ expression was confirmed in each recorded cell by co-expression of GFP. Control and $Caprola_6$-expressing cells were

maintained at 24±2 ºC using a dual TC344B temperature control system (Sutter Instruments), and were continuously perfused with oxygenated ASCF solution that contained: 125 mM NaCl, 2.5 mM KCl, 1 mM $MgCl_2$, 2 mM $CaCl_2$, 25 mM glucose, 1.25 mM NaH_2PO_4, 0.4 mM ascorbic acid, 3 mM myo-inositol, 2 mM Na-pyruvate, 25 mM $NaHCO_3$, pH 7.4, and 315 mOsm. Cells were approached and patched under DIC, using 3.0±0.5 MegaOhm glass pipettes (WPI, Inc), pulled with a PC10 puller (Narishige, Japan). In all experiments, pipettes were filled with a current-clamp internal solution that contained: Current-clamp: 125 mM K-gluconate, 20 mM KCl, 10 mM HEPES, 0.5 mM EGTA, 4 mM ATP-Magnesium, 0.3 mM GTP-Sodium, 10 mM Na-Phosphocreatine, osmolarity: 312 mOsmol; pH 7.2 adjusted with KOH. In all experiments, we used a dual-channel Multiclamp 700B amplifier (Axon instruments, Inc) controlled by Clampex 10.1 and Digidata 1440 digitizer (Molecular Devices, Inc). Resting membrane potential was measured right after breaking-in, and then offline corrected by the liquid-junction potential (estimated to be 9.683 mV under our experimental conditions). Cell capacitance and membrane resistance were estimated after challenging neurons with short (10-50 ms) pulses of negative current (-10 pA) from near -70 mV membrane potentials. For maintaining cells at ~ -70 mV, either positive or negative current was continuously injected through the recording pipette (holding current). To trigger spikes and measure the rheobase, cells were maintained at ~ -70 mV as indicated above and then challenged with increasingly larger pulses of positive current (5 pA increments, 500 ms) until action potentials were observed (rheobase). Detection and analysis of all recordings was done with Clampfit 10.1(Molecular Devices, Inc), and statistical comparisons were done using unpaired t-test (two tailed) in Prism (Graphpad, Inc).

Chemical activation of cultured neurons and signal stability measurements. Neurons seeded in 24-well glass bottom plate were used at 14-16 days *in vitro* (div). Prior to experiments, neurons were incubated with the respective fluorophore substrates at 37 °C in a humidified 5% CO_2 incubator for 30 min. Ca^{2+} influencing agents (APV/ NBQX (25 µM/10 µM) and Glutamate/Glycine (10 µM/2.5 µM)) were applied to neuronal cultures at 37 °C in a humidified 5% CO_2 incubator for 30 min. Afterwards, neurons were first washed with 1x HBSS supplemented with HaloTag protein (5 µM) for 20 min followed by washing twice with transparent NeuroBasal medium for 20 min each, prior to imaging. For Caprola signal tracking over time, neurons were incubated for 1 h with 250 nM CPY-CA at 37 °C in a humidified 5% CO_2 incubator and washed as described above. Experiments were conducted as replicates. The recorded fluorescence intensities of basally active neurons were subsequently measured, and every 24 h for three days. Before every measurement, respective laser powers were calibrated using an optical power and energy meter. Between measurements, neurons were maintained at 37 °C in a humidified 5% CO_2 incubator.

Electric field stimulation of cultured neurons. Neurons were prepared as mentioned previously. 30 min prior to the experiment a synaptic blocker solution (25 µM APV,10 µM NBQX in NeuroBasal medium) was applied to cells at 37 °C in a humidified 5% CO_2 incubator. Neuron cultures were placed on a pre-warmed (37 °C) widefield microscope stage in 5% CO_2 atmosphere and a custom-build 24-well cap stimulator with platin electrodes linked to a stimulation control unit was mounted on top (*63*). In order to elicit defined trains of action potentials, stimulation patterns of 80 Hz, 100 mA and 1 ms pulse width were delivered to live neurons in the presence of fluorophore substrates (fig. S25). Experiments were conducted as replicates. In order to evaluate the evoked Ca^{2+} levels by electrical stimulation, neurons expressing GCaMP6s (AAV transduction) were prepared as described above. Fluorescence intensities were measured on a widefield microscope at 2 ms acquisition rate. Fluorescence intensity change were calculated and represented as $\Delta F/F_0$ (fig. S17).

Measurements of calcium responses to action potentials using Caprola in neurons (*e.g.* Fig. 4G) was performed under 10 short sequences of stimulation with different numbers of action potentials (1 to 100 AP per sequence) over the course of 1 h, sequences were therefore interspaced with 6.67 min resting periods (fig. S20A). After stimulation, cells were washed with 1x HBSS supplemented with HaloTag protein (5 µM) for 20 min followed by washing twice with transparent NeuroBasal medium. Fluorescence imaging was conducted in transparent NeuroBasal medium at 37 °C and 5% CO_2.

Short-timed recordings of electrical and chemical activation of cultured neurons. Neurons seeded in 24-well glass bottom plate were used at 14-16 days *in vitro* (div). Experiments were conducted as replicates. Ca^{2+} activating agents KCl (1 mM) and Glutamate/Glycine (250 µM/100 µM)) were applied to neuronal cultures simultaneously with 100 nM CPY-CA at 37 °C in a humidified 5% CO_2 incubator for 5 min. Electrical field stimulation (10x 100 AP, 80 Hz, 100 mA, 1 ms pulse width) was performed upon 100 nM CPY-CA addition for 5 min using neurons pre-incubated with synaptic blockers (APV/NBQX (25 µM/10 µM) for 30 min. Afterwards, neurons were washed with 1x HBSS supplemented with HaloTag protein (5 µM) for 10 min followed by washing twice with transparent NeuroBasal medium for 20 min each prior to imaging.

Widefield microscopy. Wide field microscopy was performed on a commercial Leica Dmi8 inverted microscope equipped with a Leica DFC9000 GT sCMOS camera (1024x1024 pixels) and a CoolLED Pe4000 LED light source (635 nm, 635/18; 470 nm, 474/27; 365 nm, 378/52). Live cell imaging was performed at 37 °C with a 5% CO_2 atmosphere in a humidified chamber. Fixed sample were allowed to equilibrate to 37 °C for 30 min to avoid thermal drifting during image acquisition. The following settings were used for image acquisition: 20.0×/0.08 dry objective, 50 ms to 800 ms exposure times and 8-bit or 16-bit depth. Additional imaging acquisition parameters are summarized in the table S7.

Confocal microscopy. Confocal microscopy was either performed on a commercial Leica SP8 or Stellaris 5 inverted microscope both equipped with a white line laser (WLL) and hybrid photodetectors for single molecule detection (HyD SMD detector). Live cell imaging was performed at 37 °C with a 5% CO_2 atmosphere in a humidified chamber. Fixed sample were allowed to equilibrate to 37 °C for 30 min to avoid thermal drifting during image acquisition. The following settings were used for image acquisition: 20x/0.80 air objective; image size: 581.82 x 581.82 µm; scan speed 400-600 MHz; pinhole 1-2 airy units; line averages (4-8) and 8-bit or 16-bit depth. Z-stacks were performed with 2-5 µm step size. Additional imaging acquisition parameters are summarized in the table S7.

Imaging data analysis. Image analysis was performed with FIJI (*60*). For image representations, multi-plane images were converted into maximum intensity projections (MIPs). For fluorescence intensity measurements, multi-plane images were converted into average intensity projections (AIPs). ROIs were hand-segmented and mean fluorescence intensities from individual ROIs were derived for multiple fields-of-views. Cells displaying unhealthy phenotypes were excluded from analyses. Background intensities were measured as mean intensities from cell-free regions and subtracted for background correction. Ratiometric images were generated by using the BRET_analyzer plug-in (*64*). In brief, image stacks were split into their individual fluorescence channels. The mEGFP channel was used for thresholding (Chastagnier method, default settings) and fluorescence channels were divided (fluorescent probe/mEGFP), resulting in ratiometric images represented with ‘fire’ look-up table.

Flow cytometry. Cells were detached from dishes using transparent TrypLE™-Express (Gibco, 1/4 of dish volume) at 37 °C in a humidified 5% CO_2 incubator for 5 min. Cells were re-suspended in 1x PBS containing 2% FBS (3/4 of dish volume) and transferred into a flowcytometry compatible dish (non-adhering 96-U-well plate or 5 mL FACS tube, FALCON). Samples were subjected to the autosampler of a BD Fortessa X-20 flow cytometer. Cell populations were gated for live (SSC-A/FSC-A) and single cells (SSC-H/SSC-A). Fluorophores were recorded as follows: mEGFP (488 nm excitation, 530/30 nm emission), fluorophores in the range from 525 nm to 570 nm (561 nm excitation, 575/26 nm emission), fluorophores in the range from 580 nm to 620 nm (561 nm excitation, 610/20 nm emission) and fluorophores in the range from 620 nm to 680 nm (648 nm excitation, 660/20 nm emission). Photomultiplier tube detectors and fluorescence compensation parameters were adjusted such that signal saturation and signal bleed-through was avoided.

Flow cytometry data analysis. Raw data from quantitative flow cytometry measurements were imported into the FlowJo suite (BD) and processed as follows. First, live (SSC-A/FSC-A) and single cell (SSC-H/SSC-A) gates were adjusted and cells displaying fluorescence intensities of mEGFP below 10^3 a.u. were excluded from analysis. Fluorescence intensity ratios were calculated for every cell individually by dividing the fluorescence intensities from fluorophores by fluorescence intensities from mEGFP. Dot plots showing whole populations or ratio density plots were created in FlowJo's layout manager. Quantitative assessment and statistical analysis were performed using GraphPad (Dotmatics) or R.

Generation of stable Caprola-expressing glioblastoma cells. Glioblastoma were transduced with generated lentiviruses as previously described (*29*). Successfully transduced S24 cells were selected using 1 µg/mL puromycin (Applichem). Surviving cells were allowed to recover, mEGFP positive cells were sorted using a FACS Melody (Excitation 488 nm, filter 530/30 nm) and propagated for experiments as described above.

Calcium recording in glioblastoma cells. $Caprola_6$-, $Caprola_{on}$- and $Caprola_{off}$-expressing glioblastoma cells were seeded at $5x10^4$ cells/well into Matrigel®-coated 96-well Ibidi µPlates in PDGCL medium supplemented with 50 mM glucose (high-glucose medium, HGM) that stimulates diffuse growth and network formation. 48 h after seeding, S24 cells were incubated with 125 nM CPY-CA for 90 min at 37 °C in a humidified 5% CO_2 atmosphere. When needed, glioblastoma cells expressing $Caprola_6$ were treated with 100 nM thapsigargin and compared to untreated cells. Cells were further washed with HGM containing 1 µM recombinant HaloTag protein for 30 min. Lastly, S24 cells were rinsed with 1x PBS, detached using Accutase and finally analyzed via flow cytometry as described for HeLa cells expressing Caprola. Experiments were performed in replicates.

Transcriptomic data (RNA-Seq) acquisition. $Caprola_6$-expressing glioblastoma cells were plated at $12x10^6$ cells/well on Matrigel®-coated T-75 culture flasks in high-glucose medium (HGM) as previously described. 48 h after seeding, S24 cells were labeled as described above in absence of treatment and subjected to FACS sorting on a FACSAria™ Fusion Special Order System (BD Biosystems). $Caprola_6$-expressing S24 cells were sorted into three groups with high, medium and low fluorescence intensity ratios (CPY-CA/mEGFP). Three replicate samples per group were collected and RNA was isolated with the Arcturus PicoPure Kit (Thermo Fisher Scientific), according to the manufacturer´s recommendations. On-column DNAse digestion was performed with the RNAse free DNAse

set (Qiagen) and RNA integrity verified using the high-sensitivity RNA Screen Tape System (Agilent) and the 4150 Tapestation System (Agilent). Library preparation and RNA sequencing of the 2-3 replicates per condition on a NovaSeq6000 device (Illumina) were conducted by the Genomics and Proteomics Core Facility at the German Research Cancer Institute (DKFZ, Heidelberg). The same experiment was performed using Caprola$_{on}$-expressing S24 as control, with a decreased labeling time of 2.5 min.

RNA-Seq data analysis. RNA-Seq reads were aligned with STAR (*65*) (v.2.5.3a) against GRCh38 human reference genome and the gene-count matrix was generated with featureCounts (*66*) in Subread (v.1.5.3) against GENCODE (*67*) (v.32). In order to remove artefacts, we excluded the genes that only expressed in one sample. Pairwise differentially expressed genes (DEGs) between groups were identified with generalized linear models using edgeR (*68*) (v.3.34.1) (*i.e.* DEGs in High vs. Medium, High vs. Low and Medium vs. Low). We kept the DEGs which had a false discovery rate (FDR) < 0.05, a log count-per-million < 2 and were recurrently identified in at least two comparisons. We obtained 757 DEGs in Caprola$_6$ data and 57 DEGs in Caprola$_{on}$ data. The expression levels (log2 fragments per kilobase per million mapped fragments) of DEGs were scaled and centred across samples into standard scores (z-score) with scale function in R Base (v.4.1.0) and visualized in circular heatmap with circlize (*69*) (v.0.4.13). Multidimensional scaling plot of RNA-Seq datasets with the first principal coordinate (PCoA1) were plotted using plotMDS function in edgeR (*68*). ShinyGO (*70*) (RRID:SCR_019213, v.0.741) was used for the gene ontology (GO) enrichment analysis of the 757 Caprola$_6$ DEGs, 57 Caprola$_{on}$ DEGs and 31 common DEGs, respectively, and pathways obtained from the "GO Biological Process" gene set. The gene lists used for GO term analysis are disclosed as source data. Unfavourable prognostic genes of glioblastoma were retrieved from the Human Pathology Atlas (*71*). A Fisher's Exact Test for 8 worse survival genes in upregulated Caprola$_6$ DEGs (n=445) vs. 0 worse survival genes in downregulated DEGs (n=312) was performed (p-value = 0.02389).

In vivo experiments

General remarks on fly husbandry and line generation

Drosophila melanogaster were reared on standard fly medium (cornmeal agar) at room temperature and female fruit flies aged 2-4 days post enclosure were used for all experiments. Caprola was expressed in T4 and T5 visual neurons using a split-GAL4 line. The driver line was generated from the lines w[1118]; P{y[+t7.7] w[+mC]=VT043070-p65.AD}attP40 (BDSC #71655) and w[1118]; P{y[+t7.7] w[+mC]=R39H12-GAL4.DBD}attP2 (BDSC #69444) by Tabea Schilling. For the reporter line, mCD8::GFP in pJFRC7-20XUAS-IVS-mCD8::GFP (RRID:Addgene #26220, kind gift from Gerald Rubin) was replaced with NES-CaProLa$_5$_mEGFP. The plasmid was integrated into attp40 landing sites (*72*) using the PhiC31 integration system (*73*), by the BestGene Inc (Chino Hills, USA) through Drosophila Embryo Injection Service. The reporter line used was y1w67c23;P{20xUAS-IVS-NES-Caprola$_5$-meGFP}attp40;+. The genotype of the experimental flies was w$^-$; VT043070-p65.AD / 20xUAS-IVS-NES-Caprola5-meGFP; R39H12- GAL4.DBD /+..

Visual stimulation of flies

Flies underwent cold-induced anesthesia on a Peltier element before being tethered to custom plates (*74*) in order to access to the back of the fly's head. The proboscis was glued to the head capsule and wings were glued to the thorax using UV glue (Bondic). The prothoracic and the mesothoratic leg pairs were clipped. Next, the back of the fly's head was

submerged in extracellular solution (NaCl 103 mM, KCl 3 mM, TES 5 mM, Trehalose-$2H_2O$ 10 mM, Glucose 10 mM, Sucrose 2 mM, $NaHCO_3$ 26 mM, NaH_2PO_4 1 mM, $CaCl_2$-$2H_2O$ 1.5 mM, and $MgCl_2$-$6H_2O$ 4 mM (275-285 mOsm)) (*75*). A shallow incision was made at the back of the fly's head and the flies were transferred to the visual arena. The visual stimulus was presented on a 7.8 inch, fully flexible AMOLED display (Royole, 1440*1920, 60 Hz) that was bent into a half-circular shape. It covered the frontal 180° of the visual field in azimuth and 61 ° in elevation. On the unstimulated side the display was wrapped in blackout fabric to avoid reflections from the contralateral side of the screen that showed the stimulus. The fabric extended about 25 ° across the midline to cover the binocular overlap. Once flies were in the visual arena, the extracellular solution was replaced with CPY-CA solution (DMSO 5%, Pluronic F 127 0.04% [Invitrogen], CPY-CA 10 µM in extracellular solution). The visual stimulus was presented during 20 min and was generated using PsychoPy software (*76*). The visual stimulus consisted in a full-field sine wave grating (approximately 20 ° spatial frequency) that moved at 1 Hz temporal frequency. The direction of the sine wave turned every 5 sec by 45 °. A full repeat of all 8 directions was completed after 40 sec. During one experiment, 30 repeats were shown. Afterwards, the CPY-CA solution was removed and replaced by extracellular solution to wash out the dye (3x 300 µL). The brains were then prefixed by incubation with ROTI®Histofix 4% (Roth) for 5 to 10 min, during which the visual stimulus was continuously presented. After removing the flies from the arena, the brains were dissected in phosphate-buffered saline (PBS), fixed for 1h at room temperature in ROTI®Histofix 4%. The brains were subsequently washed (0.1% Triton X100 in PBS) and mounted dorsal to ventral in Vectashield (Biozol) between two cover glasses.

Confocal microscopy of fly brains

Prior to imaging, samples were allowed to equilibrate to ambient temperature. Confocal microscopy was performed on a commercial Leica SP8 microscope equipped with a white line laser (WLL), a hybrid photodetector for single molecule detection (HyD SMD detector) and an automatized stage. The following settings were used for image acquisition: 20x/0.6 multi-immersion objective with oil; image size: 456.8 µm x 456.8 µm (1024x1024 pixel); zoom 0.75 x, scan speed 600 MHz; pinhole 1 airy unit; line averages (4) and 8-bit depth. Z-stacks were recorded with 5 µm step sizes. Brains were aimed to be mounted with antennal lobes facing down for image acquisition. Additional imaging acquisition parameters are summarized in table S7.

General remarks on zebrafish husbandry

Adult and larval zebrafish were maintained on a 14:10 hours light:dark cycle at 28 °C, pH of 7-7.5, and a conductivity of 600 µS. After natural mating, up to 100 embryos were kept in petri dishes with Danieau's solution, which was exchanged every second day. The fish developmental stage was reported in days post-fertilization (dpf), corresponding to staging at standard temperature of 28.5 °C (*77*). Embryos used in this work had the *nacre* (TLN) genetic background, carrying the *mitfa*$^{-/-}$ mutation and lacking melanophore pigmentation (*78*). Experiments on zebrafish larvae were performed from 4 dpf to 6 dpf.

All animal procedures conformed to the institutional guidelines set by the Max Planck Society, with an animal protocol approved by the regional government (Regierung von Oberbayern) ROB-55.2-2532.Vet_02-21-70 and ROB-55.2-2532.Vet_02-19-16.

Generation of zebrafish lines

For the generation of transgenic zebrafish, WT Nacre zebrafish eggs were injected with mRNA encoding the Tol2 transposase (*79*) together with a pTol2 plasmid encoding Caprola driven by a partial *elavl3* pan-neuronal promoter (Tg[*elavl3*:NES-Caprola-mEGFP],

table S7). At 3 dpf, fluorescent and healthy embryos were sorted under an epifluorescence microscope (Excitation 488 nm, Emission filter 530/30 nm) and raised to adulthood (F0 generation). F0 individual fish were outcrossed to WT *nacre* and screened for germ line propagation of the Caprola constructs. The strongest fluorescent offspring were raised to adulthood constituting the F1 generation. Incross offspring (F2) from the F1 generation were used for experiments. Zebrafish lines generated are listed in the following:

- Tg(*elavl3:NES-Caprola$_{1}$-EGFP*) mnp425
- Tg(*elavl3:NES-Caprola$_{6}$-EGFP*) mnp426
- Tg(*elavl3:NES-Caprola$_{on}$-EGFP*) mnp427
- Tg(*elavl3:NES-Caprola$_{off}$-EGFP*) mnp428

Free swimming prey capture experiment

Zebrafish larvae (5 – 6 dpf) were placed in a 35 mm dish containing 1.5 mL of water. Experiments were initiated by adding CPY-CA supplemented water to reach a final dye concentration of 5 µM. Prey capture samples were provided with 2 drops of a cleared paramecia culture while control experiment did not receive paramecia. Experiments were conducted in parallel on the same day. Zebrafish larvae were incubated for 2.5 h at 28 °C in light. The prey capture behavior in bulk was verified using a binocular microscope. To terminate the experiment, larvae were de-stained in water in the dark three times for 20 min and finally 60 min prior to imaging.

Visual stimulation of embedded zebrafish larvae

At the center of a dish (100 mm x 30 mm) zebrafish larvae (4 – 6 dpf) were embedded in 2% low melting point agarose. The agarose in the vicinity of the eyes was removed to enable free movement. Black agarose (low melting agarose:squid ink (4:1)) was employed to block the vision of a given fish eye. Larvae were then placed in the center of a visual arena made of 4 miniature LCD screens (6 cm height, 8 cm width), which displayed vertical gratings at a speed of 30°/second alternating between clockwise and counter-clockwise rotation patterns every 10 s. The experiment was triggered by adding water supplemented with fluorophore substrate (5 µM final concentration). The experiment was conducted during 30 min to 6 h. Larvae were de-stained in water three times for 20 min and finally 60 min prior to imaging. For multi-color staining, the experiments were conducted as explained above despite that the larvae were recovered overnight between experiments.

Confocal microscopy of zebrafish larvae

Prior to imaging, zebrafish larvae were mounted on the bottom of petri dishes (60 mm) using 2% low melting agarose, and anaesthetized using Tricaine (0.16 mg/mL). Confocal microscopy was performed on a commercial Leica SP8 microscope equipped with a white line laser (WLL), a hybrid photodetector for single molecule detection (HyD SMD detector) and an automatized stage. The following settings were used for image acquisition: 20x/1.0 water objective; image size: 456.8 µm x 456.8 µm (1024x1024 pixel); scan speed 600 MHz; pinhole 1 airy unit; line averages (4) and 8-bit depth. Z-stacks were performed with 5 µm step sizes while recording images as two vertical tiles that were stitched together with 10% overlap in the LASX software post image acquisition. For data representation in Fig. 5D, the fluorescence measured from the eye pigmentation was omitted. Fluorescence intensities measured from the eyes were further omitted from data extraction. Additional imaging acquisition parameters are summarized in table S7.

Data representation, reproducibility and statistical analysis

Numerical data was plotted using the ggplot2 R package (*46, 47*). X-ray structures were rendered with PyMol. Imaging data was analyzed and represented using FIJI (*60*). Schemes and figures were made with Adobe Illustrator, using elements from BioRender.com.

Biochemical experiments were performed in three technical replicates. Unless stated otherwise, cell experiments were performed in three independent biological replicates including technical replicates. For mammalian cell experiments, biological replicates are defined as different passage of cells lines. For neurons, biological replicates are defined as different neuron preparations. For animal experiments, individual animals were considered biological replicates. Animal experiments were conducted at least at two different days from different clutches.

Scripts and input files for the computational design are available at https://github.com/johnsson-lab/splitHaloTag_Hpep_design (DOI: 10.5281/zenodo.8113621). Statistical analyses were performed with GraphPad Prism 9.0, or custom R scripts (*46, 47*). Statistical significances (*i.e. p*-value) were calculated using Welch's corrected one-tailed t-tests (or two-tailed for symmetric stimulation). For the analysis of fish brains after visual stimulation a paired t-test was used. The different *p*-values were classified as **** for p-value ≤ 0.0001, *** for p-value ≤ 0.001, ** for p-value ≤ 0.01, * for p-value ≤ 0.05 and non-significant (NS) for for p-value > 0.05.

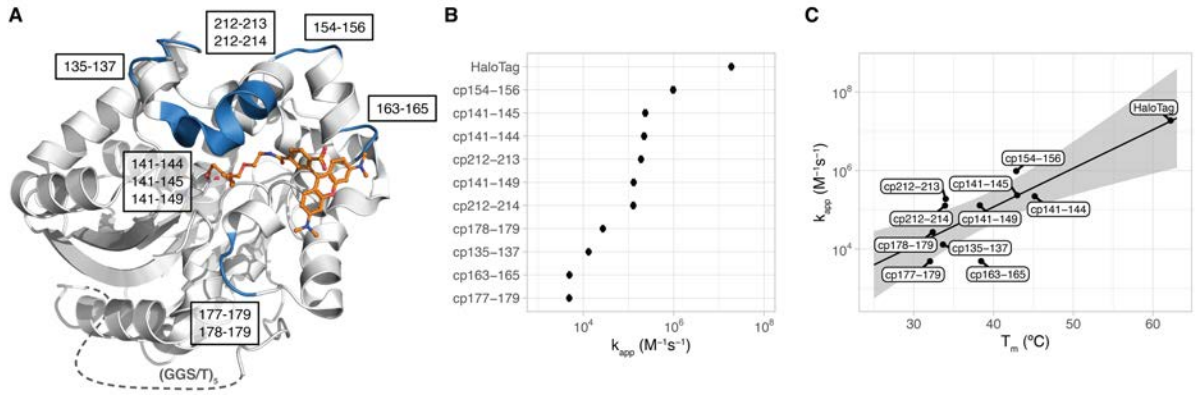

Fig. S1. Biochemical characterization of circularly permuted HaloTag variants.
(**A**) X-ray structure of HaloTag labeled with TMR-CA (PDB-ID: 6Y7A). New termini of circularly permuted HaloTag variants are highlighted in blue. The $(GGS/T)_5$ linker connecting the original termini is depicted as a dashed line. (**B**) Apparent second-order rate constants (k_{app}) of the labeling reaction of circularly permuted HaloTag variants with TMR-CA substrate measured by fluorescence polarization kinetics. Number ranges indicate the new termini according to standard HaloTag numbering. (**C**) Melting temperatures (T_m) of circularly permuted HaloTag variants measured by nanoDSF plotted against apparent second-order rate constants. Trendline: linear regression of $\log_{10}(k_{app})$ vs. T_m, $R^2 = 0.68$. Gray area: 95% confidence bands.

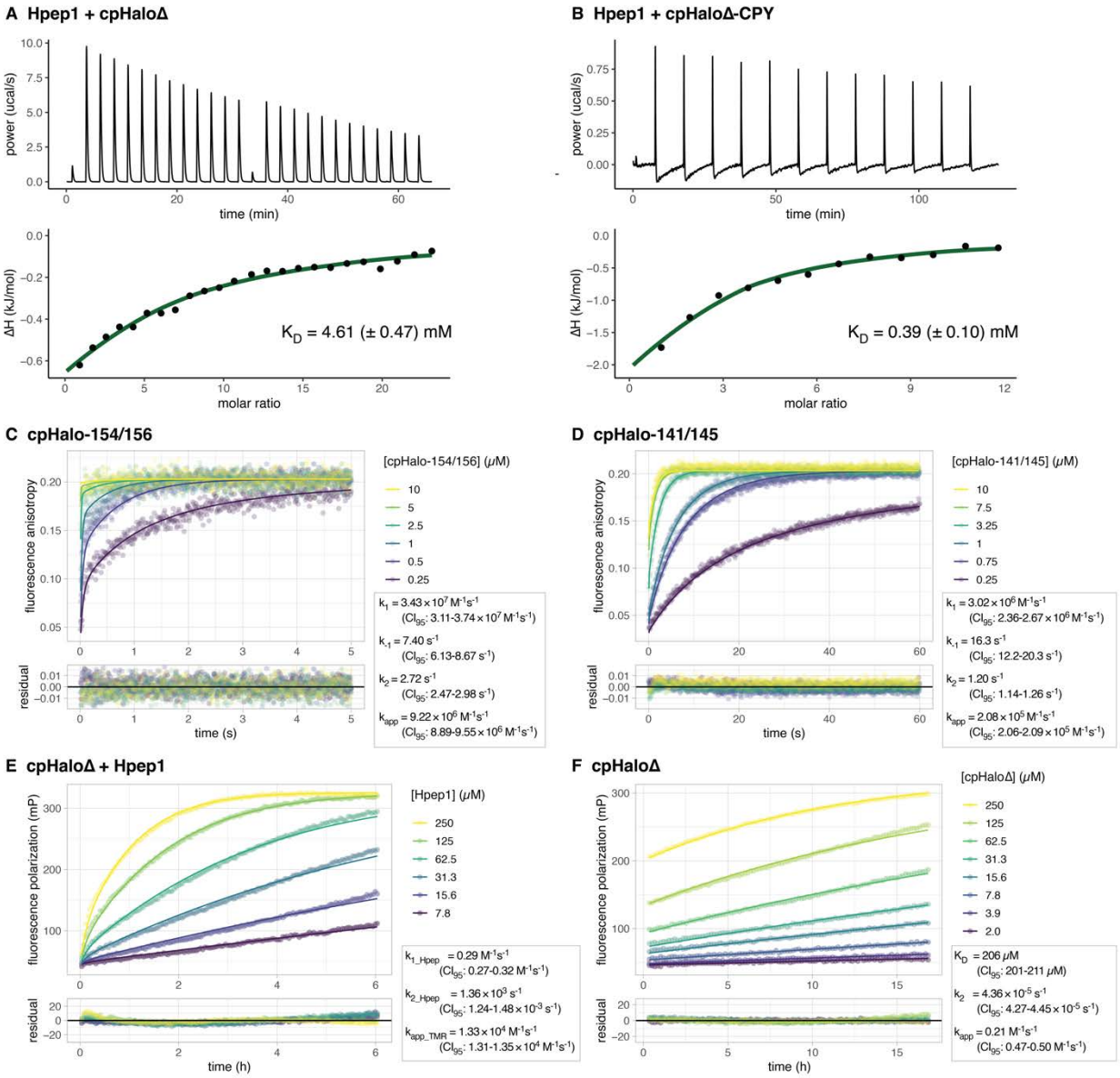

Fig. S2. Biochemical characterization of split-HaloTag.

(**A, B**) Affinity of Hpep1 for cpHaloΔ (A) or cpHaloΔ labeled with CPY-CA (B) measured by ITC. (**C**, **D**) Labeling kinetics of circularly permuted HaloTag variants (cpHalo-154/156 and cpHalo-141/145) with TMR-CA measured by fluorescence anisotropy on a stopped flow setup. A biochemical model (equations 1-2) was fit to the data and rate constants (k_1, k_{-1}, k_2, k_{app}) are given with 95% confidence intervals. (**E**) Labeling kinetics of split-HaloTag with TMR-CA at different concentrations of Hpep1 measured by fluorescence polarization. A biochemical model (equations 4-5) was fit to the data and rate constants (k_{1_Hpep1}: binding of Hpep1, k_{2_Hpep1}: unbinding of Hpep1, k_{app_TMR}: reaction with TMR-CA) are given with 95% confidence intervals. The ratio k_{1_Hpep1}/ k_{-1_Hpep1} (= K_{D_Hpep1}) was fixed to 4.61 mM. (**F**) Labeling kinetics of cpHaloΔ with TMR-CA at different concentrations of cpHaloΔ measured by fluorescence polarization. A biochemical model (equations 1-2) was fit to the data and constants (K_D, k_2, k_{app}) are given with 95% confidence intervals.

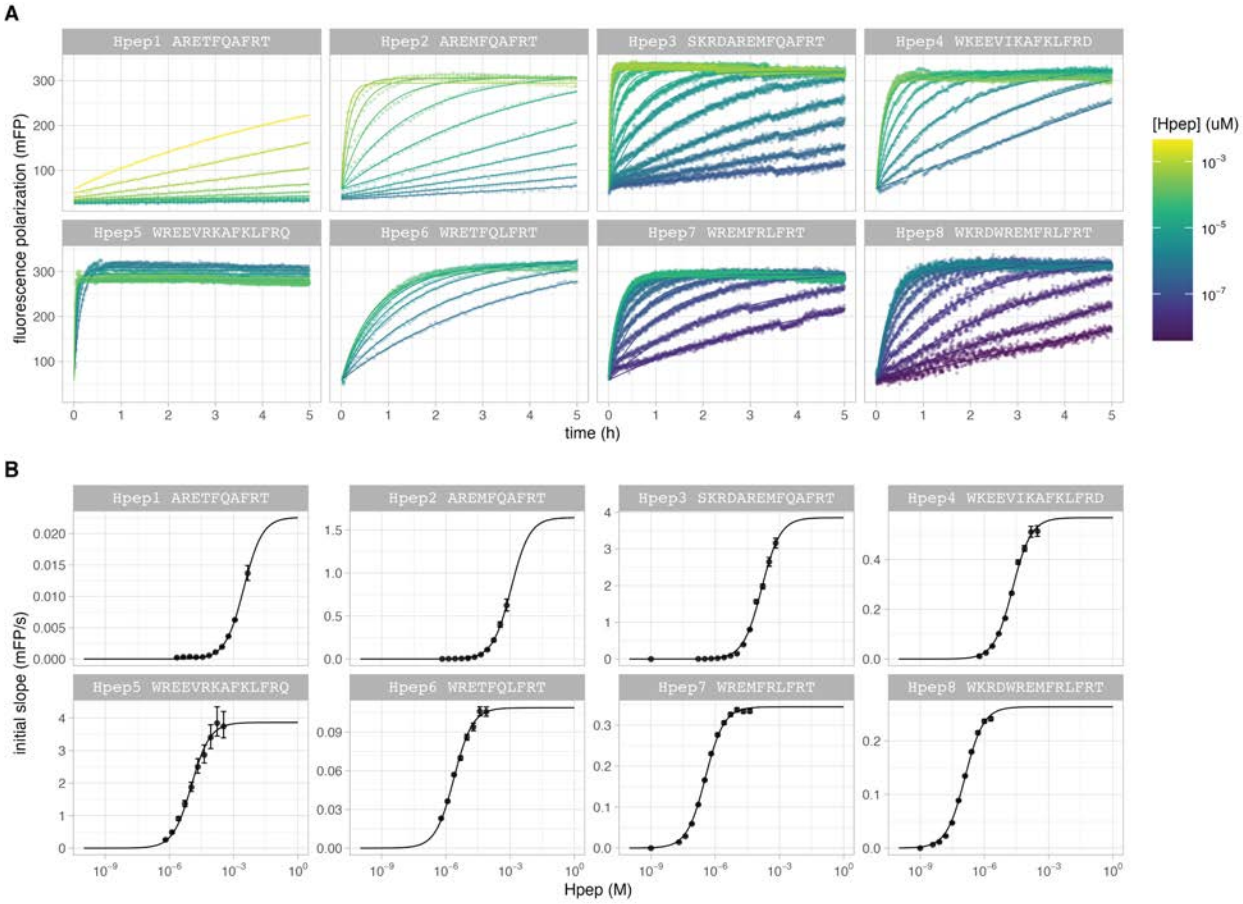

Fig. S3. Kinetic assay to determine EC_{50} values for selected Hpep variants.
(**A**) Labeling kinetics of split-HaloTag with TMR-CA at different concentrations of Hpep measured by fluorescence polarization. A second-order reaction model (or a linear model for reactions not reaching a plateau) was fit to the data and initial reaction rates were determined. (**B**) Initial rates were plotted against Hpep concentration and a sigmoidal model was fit to the data to estimate EC_{50} values. Error bars represent 95% confidence intervals.

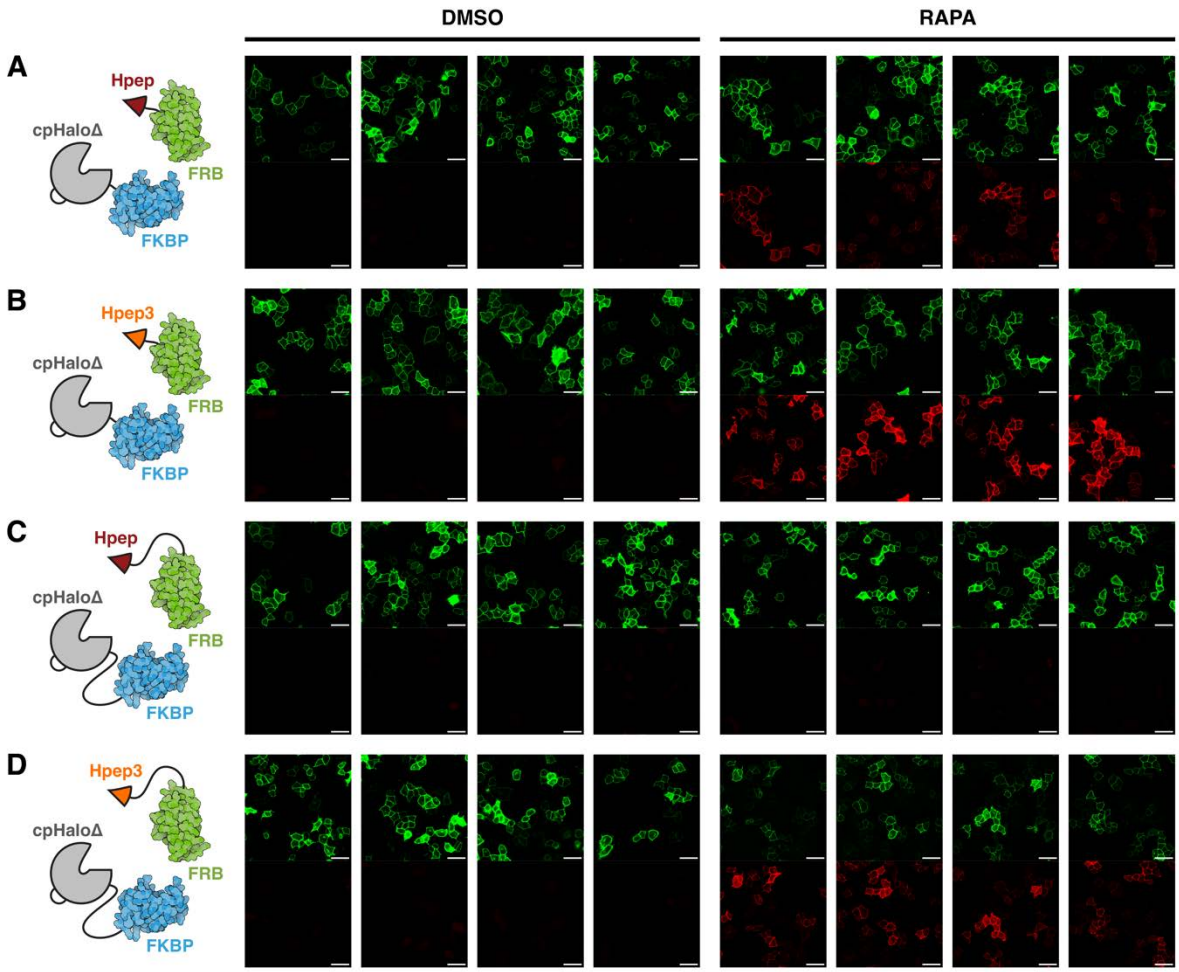

Fig. S4. Recording of rapamycin-dependent FKPB-FRB interactions in HeLa cells with split-HaloTag via fluorescence microscopy.

Fluorescence micrographs of HeLa cells co-expressing different split-HaloTag FKPB and FRB fusion proteins varying in orientation and linker length:
(**A**) Lyn11-mEGFP-FKBP-(GGS)-cpHaloΔ + FRB-(GGS)-Hpep1-mScarlet,
(**B**) Lyn11-mEGFP-FKBP-(GGS)-cpHaloΔ + FRB-(GGS)-Hpep3-mScarlet,
(**C**) Lyn11-mEGFP-cpHaloΔ-$(GGS)_9$-FKBP + Hpep1-$(GGS)_3$-FRB-mScarlet or
(**D**) Lyn11-mEGFP-cpHaloΔ-$(GGS)_9$-FKBP + Hpep3-$(GGS)_3$-FRB-mScarlet.
Cells were labeled in presence (RAPA) or absence (DMSO) of 100 nM rapamycin for 1 h. When fused to the close C-termini of FKBP/FRB (14 Å distance), cells with Hpep1 and Hpep3 are labeled in the presence of rapamycin. When fused to the more distant N-termini of FKBP/FRB (47 Å distance), only cells with Hpep3 are labeled in the presence of rapamycin. Parts of the presented data are also shown in Fig. 1M. Scale bars: 50 µm.

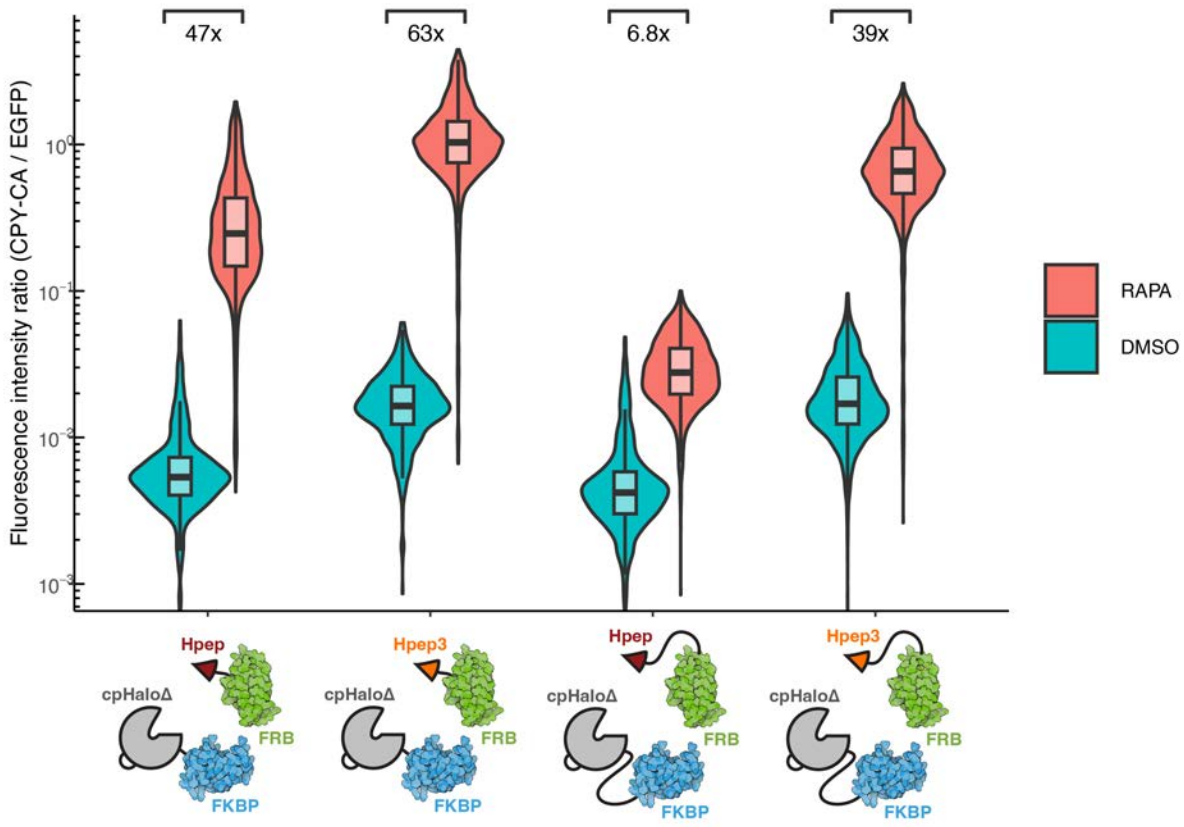

Fig. S5. Recording of rapamycin-dependent FKPB-FRB interactions in HeLa cells with split-HaloTag via flow cytometry.

Labeling ratios (CPY-CA/EGFP) of HeLa cells co-expressing different split-HaloTag FKPB and FRB fusion proteins varying in orientation and linker length:
Lyn11-mEGFP-FKBP-(GGS)-cpHaloΔ + FRB-(GGS)-Hpep1-mScarlet,
Lyn11-mEGFP-FKBP-(GGS)-cpHaloΔ + FRB-(GGS)-Hpep3-mScarlet,
Lyn11-mEGFP-cpHaloΔ-$(GGS)_9$-FKBP + Hpep1-$(GGS)_3$-FRB-mScarlet or
Lyn11-mEGFP-cpHaloΔ-$(GGS)_9$-FKBP + Hpep3-$(GGS)_3$-FRB-mScarlet.
Cells were labeled in the presence (RAPA) or absence (DMSO) of 100 nM rapamycin for 1 h. When fused to the close C-termini of FKBP/FRB (14 Å distance), cells with Hpep1 and Hpep3 are labeled in the presence of rapamycin. When fused to the more distant N-termini of FKBP/FRB (47 Å distance), only cells with Hpep3 are labeled in the presence of rapamycin. Fold changes of labeling ratios in presence of rapamycin are given for each construct. Data is partially represented in Fig. 1N.

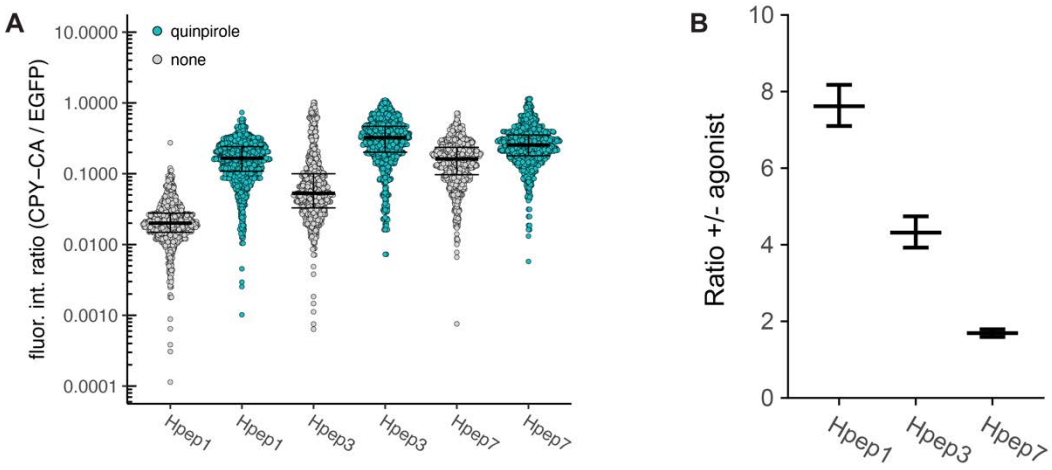

Fig. S6. Impact of Hpep affinity on the D2R GPCR recorder performances.

Quantification of labeling in HEK293 cells co-expressing D2R-cpHaloΔ-EGFP and different versions of Hpep-ß-arrestin2-T2A-mTagBFP2 treated with or without 100 µM quinpirole for 1 h in the presence of CPY-CA. Labeling was detected by fluorescence microscopy. Agonist-free labeling increases with peptide EC_{50}, indicating an increase in labeling in the absence of the GPCR/ß-arrestin interaction due to spontaneous complementation with peptides with higher affinity for cpHaloΔ. The effect of the affinity of the peptide on quinpirole-induced labeling is less pronounced. Lines indicate medians, error bars indicate 25% and 75% quantiles. Symbols indicate values from individual cells (N > 500). Fluor. int. ratio: fluorescence intensity ratio. Data for low affinity peptide Hpep1 (EC_{50} = 2.98 mM) is reproduced from Fig. 2C. (**B**) Low affinity peptide Hpep1 (EC_{50} = 2.98 mM) shows the greatest discrimination between agonist-stimulated and non-stimulated conditions. Ratio +/- agonist denotes the quotient of the geometric means of data plotted in (A). Error bars indicate 95% confidence intervals.

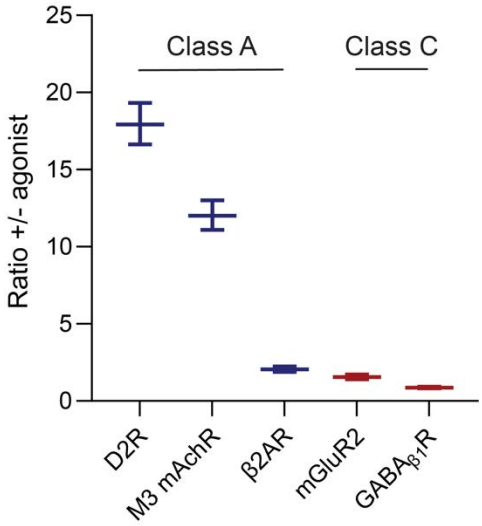

Fig. S7. Comparison between Class A and C GPCR recorder performances.
Quantification of labeling in HEK293 cells co-expressing different GPCRs fused to cpHaloΔ-EGFP and Hpep1-ß-arrestin2-T2A-mTagBFP2 treated with or without agonist for 1 h in the presence of CPY-CA. Labeling was detected by fluorescence microscopy. Class A receptors D2R and m3 mAchR show a robust response to stimulation with their cognate ligands (quinpirole and carbachol, respectively). β2AR shows a modest (2x) response to stimulation with isoproterenol, while class C GPCRs show little response to stimulation (1.5x mGluR2 stimulated with glutamate, 0.8x GABAβ1R stimulated with baclofen). Quinpirole, isoproterenol and baclofen were employed at a final concentration of 100 µM. Glutamate and carbachol were employed at a final concentration of 1 mM. Ratio +/- agonist denotes the quotient of the geometric means of cells measured in the presence or absence of agonist. Error bars indicate 95% confidence intervals.

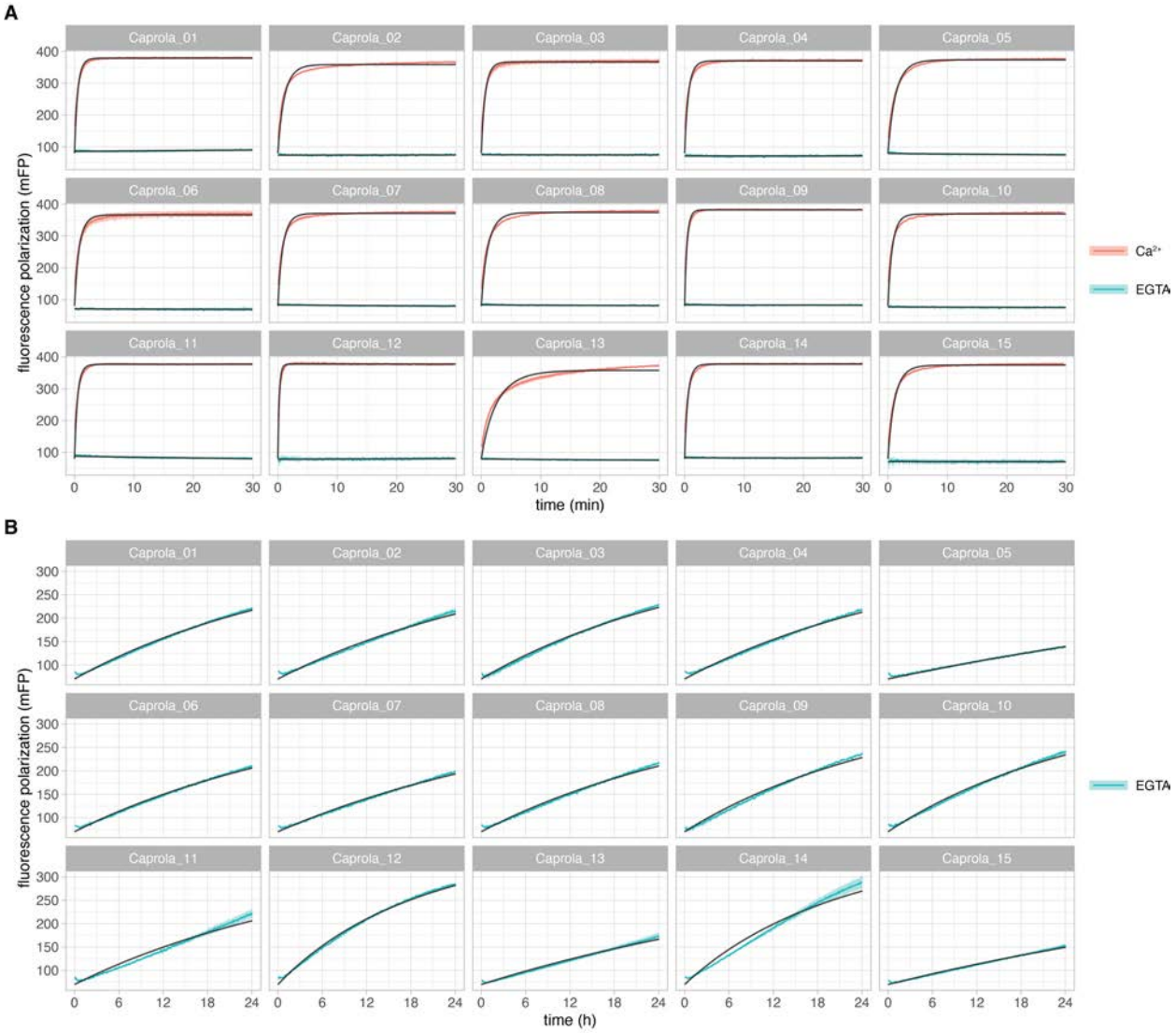

Fig. S8. Labeling kinetics of the different Caprola variants.

(**A**) Labeling kinetics of Caprola variants with TMR-CA in presence or absence of free Ca^{2+} measured by fluorescence polarization. A second-order reaction model was fit to the data in presence of Ca^{2+} to determine rate constants. (**B**) Rate constants in the absence of Ca^{2+} were determined in a long term (24 h) fluorescence polarization assay. A second-order reaction model (with fixed plateau) was fit to the data to determine rate constants.

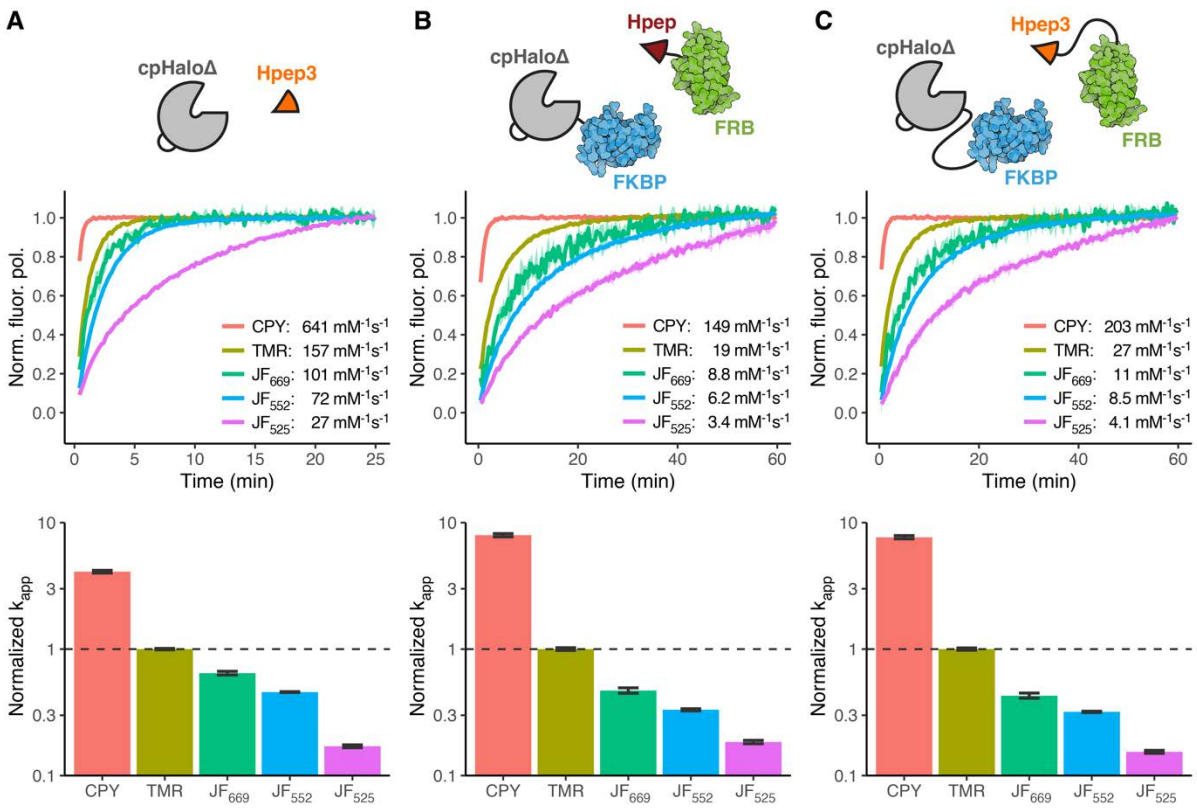

Fig. S9. Labeling kinetics of various split-HaloTag constructs with different fluorophore substrates.

Labeling reaction of (**A**) cpHaloΔ + Hpep3 (1 mM), (**B**) FKBP-(GGS)-cpHaloΔ + FRB-(GGS)-Hpep1 and (**C**) cpHaloΔ-$(GGS)_9$-FKBP and Hpep3-$(GGS)_3$-FRB. Top: Schemes representing the constructs. Middle: Labeling kinetics and apparent second-order rate constants with the different fluorophore substrates. Fluorescence polarization values were normalized for each fluorophore to its unbound and fully bound fluorescence polarization (Norm. fluor. pol.). Bottom: Apparent second-order rate constants (k_{app}) normalized to the k_{app} with TMR-CA. HaloTag substrates used: CPY-CA, TMR-CA, JF_{669}-CA, JF_{552}-CA and JF_{525}-CA. For all constructs the same substrate preference was observed: CPY-CA > TMR-CA > JF_{669}-CA > JF_{552}-CA > JF_{525}-CA.

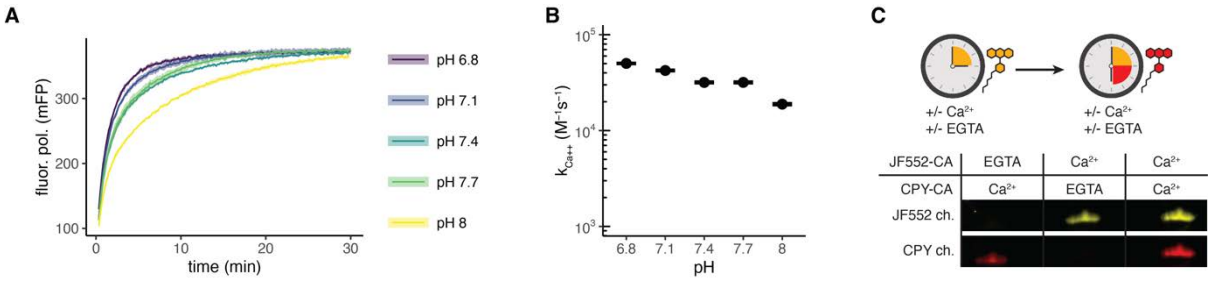

Fig. S10. Additional biochemical characterization of Caprola.

(**A**) Labeling kinetics of Caprola$_9$ variants with TMR-CA at different pH values measured by fluorescence polarization (fluor. pol.). (**B**) A second-order reaction model was fit to the data to determine rate constants (k_{Ca++}). (**C**) Multi-color recording of sequential Ca^{2+} events using Caprola$_9$. The protein was immobilized on an IMAC column and exposed to spectrally differentiable fluorophore substrates (JF$_{552}$-CA or CPY-CA) in presence or absence (EGTA) of Ca^{2+}. After protein elution, the fluorescent mark was revealed by SDS-PAGE followed by fluorescence scanning.

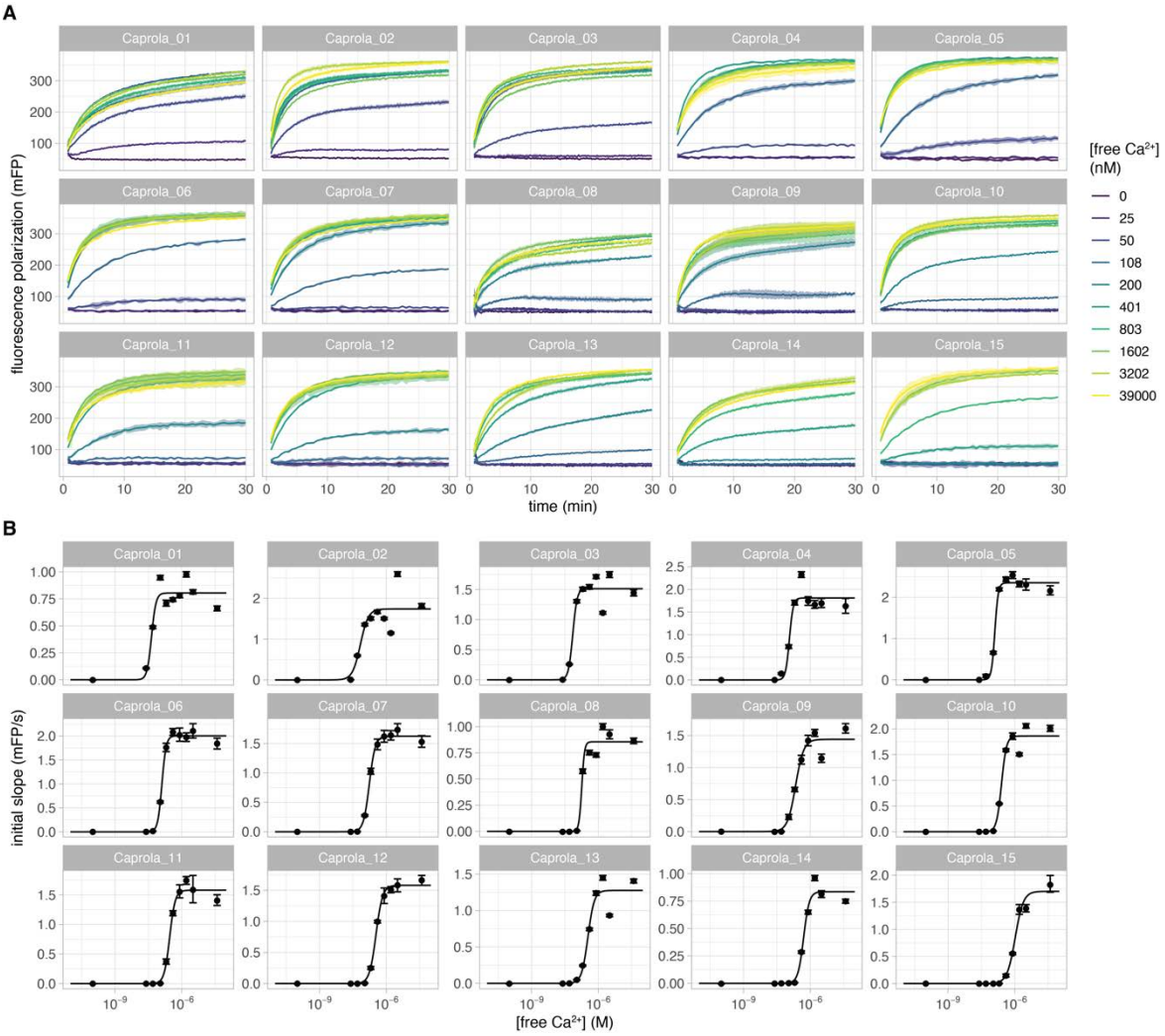

Fig. S11. Calcium sensitivity (EC_{50}) of Caprola variants.

(**A**) Labeling kinetics of Caprola variants with TMR-CA at different concentrations of free Ca^{2+} were followed by fluorescence polarization. A second-order reaction model (or a linear model for reactions not reaching a plateau) was fit to the data and initial reaction rates were determined. (**B**) Initial rates were plotted against free Ca^{2+} concentration and a sigmoidal model was fit to the data to estimate EC_{50} values.

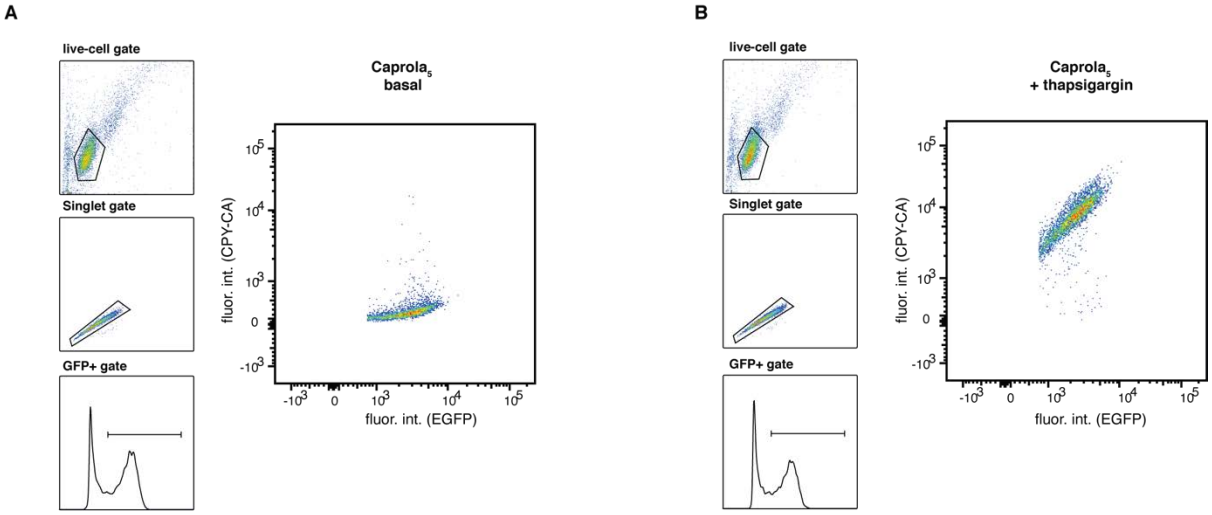

Fig. S12. Exemplary flow cytometry gating strategy for HeLa cells expressing Caprola$_5$-EGFP.

(**A**) Hierarchical gating of live-cells (FSC-A x SSC-A), singlets (SSC-A x SSC-H) and GFP positive cells (GFP*, fluor. Int. of mEGFP > 10^3) of HeLa cells expressing Caprola$_5$-EGFP incubated with 62.5 nM CPY-CA for 60 min without stimulation (basal). (**B**) Hierarchical gating of Caprola$_5$-EGFP-expressing HeLa cells incubated with 62.5 nM CPY-CA for 60 min in the presence of 100 nM thapsigargin.

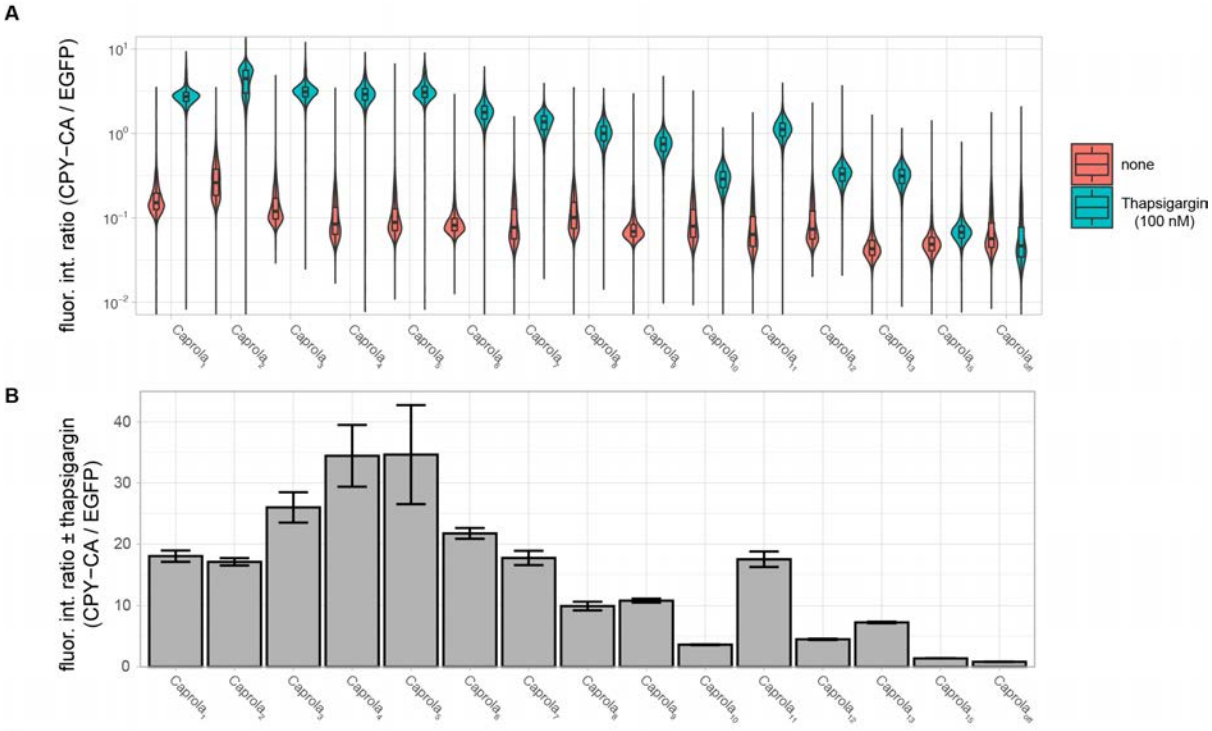

C

Application	Caprola version	Addgene plasmid #
Mammalian cells – low sensitivity	Caprola$_{10}$	194685
Mammalian cells – medium sensitivity	Caprola$_5$	194683
Mammalian cells – high sensitivity	Caprola$_1$	194681
Rat hippocampal neurons - – low sensitivity	Caprola$_6$	194690
Rat hippocampal neurons - – medium sensitivity	Caprola$_5$	194689
Drosophila	Caprola$_6$	TBD
Zebrafish	Caprola$_1$	194696

Fig. S13. Flow cytometry analysis of Caprola variants.

(**A**) Violin plots of fluorescence intensity ratios (fluor. Int. ratio) of HeLa cells expressing different Caprola-EGFP variants. Cells were incubated with 125 nM CPY-CA for 60 min ± 100 nM thapsigargin. (**B**) Fluorescence intensity ratio changes (fluor. int. ratio ± thapsigargin, 100 nM) from (A). Error bars represent propagated SEM. (**C**) Selection guide for Caprola variants.

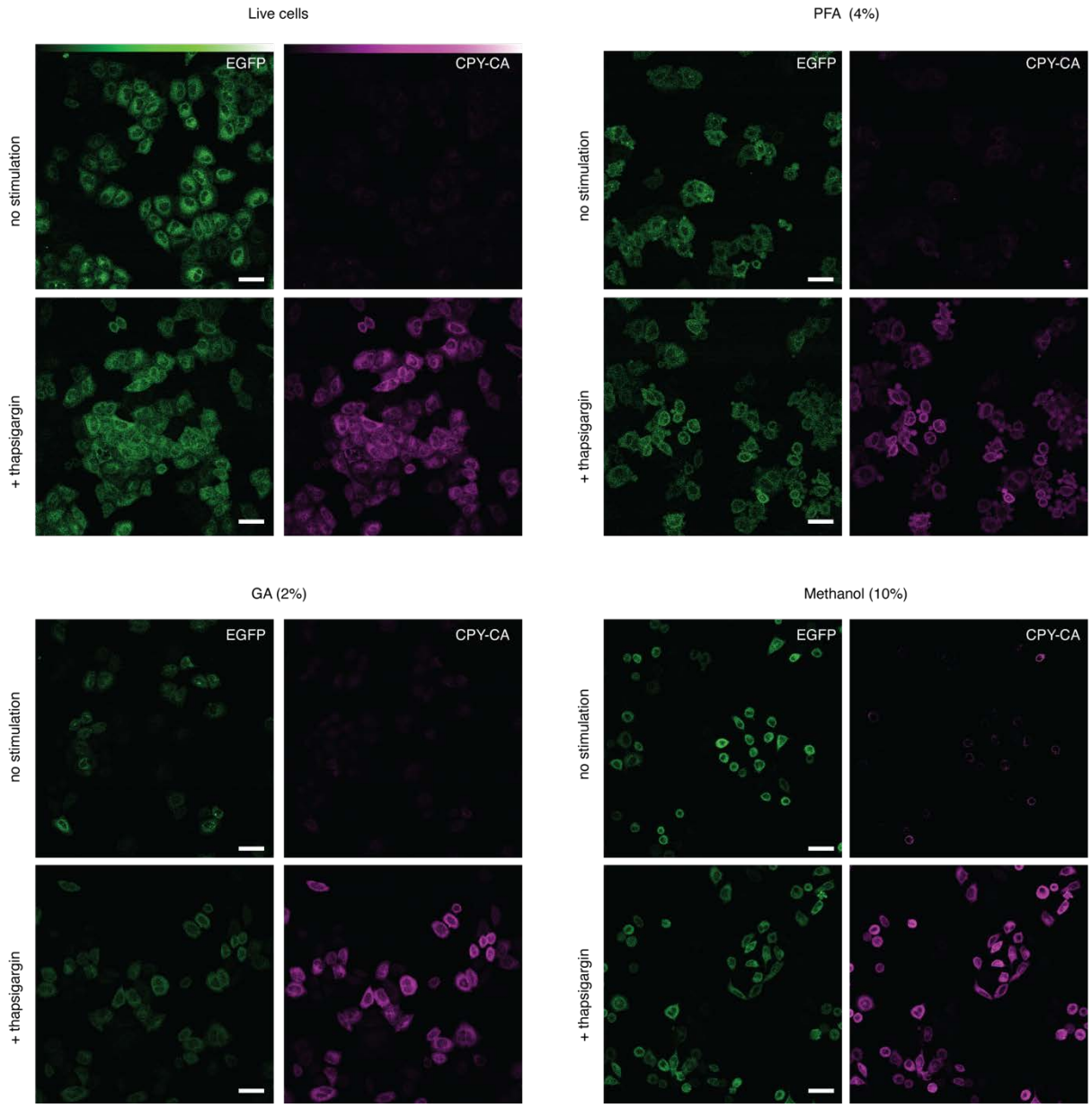

Fig. S14. Resistance of fluorescent Caprola signal to chemical fixation.

Fluorescence micrographs of Caprola$_5$-EGFP-expressing HeLa cells labeled with 125 nM CPY-CA for 60 min ± 100 nM thapsigargin. After labeling, cells were exposed to different chemical fixatives and subsequently imaged. PFA: paraformaldehyde and GA: glyceraldehyde. Scale bars: 50 µm. Best results were obtained with 4% PFA.

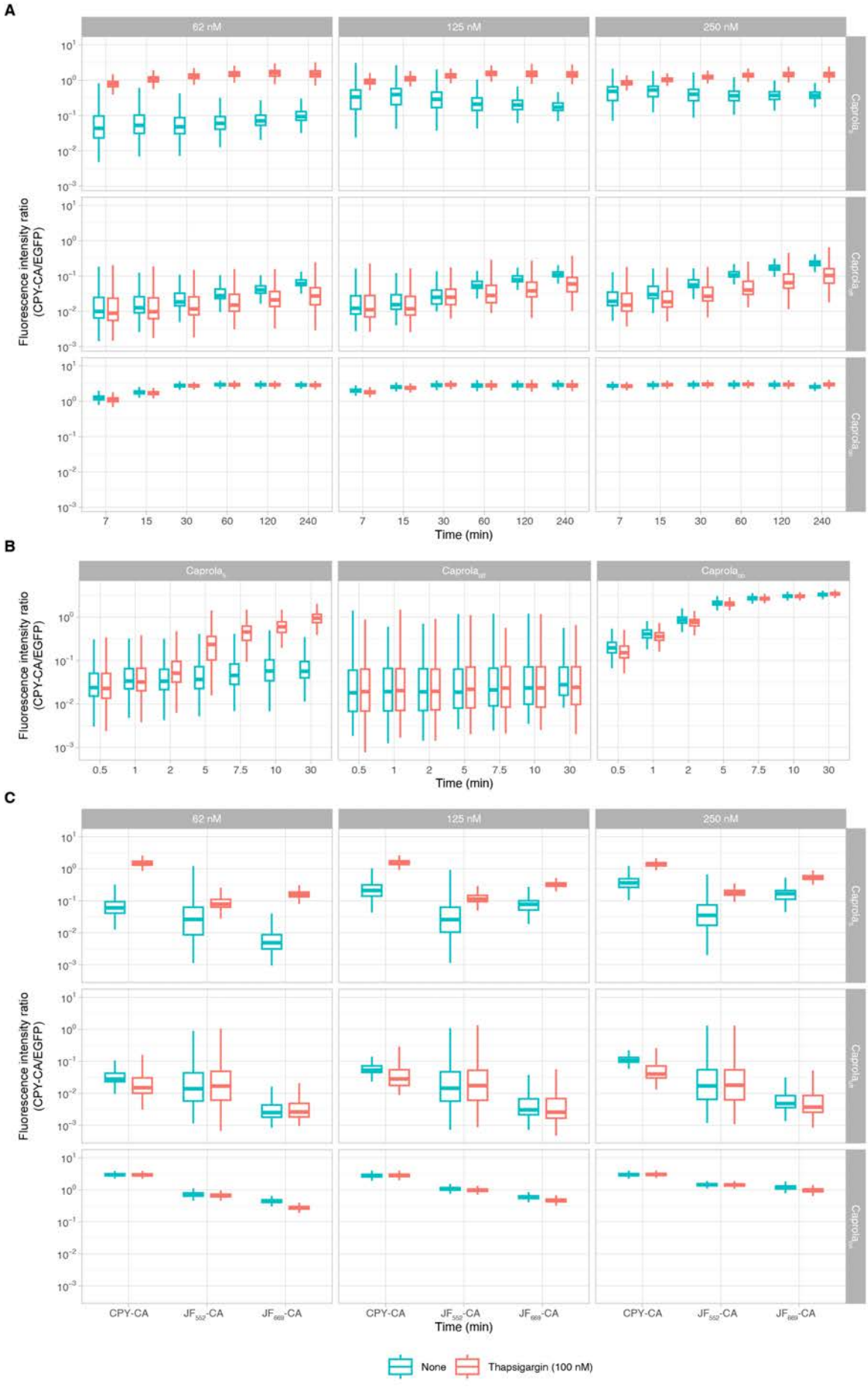
A
62 nM
125 nM
250 nM
Caprola6
Caprola6E
Caprola6S
Fluorescence intensity ratio (CPY-CA/EGFP)
7
15
30
60
120
240
Time (min)
B
Caprola6
Caprola6E
Caprola6S
Fluorescence intensity ratio (CPY-CA/EGFP)
0.5
1
2
5
7.5
10
30
Time (min)
C
62 nM
125 nM
250 nM
Caprola6
Caprola6E
Caprola6S
Fluorescence intensity ratio (CPY-CA/EGFP)
CPY-CA
JF552-CA
JF669-CA
Time (min)
None
Thapsigargin (100 nM)

Fig. S15. Time- and substrate-dependency of Caprola$_5$ labeling in HeLa cells.
(**A**) Flow cytometry analysis of Caprola labeling ± 100 nM thapsigargin over time at different CPY-CA concentrations. Fluorescence intensity ratios of Caprola$_5$-EGFP-, Caprola$_{on}$-EGFP- or Caprola$_{off}$-EGFP-expressing HeLa cells labeled with CPY-CA ± 100 nM thapsigargin are shown. Maximum differences are observed at low (62.5 nM) fluorophore substrate concentration. (**B**) Flow cytometry analysis of conditional Caprola labeling on short time scales. Fluorescence intensity ratios of Caprola$_5$-EGFP-, Caprola$_{on}$-EGFP- or Caprola$_{off}$-EGFP-expressing HeLa cells incubated with 62.5 nM CPY-CA ± 100 nM thapsigargin are shown. Differences are observed after 5 min. (**C**) Flow cytometry analysis of conditional Caprola labeling with different fluorophore substrates. Fluorescence intensity ratios of Caprola$_5$-EGFP-, Caprola$_{on}$-EGFP- or Caprola$_{off}$-EGFP-expressing HeLa cells with different concentrations of JF$_{552}$-CA, CPY-CA or JF$_{669}$-CA over 60 min ± 100 nM thapsigargin are shown. Largest differences were observed with CPY-CA > JF$_{669}$-CA > JF$_{552}$-CA.

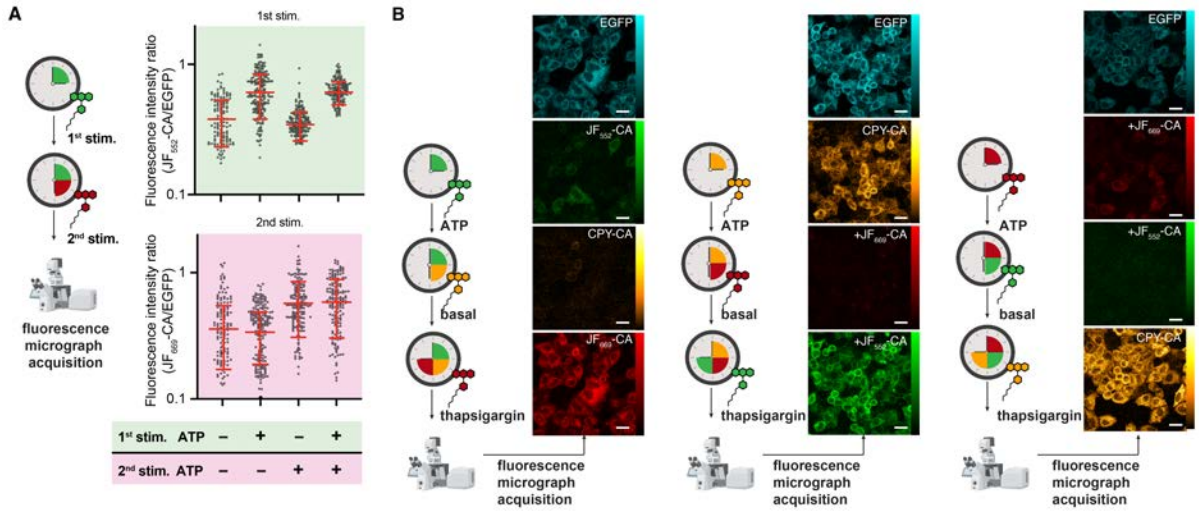

Fig. S16. Recordings of successive periods of Ca^{2+}-activity in HeLa cells with Caprola.
(**A**) Dot plots of successive recordings of Ca^{2+} levels in $Caprola_5$-EGFP-expressing HeLa cells. Cells were treated ± 100 µM ATP in the presence of fluorophore substrates in two consecutive stimulation periods and labeling was detected after the two incubation periods by fluorescence microscopy. First stimulation: JF_{552}-CA for 60 min (green, top); second stimulation: JF_{669}-CA for 60 min (red, bottom). Lines indicate means ± standard deviations (N > 100). The quantitative evaluation shows that the labeling ratio observed in the second stimulation period is independent of the extent of labeling that happened during the first stimulation period. In conclusion, ATP stimulation in the first period does not lead to a saturation of Caprola labeling that would hamper the next recording step. (**B**) Fluorescence micrographs of successive recordings of Ca^{2+} levels in $Caprola_5$-EGFP-expressing HeLa cells. First stimulation: ATP (100 µM); second stimulation: no treatment; third stimulation: thapsigargin (100 nM), in presence of JF_{669}-CA or JF_{552}-CA or CPY-CA. The extent of labeling is proportional to the strength of the stimulation independent of the fluorescent substrate. Stimulation strength: basal < ATP < thapsigargin. Fluorescence micrographs were all acquired after the third incubation period. Scale bars: 50 µm.

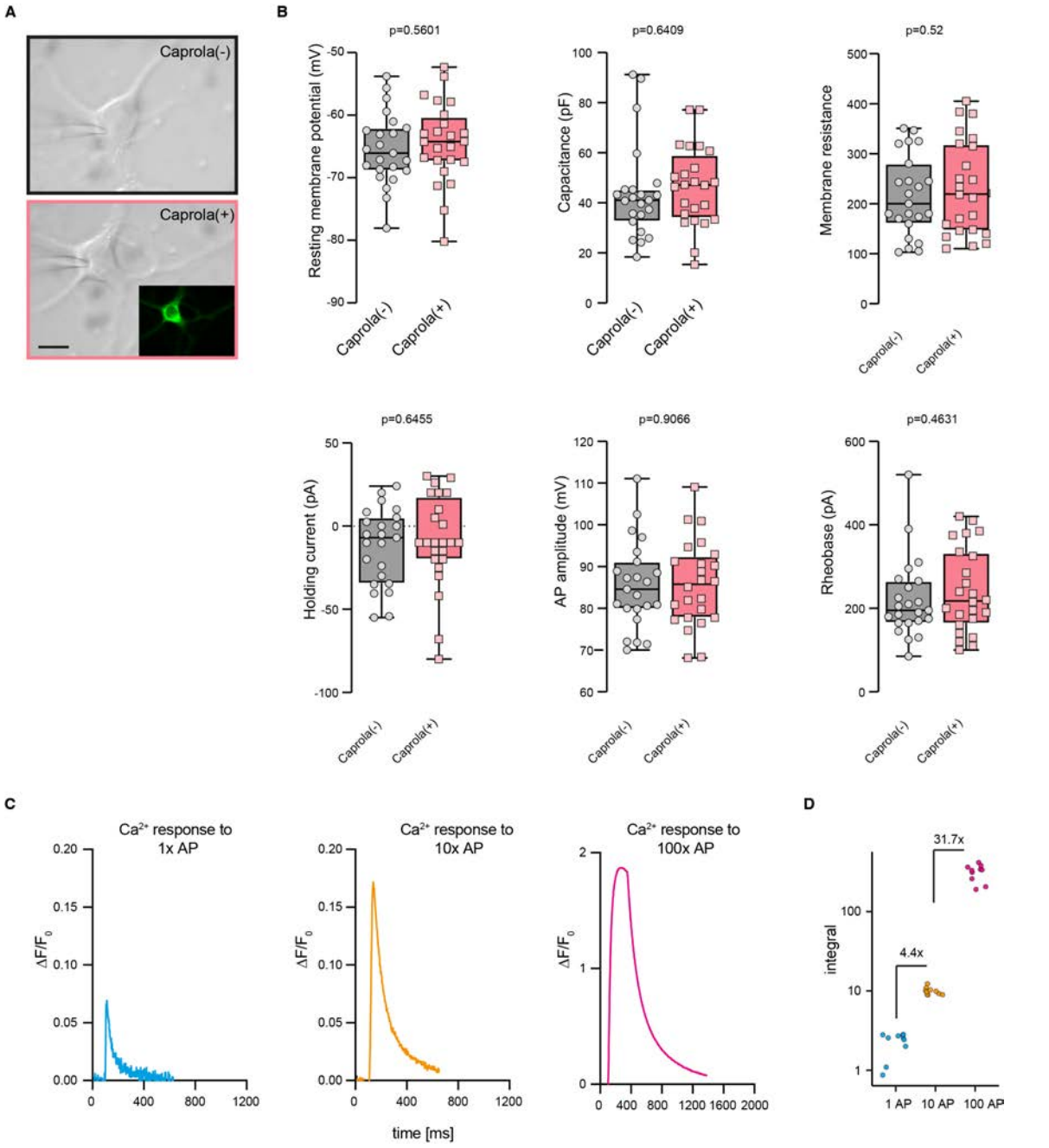

Fig. S17. Neuron physiology and electrical excitability.

(**A**) Micrographs of patched cultured neurons with or without AAV-mediated Caprola$_6$-EGFP expression. (**B**) Neuronal electrophysiology comparison between transduced (Caprola(+)) and non-transduced (Caprola(-)) neurons. No significant differences were observed in the 6 different parameters assessed. (**C**) Representative traces of Ca^{2+} responses of GCaMP6s-expressing cultured neurons to action potentials evoked by electrical field stimulation (80 Hz, 100 mA, 1 ms pulse-width). Trains of 1, 10 and 100 consecutive action potentials (AP) were applied. (**D**) Dot plot showing the integrals (*i.e.* area under the curve) for 10 individual Ca^{2+} responses per condition measured as described in (C). The GCaMP6s-measured calcium response of neurons is not proportional between trains of 1, 10 and 100 consecutive APs.

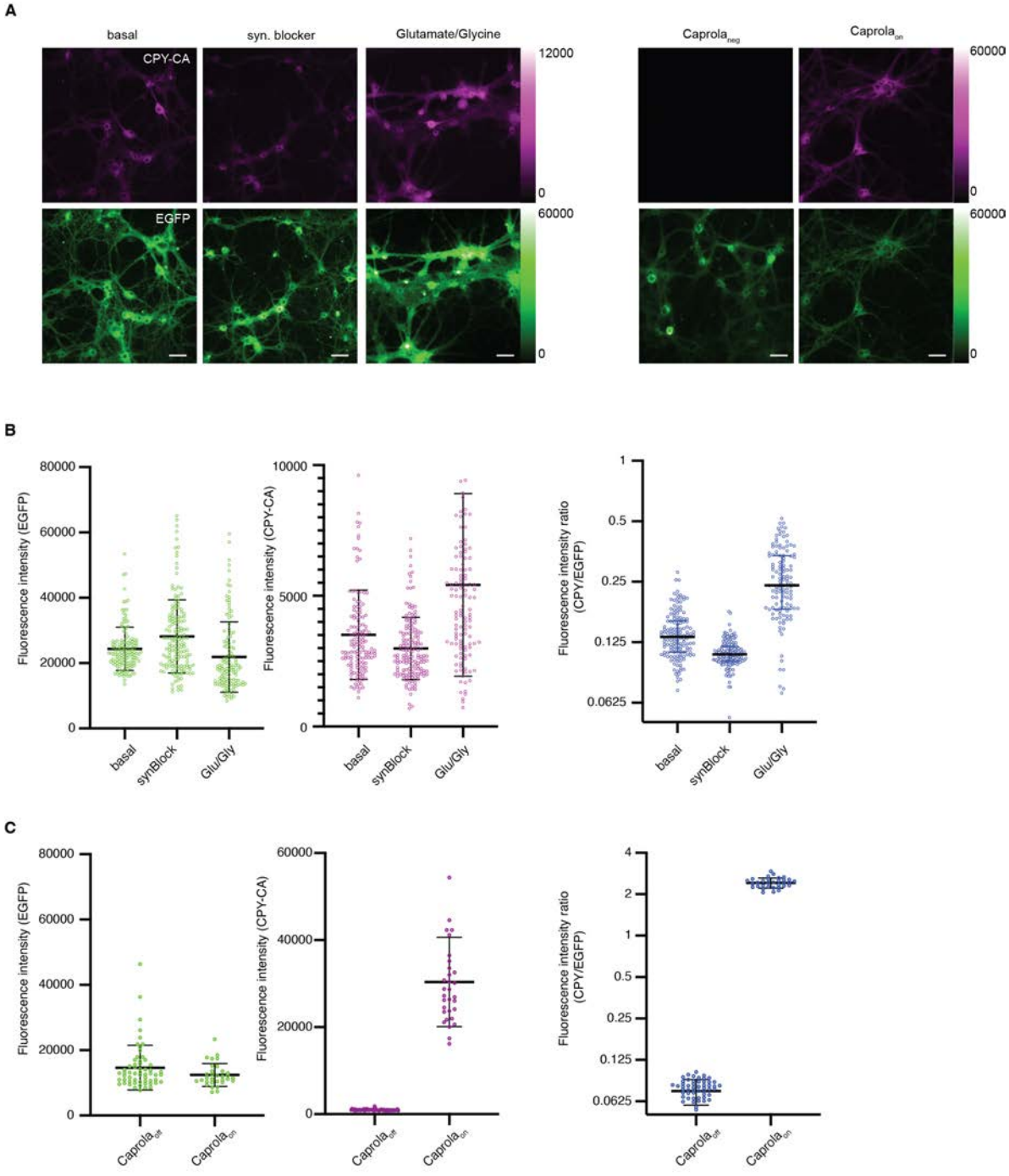

Fig. S18. Recordings of drug-induced Ca^{2+} signals in primary hippocampal neurons with Caprola.

(**A**) Fluorescence micrographs of Caprola$_4$-EGFP-expressing primary hippocampal neurons (14 div). Labeling was performed with 250 nM CPY-CA for 30 min in basal condition or in the presence of either synaptic blockers (APV, 25 µM / NBQX, 10 µM) or glutamate/glycine (10 µM/2.5 µM). (**B, C**) Quantification of fluorescence intensities (mEGFP and CPY-CA) and fluorescence intensity ratios from experiments described in (A). Lines indicate means ± standard deviations (N > 50). Scale bars: 50 µm.

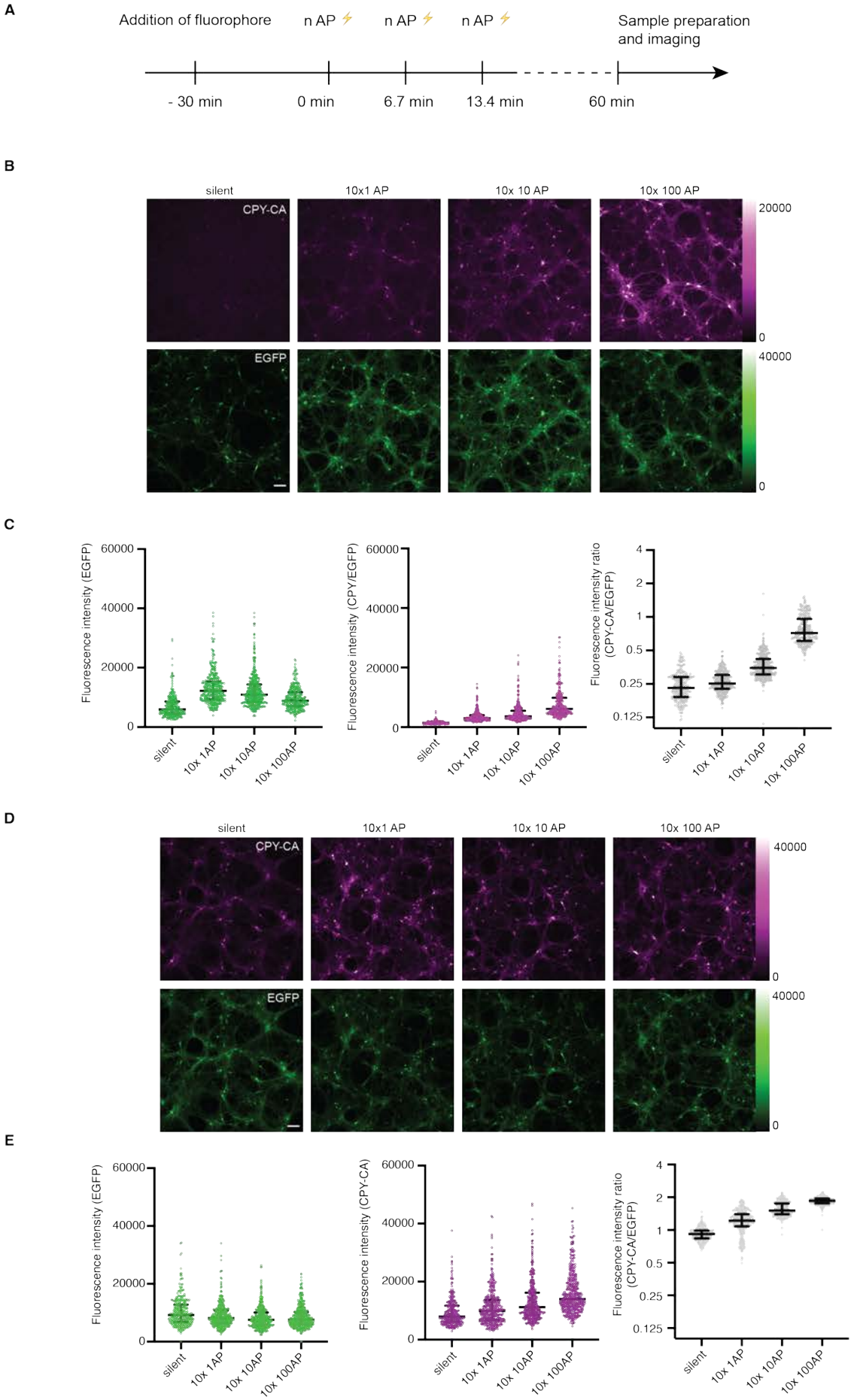
A
Addition of fluorophore
n AP
n AP
n AP
Sample preparation and imaging
- 30 min
0 min
6.7 min
13.4 min
60 min
B
silent
10x1 AP
10x 10 AP
10x 100 AP
CPY-CA
EGFP
20000
0
40000
0
C
Fluorescence intensity (EGFP)
Fluorescence intensity (CPY/EGFP)
Fluorescence intensity ratio (CPY-CA/EGFP)
60000
40000
20000
0
4
2
1
0.5
0.25
0.125
silent
10x 1AP
10x 10AP
10x 100AP
D
silent
10x1 AP
10x 10 AP
10x 100 AP
CPY-CA
EGFP
40000
0
40000
0
E
Fluorescence intensity (EGFP)
Fluorescence intensity (CPY-CA)
Fluorescence intensity ratio (CPY-CA/EGFP)
60000
40000
20000
0
4
2
1
0.5
0.25
0.125
silent
10x 1AP
10x 10AP
10x 100AP

Fig. S19. Electrical field stimulation of primary hippocampal neurons expressing Caprola.

(**A**) Timeline of the conducted stimulations. Neurons were pre-incubated with the fluorophore substrate in presence of synaptic blockers (APV, 25 µM / NBQX, 10 µM) for 30 min prior to stimulations. Stimulations consisted of trains of 1, 10 or 100 action potentials (APs) delivered at 80 Hz every 6 min over 60 min. 10 stimulations were delivered in the course of 60 min. (**B**) Fluorescence micrographs of $Caprola_6$-EGFP-expressing primary hippocampal neurons (14 div) labeled with 100 nM CPY-CA under previously described electrical field stimulations. (**C**) Quantification of fluorescence intensities (mEGFP and CPY-CA) and fluorescence intensity ratios from the experiment described in (B). Lines indicate means ± standard deviations (N > 100). Differences between non-stimulated and 10x10 or 10x100 APs stimulated neurons can be observed. However, 10x1 AP stimulation did not result in a detectable difference. (**D**) Fluorescence micrographs of $Caprola_6$-EGFP-expressing primary hippocampal neurons (14 div) labeled with 1000 nM CPY-CA in previously described conditions. (**E)** Quantification of fluorescence intensities (mEGFP and CPY-CA) and fluorescence intensity ratios from the experiment described in (D). Due to the increased fluorophore substrate concentration of 1000 nM, differences between non-stimulated and 10x1 AP stimulated neurons were observed. In conclusion, adjusting the fluorophore substrate concentration allows to tune the sensitivity of Caprola. Scale bars: 50 µm. Data is partially represented in Fig. 4G and H.

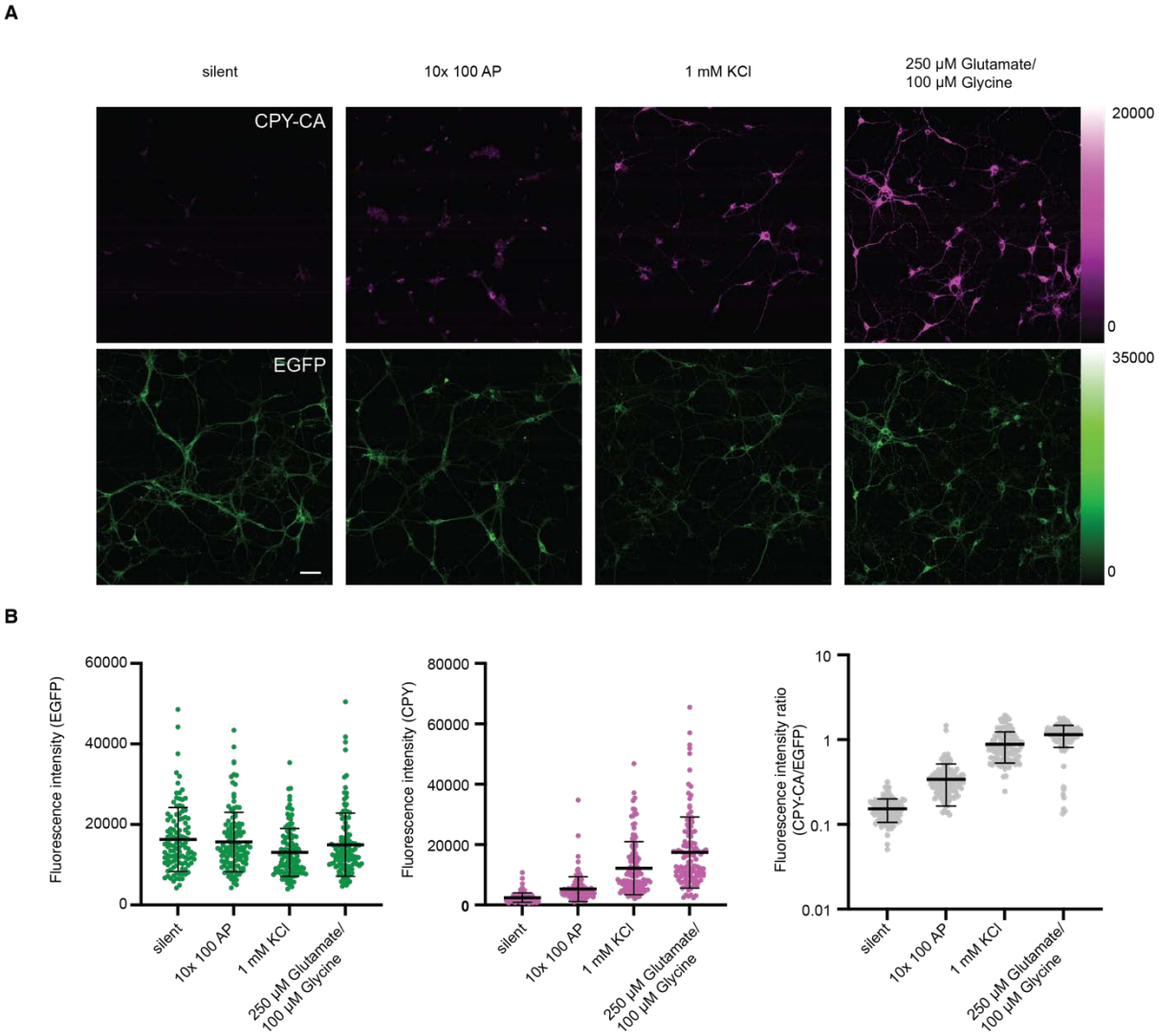

Fig. S20. Short-time recording of stimulations in primary hippocampal neurons with Caprola.

(**A**) Fluorescence micrographs of Caprola$_6$-EGFP-expressing primary hippocampal neurons (14 div) labeled for 5 min with 100 nM CPY-CA under different stimulations: synaptic blockers (silent, APV, 25 µM / NBQX, 10 µM), electric field stimulation with 10 trains of 100 action potentials (APs), KCl (1 mM) or glutamate/glycine (250 µM/100 µM). (**B**) Dot plots of fluorescence intensities (mEGFP and CPY-CA) and fluorescence intensity ratios from experiments described in (A). Lines indicate means ± standard deviations (N > 100). Scale bars: 50 µm. Stimulated neurons show a clear signal increase compared to non-stimulated neurons already after 5 min of recording.

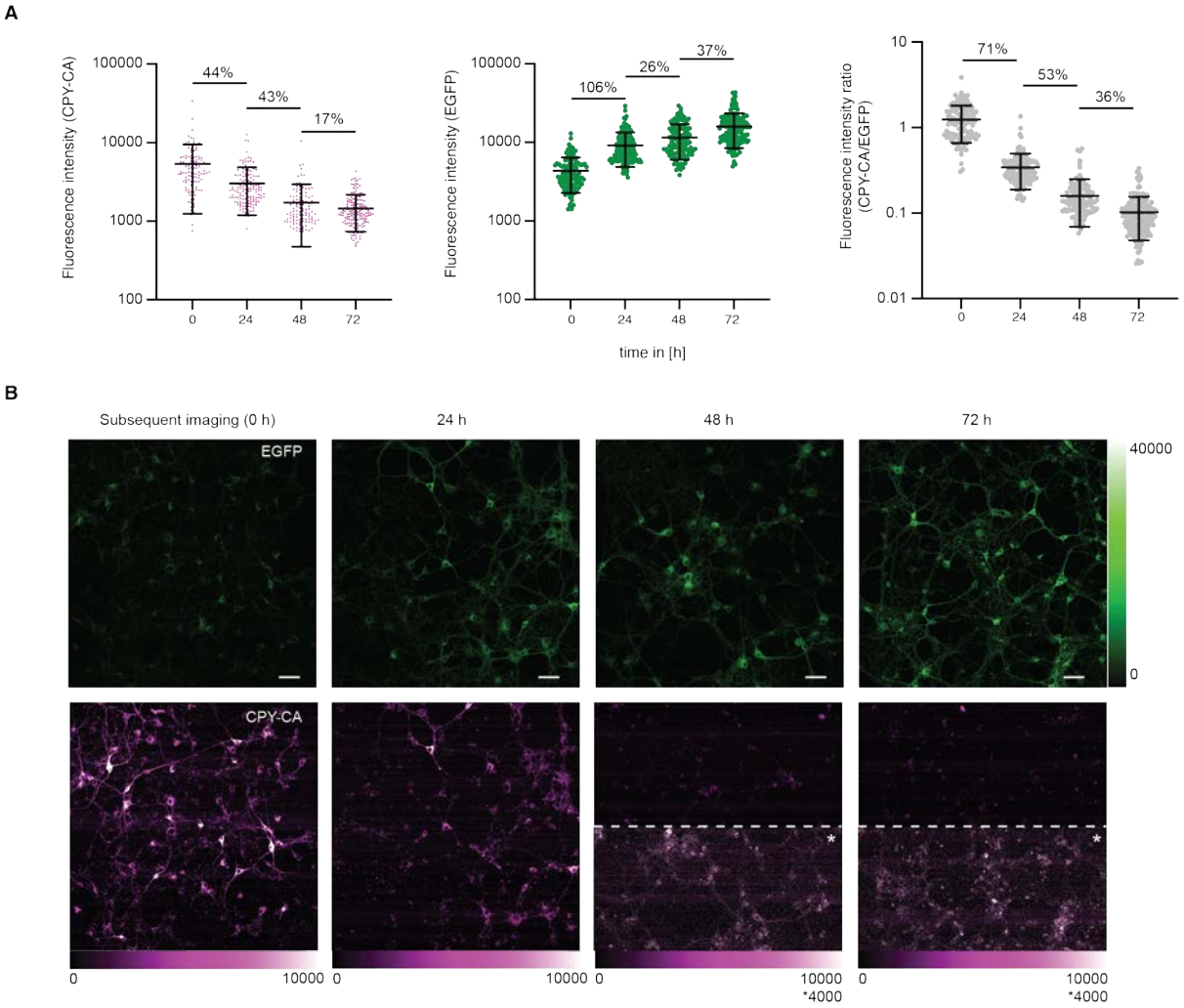

Fig. S21. Stability of fluorescent Caprola signal in primary hippocampal neurons over time.

(**A**) Dot plots of the fluorescence intensities (mEGFP and CPY-CA) and fluorescence intensity ratios of Caprola$_4$-EGFP-expressing primary hippocampal neurons (14 div). Neurons were labeled with 250 nM CPY-CA for 60 min without external stimulation. Images were acquired right after labeling and every 24 h over 3 days. Lines indicate means ± standard deviations (N > 50). (**B**) Representative fluorescence micrographs of the experiment described in (A). Contrast of images after 48 and 72 hours was adjusted (CPY channel, bottom half) to highlight that Caprola labeling can still be reliably detected after prolonged time. Scale bars: 50 µm. The decrease of fluorescence intensity ratios is due to degradation of labeled Caprola and re-synthesis of Caprola-EGFP protein. The latter manifests itself by an increase of EGFP intensities.

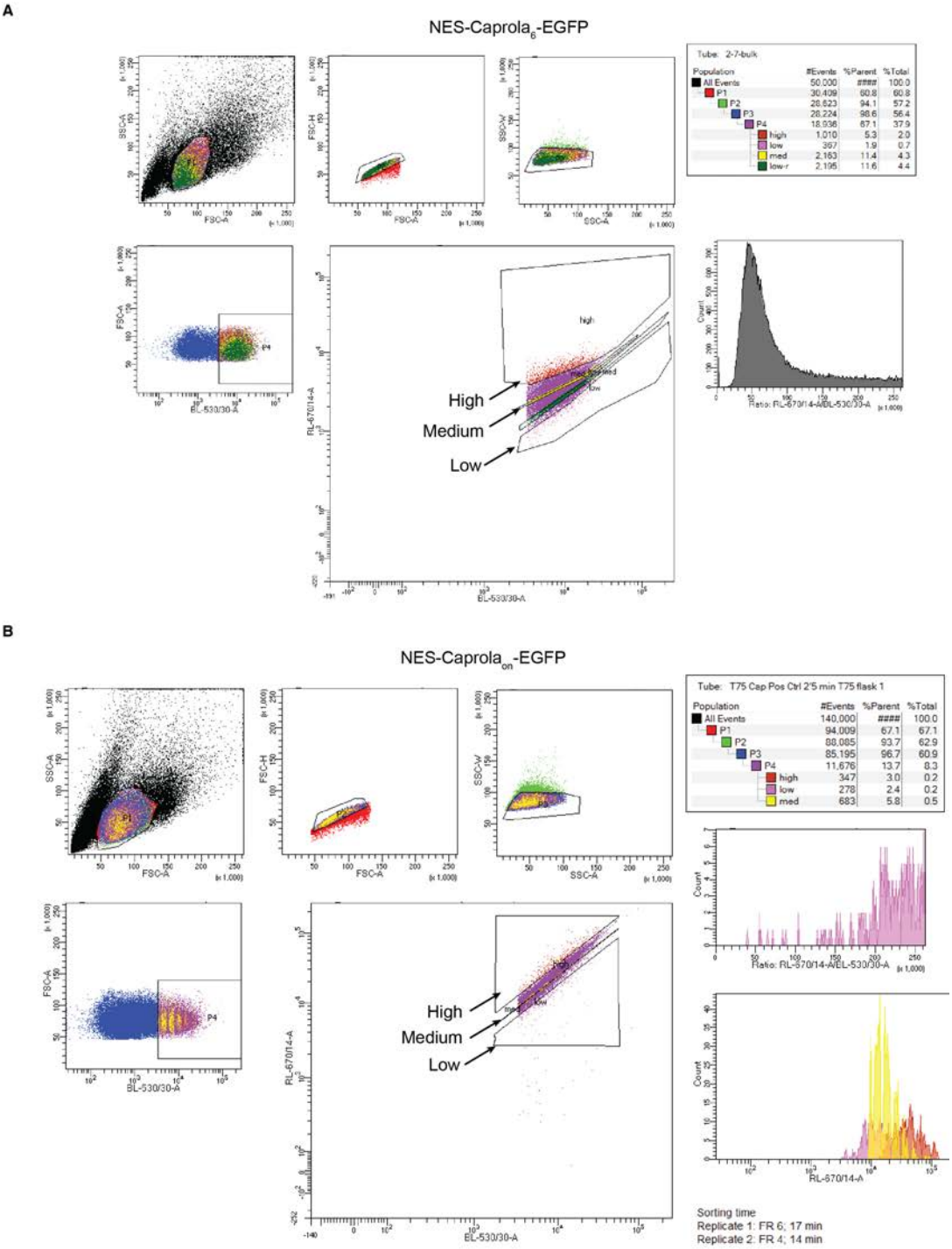

Fig. S22. Gating strategies of Caprola-EGFP-expressing glioblastoma cells.

(**A**) Gating and sorting strategies of Caprola$_6$-EGFP-expressing glioblastoma cells that were submitted to RNA-Seq. Data is also partially shown in Fig. 4I. (**B**) Gating and sorting strategies of Caprola$_{on}$-expressing glioblastoma cells that were submitted to RNA-Seq.

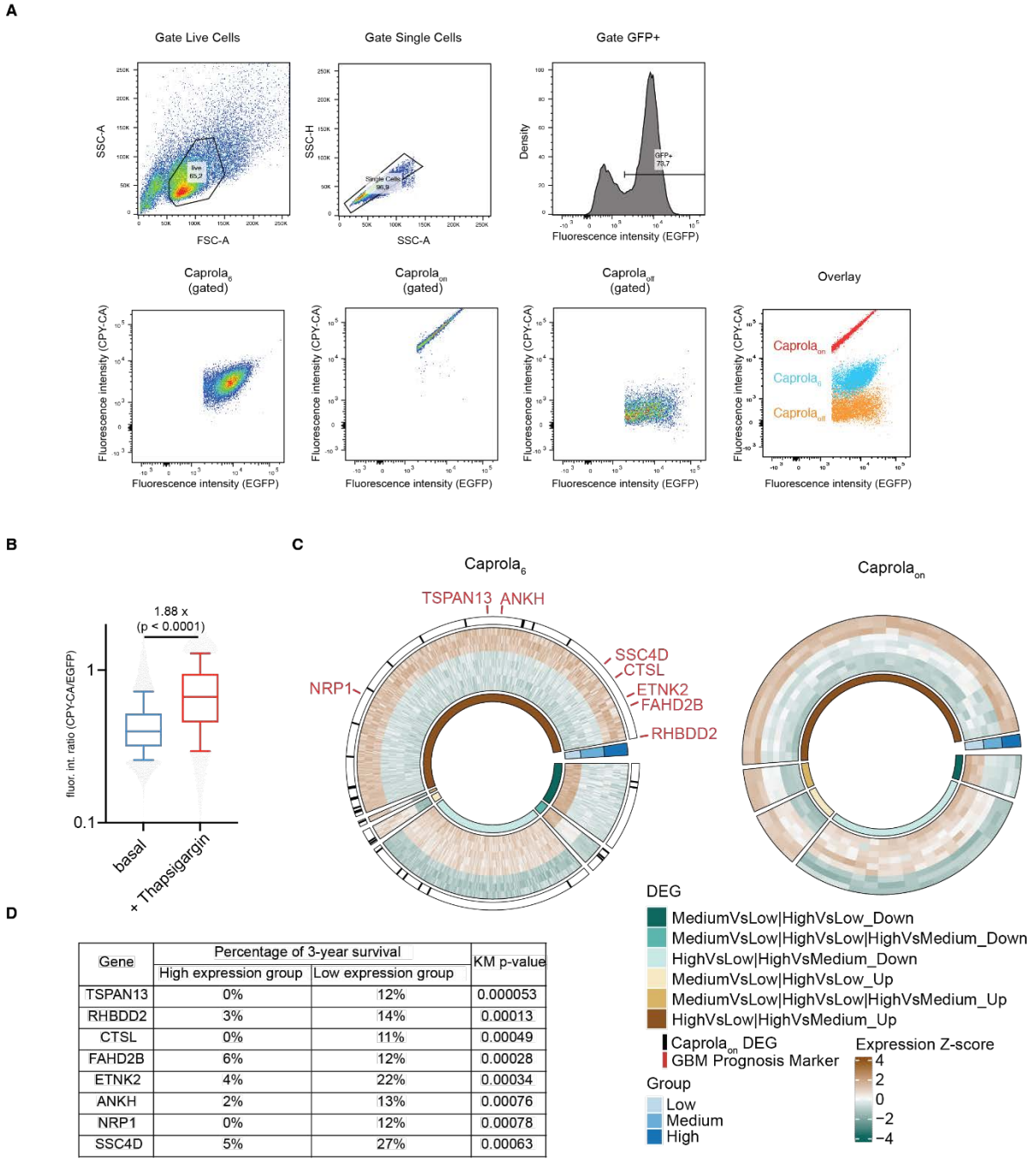

D

Gene	Percentage of 3-year survival		KM p-value
	High expression group	Low expression group	
TSPAN13	0%	12%	0.000053
RHBDD2	3%	14%	0.00013
CTSL	0%	11%	0.00049
FAHD2B	6%	12%	0.00028
ETNK2	4%	22%	0.00034
ANKH	2%	13%	0.00076
NRP1	0%	12%	0.00078
SSC4D	5%	27%	0.00063

Fig. S23. Transcriptomic analysis of glioblastoma cells.

(**A**) Gating strategy and flow cytometry profiles of labeled Caprola$_6$-EGFP-, Caprola$_{on}$-EGFP- and Caprola$_{off}$-EGFP-expressing glioblastoma cells. Cells were labeled with 125 nM CPY-CA for 90 min without external stimulation. Caprola$_6$-EGFP-expressing cells show an intermediate CPY intensity between the negative (Caprola$_{off}$) and positive controls (Caprola$_{on}$). (**B**) Box plot comparing fluorescence intensity ratios (CPY-CA/EGFP) of Caprola$_6$-EGFP-expressing glioblastoma cells in presence or absence of 100 nM thapsigargin. Thapsigargin treatment leads to an increase in intracellular Ca^{2+} levels through ER store release and hence fluorescence intensity ratio. This highlights the capacity of Caprola to record Ca^{2+} signals in different glioblastoma cell populations. (**C**) Circular heatmaps of differentially expressed genes (DEGs) from RNA-Seq data analysis of sorted Caprola$_6$-EGFP-expressing glioblastoma cells. Cell populations were sorted in three groups as depicted

in fig. S22. Left: Caprola$_6$, right: Caprola$_{on}$. The Caprola$_{on}$ experiment was conducted to identify genes involved in the modulation of the fluorophore substrate uptake. These genes would be false positive hits in the Caprola$_6$ experiment. Such overlapping DEGs identified in both experiments (31 in total) are highlighted on the outer ring of the circular heatmap of the Caprola$_6$ experiment with black stripes. Additionally, known prognosis markers of glioblastoma are highlighted and named (red) on the Caprola$_6$ heatmap. Data from the Caprola$_6$ experiment is partially represented in Fig. 4J. (**D**) 3-year survival of patients in respect to expression of glioblastoma prognosis markers identified in the Caprola$_6$ experiment depicted in (C).

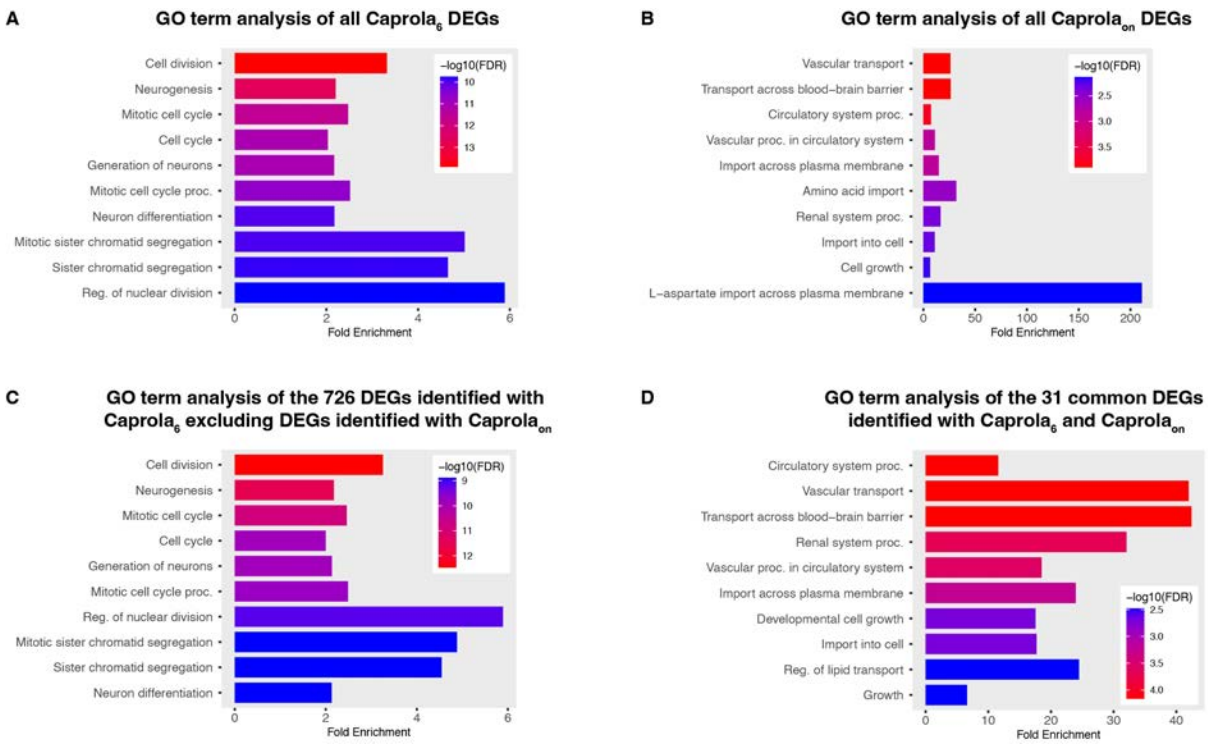

Fig. S24. Gene ontology (GO) term analysis of Caprola-identified DEGs

(**A**) GO term analysis of all Caprola$_6$-identified DEGs. (**B**) GO term analysis of all Caprola$_{on}$-identified DEGs. (**C**) GO term analysis of the exclusively Caprola$_6$-identified 726 DEGs. (**D**) GO term analysis of the 31 overlapping DEGs identified with Caprola$_6$ and Caprola$_{on}$. The GO terms enriched in overlapping Caprola$_{on}$ and Caprola$_6$ DEGs are mostly related to solute transporters and have a high overlap with the GO terms that were most enriched in the total Caprola$_{on}$ DEGs. In contrast, the Caprola$_6$- and exclusively Caprola$_6$-identified DEGs are enriched in GO terms related to neuronal and tumor growth associated processes that comprise Ca^{2+} dependent pathways. A list of all DEGs in each group are provided as source data.

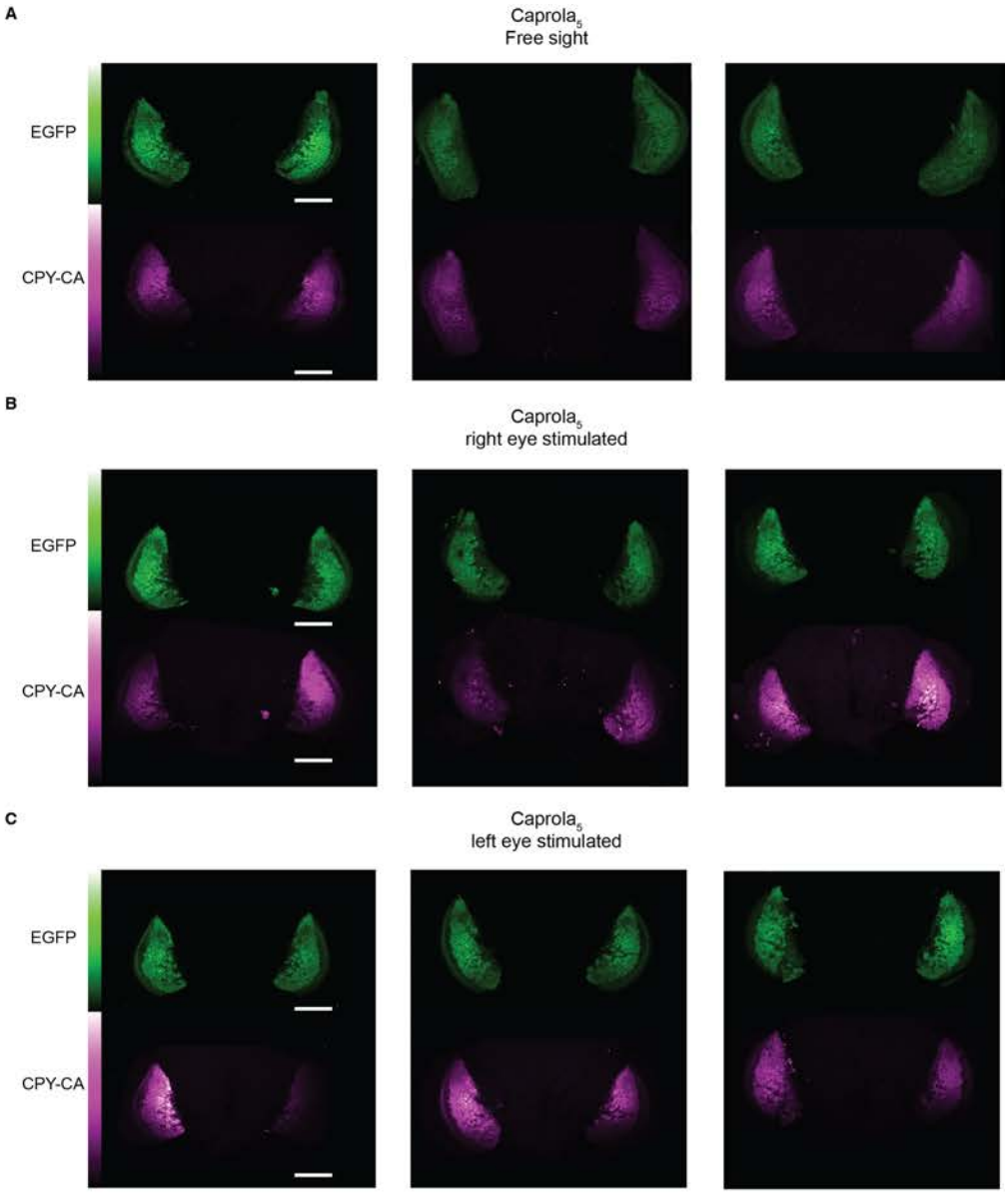

Fig. S25. Caprola labeling in adult flies.

Representative fluorescence micrographs (maximum intensity projections (MIPs) of whole brain volumes) of Caprola$_5$-EGFP-expressing adult flies incubated with 5 µM CPY-CA for 20 min while being visually stimulated on (**A**) both eyes, (**B**) the right eye or (**C**) the left eye. Scale bars: 100 µm. The observation of inter-individual variabilities in the experiment could arise from a combination of technical and biological factors. These may include variances in overall protein expression, small differences in the dissection of the fly cuticle and resulting dye delivery, as well as potential biological factors. The latter could include small visual responses in the non-stimulated (but non-blinded) eye, as well as intrinsic calcium activity that depends on the behavioral state of the animal. All fluorescence micrographs are enclosed in Data S1.

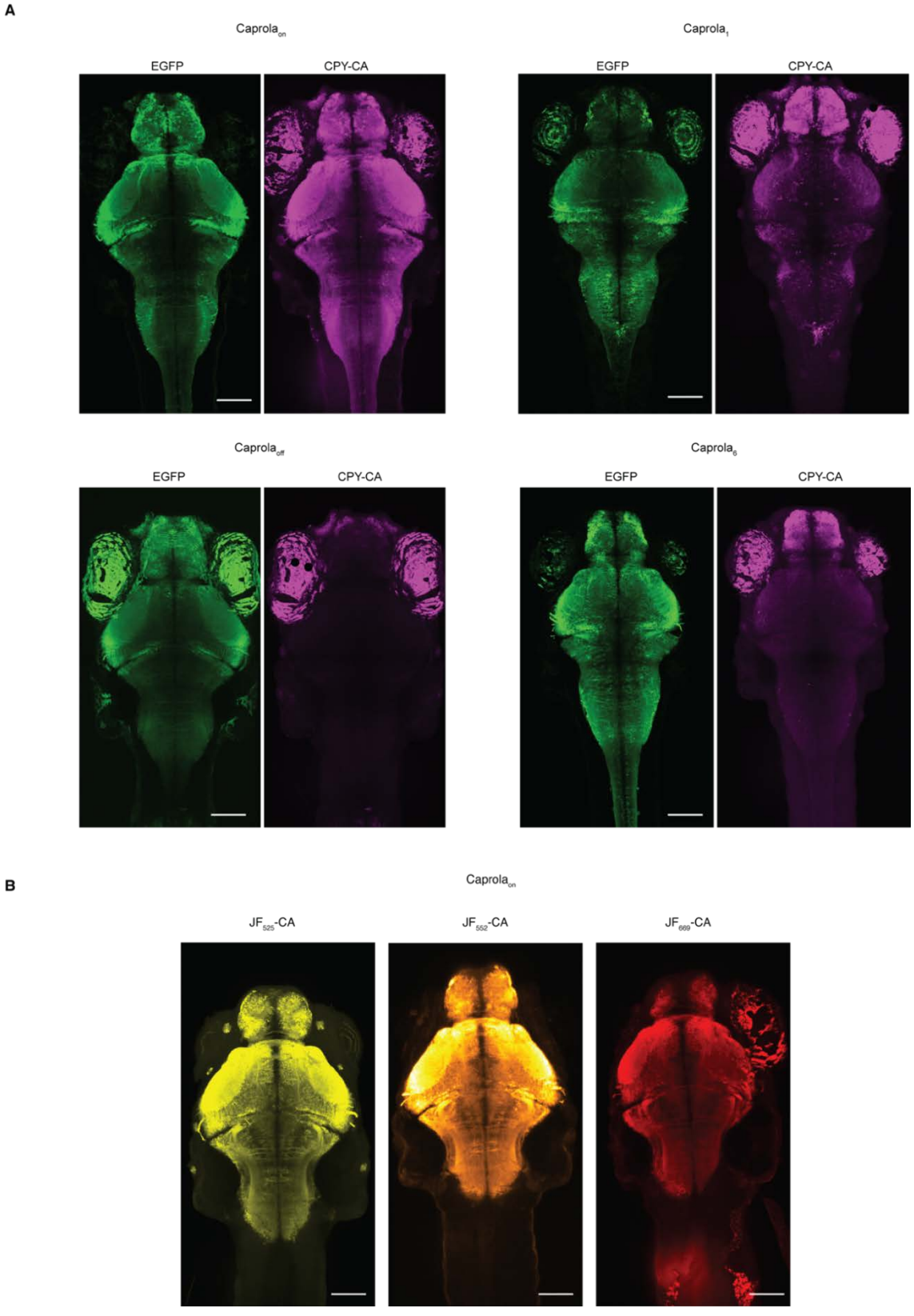

Fig. S26. Caprola labeling in zebrafish larvae.

(**A**) Fluorescence micrographs (maximum intensity projections (MIPs) of 50 µm brain volumes) of different Caprola-EGFP-expressing zebrafish larvae incubated with 5 µM CPY-CA for 6 h. (**B**) Fluorescence micrographs (MIPs of 50 µm brain volume) of different Caprola$_{on}$-EGFP-expressing zebrafish larvae incubated with 5 µM JF$_{525}$-CA, JF$_{552}$-CA and

JF_{669}-CA for 3 h. The fluorescence signal measured from the eyes of zebrafish are a product of melanin pigmentation as well as iridophores and probably a non-specific sticking of fluorophore substrate. Scale bars: 100 µm.

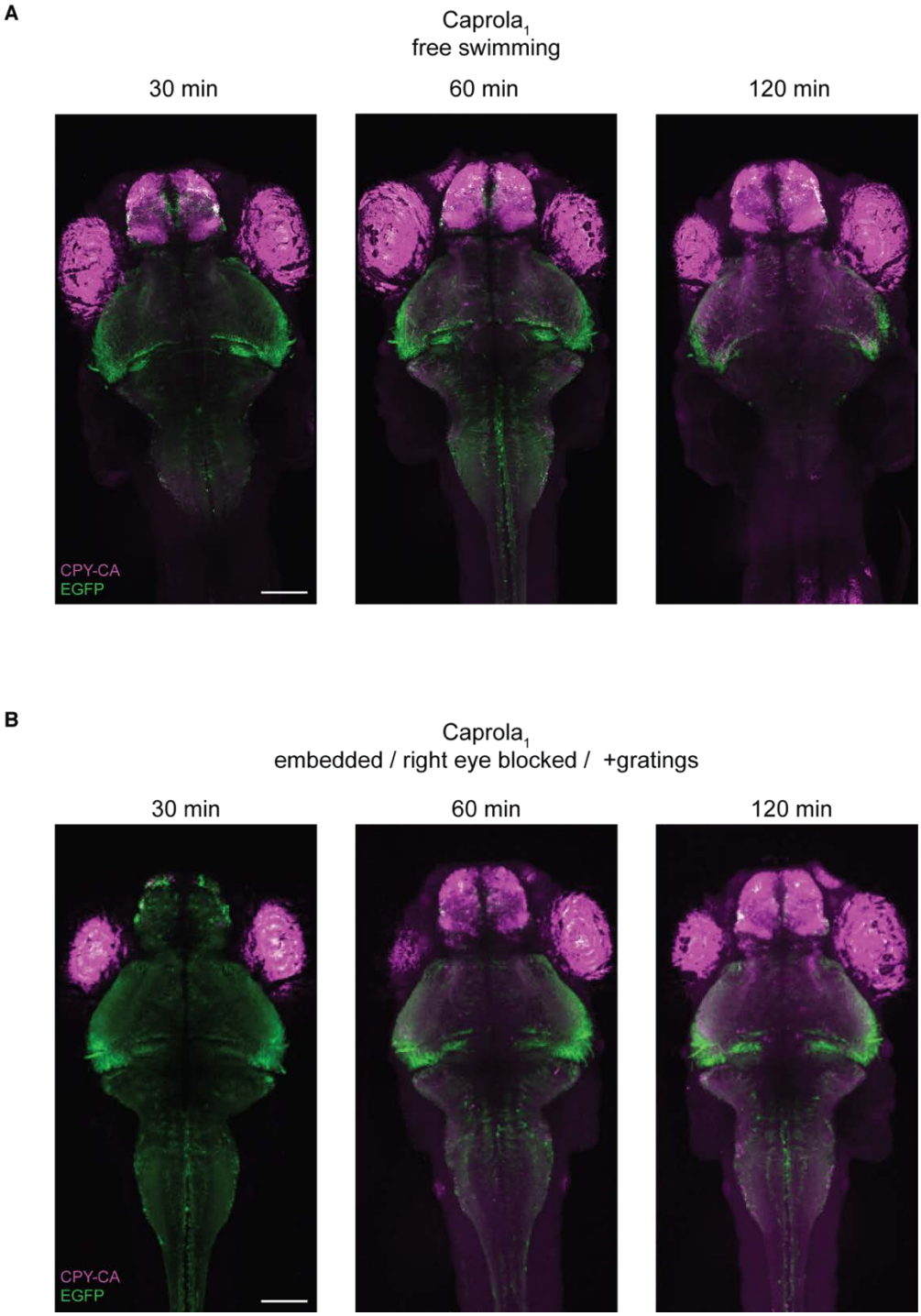

Fig. S27. Time-dependency of Caprola labeling in zebrafish larvae.

(**A, B**) Fluorescence micrographs (MIPs of 50 µm brain volume) of Caprola$_1$-EGFP-expressing zebrafish larvae incubated with 5 µM CPY-CA for 30 min, 60 min or 120 min. Cohorts of zebrafish larvae were either left free swimming (A) or immobilized (B) in ambient conditions. Scale bars: 100 µm. Labeling could be observed in the forebrain after 30 min for freely swimming larvae, signal starts to appear in deeper brain regions after 1 hour and becomes more distinct after 2 hours incubation of the larvae, independent of embedding.

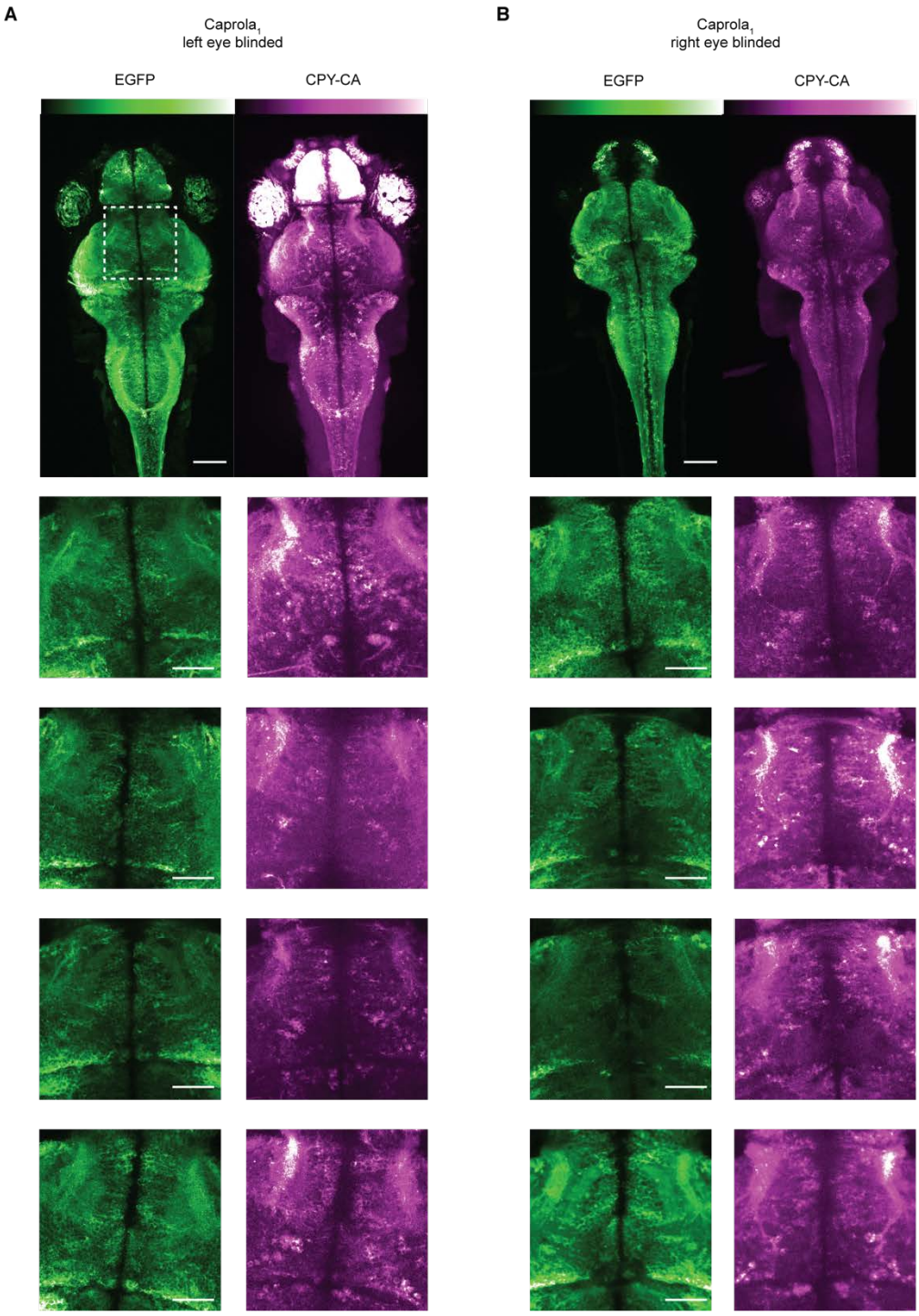

Fig. S28. Recording of neuronal activity in visually stimulated zebrafish larvae with Caprola.

(**A, B**) Representative fluorescence micrographs (MIPs of 50 µm brain volume) of Caprola$_1$-EGFP-expressing zebrafish larvae incubated with 5 µM CPY-CA for 6 h with focus on pretectal areas. Cohorts of zebrafish larvae were immobilized and either had their left (A) or right eye (B) blocked while being visually stimulated. Scale bars: 100 µm (whole brain); 50 µm (zooms). All fluorescence micrographs are enclosed in Data S1.

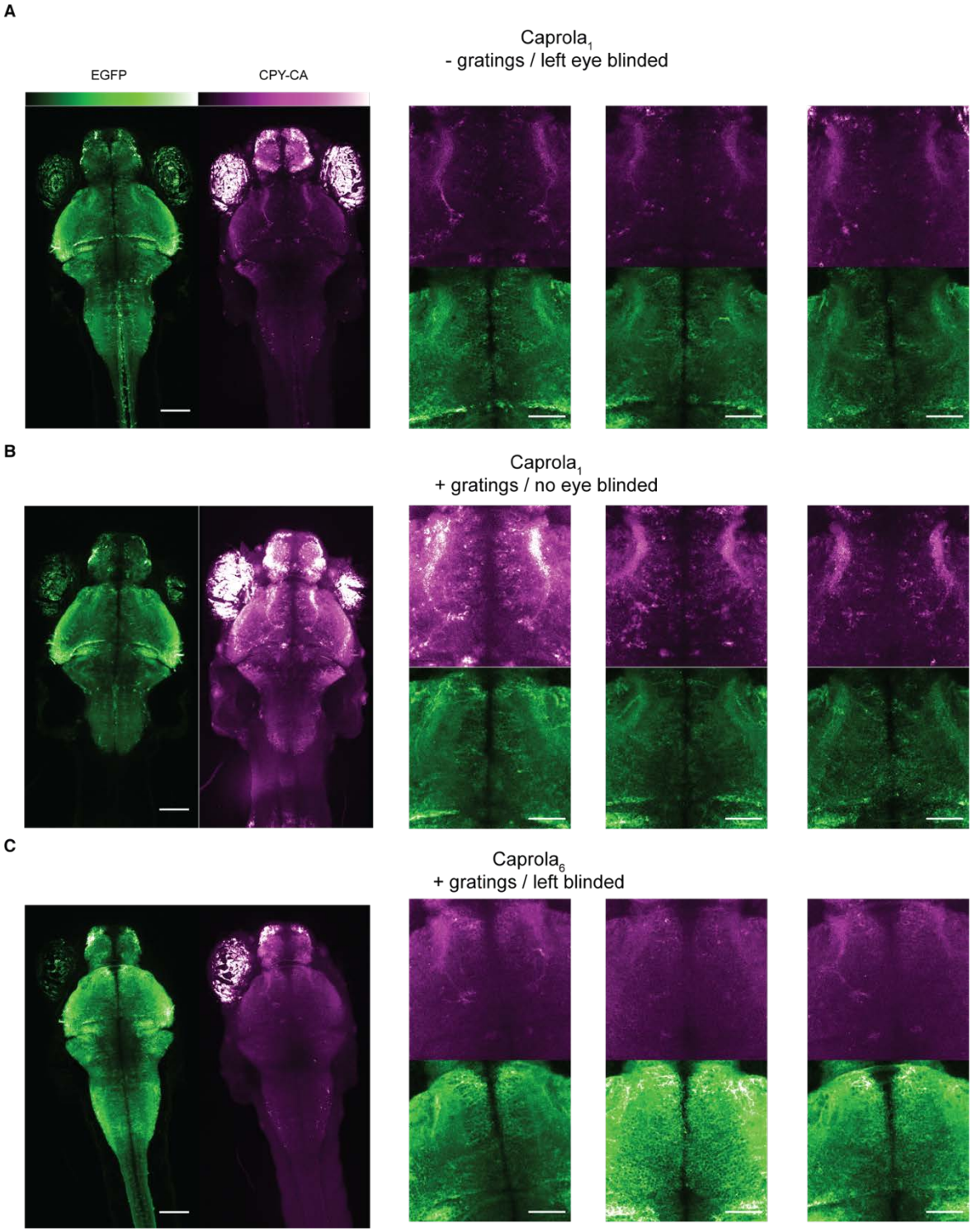

Fig. S29. Control experiments for visual stimulation in zebrafish larvae.

(**A, B**) Fluorescence micrographs (MIPs of 50 µm brain volume) of Caprola$_1$-EGFP-expressing zebrafish larvae incubated with 5 µM CPY-CA for 6 h with focus on pretectal areas. Cohorts of zebrafish larvae were immobilized and either had their left eye blocked without visual stimulation (A) or both eyes free during visual stimulation (B). Results show that visual stimulation leads to even labeling in both hemispheres if no eye is blinded and that, even if one eye is blinded, without stimulation no asymmetric signal is recorded. (**C**) Caprola$_6$-EGFP-expressing zebrafish larvae were immobilized and had their left eye blocked during visual stimulation. Scale bars: 100 µm (whole brain); 50 µm (zooms). Caprola$_6$, which

features a lower $EC50_{Ca2+}$ than $Caprola_1$, was unable to record distinct signals in visual stimulation experiments.

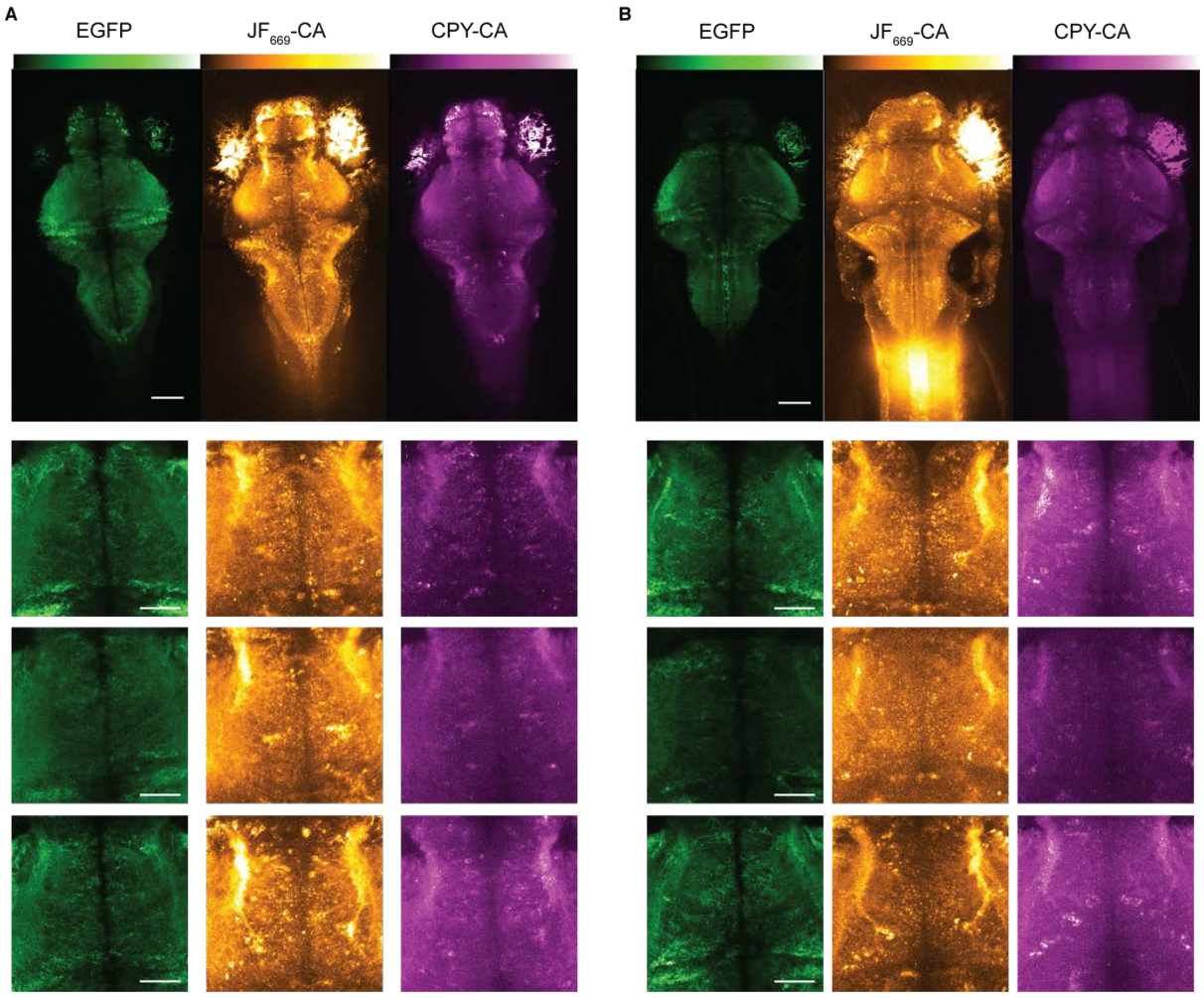

Fig. S30. Sequential recording of neuronal activity in visually stimulated zebrafish larvae.

(**A, B**) Fluorescence micrographs (MIPs of 50 µm brain volume) of Caprola$_1$-EGFP-expressing zebrafish larvae incubated first with 5 µM JF$_{669}$-CA for 6 h and the following day with 5 µM CPY-CA with focus on pretectal areas. Cohorts of zebrafish larvae were immobilized and either had their left eye (A) or right eye (B) blocked on the first day, while the other respective eye was blocked on the following day. Scale bars: 100 µm (whole brain); 50 µm (zooms).

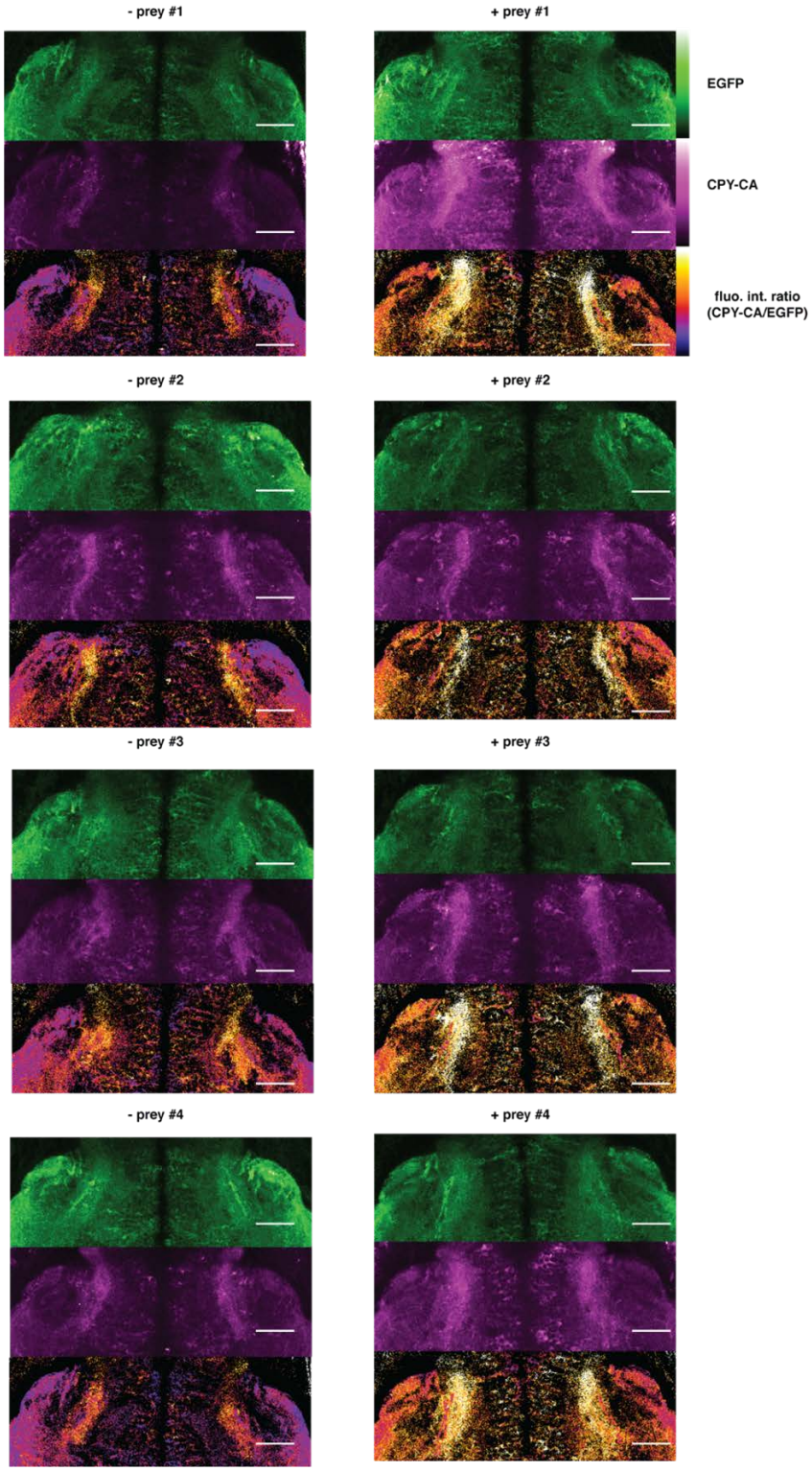

Fig. S31. Recording of neuronal activity of larval zebrafish in prey-capture experiments.

Fluorescence micrographs (MIPs of 50 µm brain volume) of Caprola$_1$-EGFP-expressing zebrafish larvae incubated with 5 µM CPY-CA for 2.5 h with focus on pretectal areas. Cohorts of zebrafish larvae either chased prey or were left in ambient conditions. Scale bars: 50 µm.

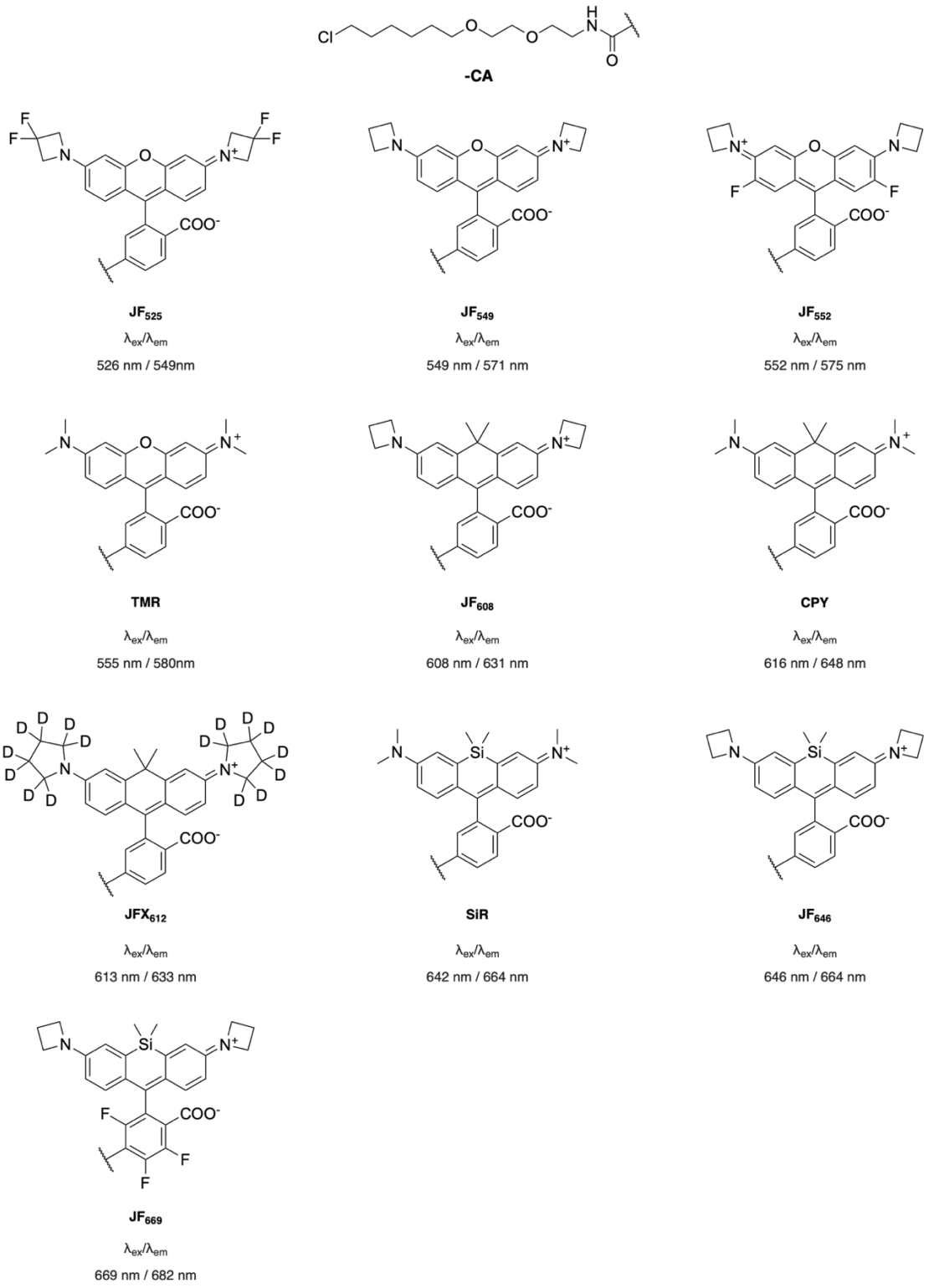

Fig. S32. Fluorescent probes used in this study.

Chemical structures of fluorescent HaloTag substrates with excitation and emission maxima. Janelia Fluor (JF) fluorescent substrates were kind gifts of L. D. Lavis (HHMI, Ashburn, VA, USA). TMR-, CPY-CA and SiR-Halo were synthesized in house.

Table S1. Relative activity of the initial Hpep library.

sequence	rel. activity	sequence	rel. activity	sequence	rel. activity	sequence	rel. activity	sequence	rel. activity	sequence	rel. activity
AIRTFILFRQ	< 0.01	AVETFQAFRT	0.86	AIETFKLFRQ	2.14	VIETFKLFRD	10.55	MREDARETFQAFRT	40.68	LGDDARETFQAFRT	165.98
ARKTFILFRS	< 0.01	TGEEARETFQAFRT	0.86	KSEEARETFQAFRT	2.15	FKEEARETFQAFRT	11.30	SRETFQAFRT	41.71	WKEDVIDAFRKFRD	172.46
SIRAFILFRS	< 0.01	ARETFQAFRE	0.88	QKDEARETFQAFRT	2.26	DGDDARETFQAFRT	11.46	TRDTFQAFRT	43.34	LVETFKLFRS	176.98
WIETFKLFRS	< 0.01	AVKTFILFRE	0.90	AIEAFKLFRQ	2.27	DKEEARETFQAFRT	11.55	SRDEARETFQAFRT	43.98	WKEEVIKAFRLYRE	177.93
AIRAFIKFRS	< 0.01	ARETFQAFRTAKDS	0.91	YTEEARETFQAFRT	2.30	WEDEARETFQAFRT	11.57	WEEEARETFQAFRT	44.20	WEKEARETFQAFRT	184.16
AIRTFILFRS	< 0.01	QEEEARETFQAFRT	0.93	SRDTFKAFQS	2.35	ARETFQAFRTALKD	11.63	AIRTFQLFRQ	44.92	TRDTFQAFQS	192.59
ARKAFILFRS	0.06	ARETFQAFRTGAES	0.94	VRKTFELFRS	2.46	AKETFQAFRT	12.29	SKEIARETFQAFRT	47.40	SRDAFKAYRS	194.89
ARKTFILFRQ	0.12	YSEDARETFQAFRT	0.94	MRETFQAFRT	2.46	DGEEARETFQAFRT	12.44	FSEDARETFQAFRT	47.58	VRTAFKLFRS	197.26
VRKTFKLFRS	0.18	TRETFKAFRD	0.96	AVEMFKLFRD	2.51	WFDEARETFQAFRT	12.73	MSEEARETFQAFRT	47.86	RDEDARETFQAFRT	203.92
IRDTFQAFQS	0.21	SRKAFELFRQ	0.96	WWEEARETFQAFRT	2.70	WKEEVVKAFIKFRD	12.73	WSEEARETFQAFRT	47.92	YSEEARETFQAFRT	208.67
ARDTFKAFQS	0.28	LIEAFIQFRS	0.97	SRDTFKAFQT	2.73	TREAFEAFRS	12.80	YGEELIKMFIKFRD	48.04	LIKTFQLYRS	217.70
IRETFEAYQS	0.34	ARETFQAFRT	1.00	YNEEARETFQAFRT	2.74	FQEEARETFQAFRT	13.37	LGEDARETFQAFRT	48.10	SRDAFKAFRS	222.76
ARETFQAFQT	0.36	YGRDARETFQAFRT	1.02	KEEEARETFQAFRT	2.80	QAEEARETFQAFRT	13.55	LKEDARETFQAFRT	48.49	ARKAFELFRS	223.61
ARETFQAFMT	0.39	AIRAFQLFRQ	1.03	TRETFEAFQS	2.82	TGEDARETFQAFRT	14.29	TREAFKAFRA	48.88	LIKTFQLFRS	243.50
GRDTFQAFQS	0.39	GRDTFKAFQS	1.03	AIKAFQLFRE	2.86	QGEEARETFQAFRT	14.38	SGEDARETFQAFRT	50.85	WKEEVIKAFRLFRE	253.66
IRETFEAFQS	0.39	MRDEARETFQAFRT	1.04	AREAFEAFRS	2.87	FGDEARETFQAFRT	15.25	WAQEARETFQAFRT	51.44	WDEEVKDAFKKFRD	259.31
SRDAFQAFQS	0.42	QKEDARETFQAFRT	1.05	SKEEARETFQAFRT	3.04	PKEDARETFQAFRT	15.57	ARDTFQAFRS	52.15	WREEVIKAFKLFRQ	265.38
TRDTFKAFKS	0.43	ARKTFQAFRT	1.13	WQEEARETFQAFRT	3.07	ESEDARETFQAFRT	15.75	LKEEARETFQAFRT	52.52	SKKEARETFQAFRT	268.50
AIRFFILARD	0.44	LIKTFILFRD	1.15	TRETFEAFRS	3.11	YGEEARETFQAFRT	15.99	WDEDARETFQAFRT	53.04	LIKAFQLFRS	276.56
AIRAFILFRE	0.44	ARETFQAFRTGASS	1.17	NGEDARETFQAFRT	3.11	DGEIARETFQAFRT	16.29	FIETFKLFRD	53.08	WKEEVIKAFKLFRD	285.96
SREAFEAFQS	0.44	KKEDARETFQAFRT	1.18	FKDDARETFQAFRT	3.20	VIKAFQLFRE	17.13	DKEDARETFQAFRT	53.45	WKEEVIKAFKLFRQ	293.44
GRDAFKAFQS	0.45	GRDTFQAFRS	1.18	WSETARETFQAFRT	3.20	YREEARETFQAFRT	17.82	AVETFKLFRQ	54.13	WRETFQAFRT	294.43
IRDTMKAFQN	0.45	EKEEARETFQAFRT	1.20	SSEEARETFQAFRT	3.23	WKDDARETFQAFRT	18.10	WHEEARETFQAFRT	54.83	DGRDARETFQAFRT	308.00
ARETFQAFRTPPEG	0.48	VIKAFIKFRE	1.20	LIETFKLFRQ	3.26	LIETFKLFRE	18.12	MKEEARETFQAFRT	57.76	WKKEARETFQAFRT	309.63
ARETFKAFQS	0.48	LAEEARETFQAFRT	1.23	ARETFQAFRD	3.40	FREEARETFQAFRT	18.20	ARDTFRAFRS	58.16	SRDTFQAFRS	309.89
TREAFEAFQS	0.50	VVRTFKLFRS	1.24	WRDEARETFQAFRT	3.47	ARETFRAFRT	18.37	WDRDARETFQAFRT	58.70	WKEEVIKAFKLFRS	322.27
IRDTFQAFRS	0.50	FWEEARETFQAFRT	1.27	WSDEARETFQAFRT	3.51	DAEDARETFQAFRT	18.45	AQETFKAYRS	60.80	YKEDLIKTFILFRQ	348.07
VVKAFIKFRD	0.50	AQETFKAFRS	1.28	WGQEARETFQAFRT	3.52	WLEEARETFQAFRT	18.52	QREEARETFQAFRT	61.04	LGEEARETFQAFRT	350.13
ARETFQAART	0.51	ARDTFKAFRS	1.31	WKDEARETFQAFRT	3.57	FGEEARETFQAFRT	18.53	WKEEVIKAFILYRQ	61.60	YKDDLIKTFILFRQ	360.10
AIRTFILFRE	0.52	SKEDARETFQAFRT	1.31	ARETFIAFRT	3.57	WDEIARETFQAFRT	18.78	SRDAFQAFRS	64.06	WRKEARETFQAFRT	361.66
YSEIARETFQAFRT	0.52	IREAFEAYRS	1.31	WREEARETFQAFRT	3.65	FTEEARETFQAFRT	19.13	VIKTFQLFRQ	66.44	ARDMFIKFRD	367.76
IRDTFRAFQS	0.53	IREAFEAFRS	1.32	ARETFKAFRT	3.69	LRETFQAFRT	20.58	SRDTFQAFRT	66.56	FKQDARETFQAFRT	376.88
SRDAFQAFQT	0.53	SSEDARETFQAFRT	1.33	ARETFQAFRTIFEH	3.77	WTEEARETFQAFRT	20.71	TRETFKAFRS	67.28	WDREARETFQAFRT	380.13
AIRAFILFRD	0.54	ARETFQAFRTAHQK	1.34	WSEMARETFQAFRT	3.77	STEEARETFQAFRT	21.15	HKDEARETFQAFRT	67.42	AIKAFQLFRS	381.00
VRETFEAFRS	0.54	VIKAFQLFRS	1.36	ARDTFRAFRD	3.79	LIEAFKLFRD	21.29	SRDTFRAFRS	68.65	IRDAFQAFRS	394.10
TGEIARETFQAFRT	0.55	YKEDLIDTFRKFRQ	1.36	LIETFRQFRE	3.87	EKEDARETFQAFRT	21.39	ARETFQAYRS	68.70	AQEAFKAFRS	405.63
TRDTFRAFQS	0.55	VRDTFILFRS	1.38	DKEIARETFQAFRT	3.90	ARETFKAFRS	21.42	AIKTFQLFRS	71.38	WKETARETFQAFRT	409.06
IRDTFRAFKS	0.56	ARDTFILFRE	1.42	LIKTFQLFRD	3.95	FAEDARETFQAFRT	22.18	WGDEARETFQAFRT	72.85	LIKTFQLFRQ	419.30
VRKTFILFRD	0.58	VVETFKLFRS	1.45	ARETFQAFRQ	3.97	ARETFQAYRT	22.28	YKDDARETFQAFRT	78.52	WEETARETFQAFRT	441.21
AIETFQAFRT	0.58	AIETFKLFRE	1.50	AQETFKAFRD	4.01	WNEEARETFQAFRT	23.71	TRDTFQAFRS	78.67	LIETFKLFRS	444.81
ARETFQAFR	0.58	SRDTFKAFRS	1.51	SRETFILFRQ	4.03	QKDVARETFQAFRT	23.94	WKEEVIKAFRLYRD	79.07	WRETARETFQAFRT	453.59
LIETFIQFRS	0.60	VRTAFKLFRQ	1.51	YEEEARETFQAFRT	4.13	FSEEARETFQAFRT	24.49	FGREARETFQAFRT	79.77	LRKTFKLFRS	476.55
FGEDARETFQAFRT	0.60	WGKEARETFQAFRT	1.51	YAEIARETFQAFRT	4.15	WSEDARETFQAFRT	24.96	VIKAFQLFRQ	85.12	QERDARETFQAFRT	515.29
VIETFIQFRS	0.63	VIRAFQLFRQ	1.54	WKEEVIKAFILYRE	4.19	LIDTFRKFRS	25.18	VIETFKLFRS	88.76	AREMFQAFRT	519.10
SREAFEAYRS	0.63	LIEAFRQFRS	1.56	GRDTFKAFRS	4.22	WDEEARETFQAFRT	25.36	WYEEARETFQAFRT	88.83	DGEDARETFQAFRT	536.24
QKEEARETFQAFRT	0.64	KDEEARETFQAFRT	1.60	LIETFKKFRD	4.25	WKDEVIDAFRKFRE	25.88	WKEEVIKAFILYRS	89.82	ARLFFQLFRT	554.77
WKEEARETFQAFRT	0.65	AREAFQAFRT	1.61	YKEEARETFQAFRT	4.45	VRETFQAFRT	26.65	QKKEARETFQAFRT	91.08	DKETARETFQAFRT	567.46
AVKTFILFRD	0.65	AIKTFILFRE	1.64	MGEDARETFQAFRT	4.65	WKEIARETFQAFRT	27.26	IRETFQAFRT	92.72	AREAFKAFRS	592.67
TRDTFKAFQS	0.65	YKEELIKTFRLFMQ	1.70	VRDTFQAFRT	4.82	AREFFQAFRT	27.40	ARETFQKFRT	94.09	VREAFKLFRS	599.08
ARETFQAFRTAKEK	0.65	IRETFEAFRS	1.71	FSDEARETFQAFRT	4.89	YWEEARETFQAFRT	28.73	GRETFQAFRS	96.35	WKEKARETFQAFRT	697.62
FEEEARETFQAFRT	0.66	VRETFKLFRS	1.71	FKEIARETFQAFRT	4.90	IRDTFQAYRS	29.49	WGRDARETFQAFRT	96.68	RKKEARETFQAFRT	711.89
AIRAFQLYRS	0.66	NRDTFQAFRS	1.76	YGEIARETFQAFRT	4.90	YGEDARETFQAFRT	29.80	HKEEARETFQAFRT	97.93	SKRDARETFQAFRT	808.46
ARETFEAFRS	0.67	WAKEARETFQAFRT	1.77	WREIARETFQAFRT	4.92	KKEEARETFQAFRT	30.01	LIETFRLFRQ	106.52	WREEVRKTFKLFRS	828.94
YAEEARETFQAFRT	0.72	VREFFKLARD	1.81	YKEDARETFQAFRT	4.96	WGEDARETFQAFRT	31.15	LAEDARETFQAFRT	118.39	WDKEARETFQAFRT	887.88
SAEEARETFQAFRT	0.72	LIETFKLFRT	1.83	ARDTFQAFRT	6.39	ARRTFQAFRT	33.23	VIKTFQLFRS	119.52	WREEVRKAFKLFRS	930.10
TRDAFRAYQS	0.73	SRDAFQAYRS	1.86	AIEAFKLFRE	7.82	WGEEARETFQAFRT	33.52	WKEDARETFQAFRT	119.99	WSKEARETFQAFRT	943.09
SRDAFKAFQS	0.74	VIRTFQLFRQ	1.88	TRETFQAFRT	8.35	WGEIARETFQAFRT	34.30	SREAFEAFRS	124.17	WKREARETFQAFRT	962.45
AQETFQAFRT	0.76	SRDTFQAFQS	1.89	YQEEARETFQAFRT	8.63	LKDIARETFQAFRT	36.26	VREAFKLFRQ	128.90	LSEEARETFQAFRT	976.73
SRDAFQAYQS	0.79	STEIARETFQAFRT	1.92	SRETFEAFRS	9.16	FKEDARETFQAFRT	36.39	WKEEVIKAFIKFRE	134.28	WREEVRKTFKLFRQ	989.97
ARETFQAFRTTSDS	0.79	MGEEARETFQAFRT	1.95	WTDEARETFQAFRT	9.44	VIRMFQLFRE	36.43	WKELARETFQAFRT	135.29	AIRMFQLFRE	1038.03
WFEEARETFQAFRT	0.80	VRKTFKLFRQ	1.97	ARETFKAFRD	9.45	KDETARETFQAFRT	37.37	FGKEARETFQAFRT	138.74	WREEVRKAFKLFRQ	1189.69
ARETAQAFRT	0.80	VRDTFQAFRS	1.98	WADEARETFQAFRT	9.69	ARETFQLFRT	37.74	ARETFQAFRS	144.80	WIETFKLYRE	1333.05
FAEEARETFQAFRT	0.83	WTKEARETFQAFRT	2.01	GRETFQAFRT	10.24	YKEIARETFQAFRT	38.27	VVKTFQLFRS	156.13	WREEVRKAFKLFRD	1525.72
ARETFEAFRT	0.84	WAEEARETFQAFRT	2.02	LIETFIQYRQ	10.35	RKEEARETFQAFRT	39.66	MKEDARETFQAFRT	163.83	WKRDARETFQAFRT	1641.32

Labeling kinetics of split-HaloTag with each Hpep variant measured by fluorescence polarization. A linear or exponential model was fit to the data and initial reaction rates were determined as a measure of activity. Activities were normalized to the original Hpep1.

Table S2. EC_{50} values and sequences of Hpep variants.

variant	sequence	EC_{50} (μM)	
Hpep1	ARETFQAFRT	2979	(2628 - 3417)
Hpep2	AREMFQAFRT	1116	(928 - 1350)
Hpep3	SKRDAREMFQAFRT	149	(128 – 176)
Hpep4	WKEEVIKAFKLFRD	21.0	(18.3 – 24.1)
Hpep5	WREEVRKAFKLFRQ	10.7	(8.84 – 13.0)
Hpep6	WRETFQLFRT	2.39	(2.08 – 2.77)
Hpep7	WREMFRLFRT	0.35	(0.32 – 0.38)
Hpep8	WKRDWREMFRLFRT	0.12	(0.11 – 0.14)

EC_{50}: Hpep concentration leading to half maximal split-HaloTag labeling rate. 95% confidence intervals are given in brackets.

Table S3. Biochemical characterization of Caprola *in vitro.*

Caprola variant	EC_{50} (nM)	k_{Ca++} ($M^{-1}s^{-1}$)	k_{EGTA} ($M^{-1}s^{-1}$)	k_{Ca++} / k_{EGTA}	hill-coefficient
Caprola_01	44 (32 - 64)	1.88×10^5 ($1.77 - 1.98 \times 10^5$)	41.6 (41.1 - 42.2)	4510 (4260 - 4770)	4.09 (1.52 - 8.49)
Caprola_02	68 (29 - 186)	0.87×10^5 ($0.82 - 0.93 \times 10^5$)	44.2 (43.7 - 44.6)	1980 (1860 - 2100)	2.82 (0.46 - 8.29)
Caprola_03	70 (52 - 94)	1.50×10^5 ($1.40 - 1.60 \times 10^5$)	35.9 (35.5 - 36.3)	4170 (3910 - 4470)	4.62 (1.95 - 9.98)
Caprola_04	120 (80 - 168)	1.55×10^5 ($1.45 - 1.64 \times 10^5$)	31.4 (31 - 31.8)	4920 (4620 - 5240)	4.61 (1.87 - 10.18)
Caprola_05	130 (117 - 147)	0.73×10^5 ($0.7 - 0.75 \times 10^5$)	37.2 (36.6 - 37.8)	1950 (1860 - 2040)	5.92 (3.94 - 9.73)
Caprola_06	131 (117 - 147)	1.22×10^5 ($1.13 - 1.32 \times 10^5$)	38.3 (37.8 - 38.8)	3190 (2930 - 3460)	4.79 (3.51 - 6.92)
Caprola_07	172 (151 - 195)	1.16×10^5 ($1.08 - 1.23\times 10^5$)	47.5 (46.8 - 48.1)	2440 (2280 - 2600)	3.31 (2.58 - 4.25)
Caprola_08	173 (145 - 207)	0.84×10^5 ($0.79 - 0.89 \times 10^5$)	75.3 (74.6 - 76)	1110 (1050 - 1180)	5.65 (2.75 - 10.4)
Caprola_09	243 (186 - 319)	2.61×10^5 ($2.46 - 2.78 \times 10^5$)	38 (37.4 - 38.5)	6870 (6460 - 7330)	2.64 (1.39 - 5.12)
Caprola_10	253 (210 - 312)	1.33×10^5 ($1.24 - 1.41 \times 10^5$)	23.7 (23.3 - 24.1)	5600 (5230 - 5970)	4.3 (2.23 - 8.32)
Caprola_11	278 (227 - 344)	1.99×10^5 ($1.89 - 2.1 \times 10^5$)	28.5 (28.2 - 28.9)	6970 (6600 - 7390)	3.62 (2.4 - 5.23)
Caprola_12	336 (311 - 364)	4.77×10^5 ($4.38 - 5.21 \times 10^5$)	48.1 (47.5 - 48.7)	9930 (9080 - 10870)	2.98 (2.44 - 3.63)
Caprola_13	343 (245 - 483)	0.36×10^5 ($0.34 - 0.38 \times 10^5$)	70.8 (69 - 72.7)	510 (470 - 540)	3.43 (1.39 - 7.48)
Caprola_14	500 (414 - 608)	1.81×10^5 ($1.72 - 1.91 \times 10^5$)	40.5 (40.1 - 40.9)	4470 (4240 - 4710)	3.69 (2.06 - 6.73)
Caprola_15	1050 (847 - 1300)	0.83×10^5 ($0.8 - 0.87 \times 10^5$)	16.2 (15.8 - 16.5)	5150 (4910 - 5400)	2.51 (1.69 - 3.85)

Biochemical characterization of Caprola. EC_{50}: free Ca^{2+} concentration leading to half maximal Caprola labeling rate. k_{Ca++}: second-order rate constant in saturating Ca^{2+} concentration. k_{EGTA}: second-order rate constant in absence of free Ca^{2+}. hill-coefficient: hill coefficient of the sigmoidal model fitted to free Ca^{2+} titrations. 95% confidence intervals are given in brackets.

Table S4. Composition of buffers used in the study.

Buffer	Composition
IMAC lysis buffer	50 mM KH_2PO_4, 150 mM NaCl, 5 mM imidazole, 1 mM PMSF, 0.25 mg/mL lysozyme, pH 8.0
IMAC wash buffer	50 mM KH_2PO_4, 300 mM NaCl, 10 mM imidazole, pH 7.5
IMAC elution buffer	50 mM KH_2PO_4, 300 mM NaCl, 500 mM imidazole, pH 7.5
Strep wash buffer	100 mM TrisHCl, 150 mM NaCl, 1 mM EDTA, pH 8
Strep elution buffer	100 mM TrisHCl, 150 mM NaCl, 1 mM EDTA, 2.5 mM desthiobiotin, pH 8
Activity buffer	50 mM HEPES, 50 mM NaCl, pH 7.3
FP buffer	50 mM HEPES, 50 mM NaCl, 0.5 g/l BSA, pH 7.3

Table S5. Plasmids and stable cell lines used in the study.

Name	Purpose	Addgene #	Gene of interest
Building blocks			
pAAV_hSyn_NES-his-CaMPARI2-WRPE-SV40	Primary neuron culture of the light gated Ca^{2+} integrator	#101060	CaMPARI2 (*80*)
pTol2_elavl3(HuC)_CaMPARI2	Zebrafish expression of light gated Ca^{2+} integrator	#137185	CaMPARI2 (*80*)
pJFRC7-20XUAS-IVS-	*Drosophila* GAL4-driven expression of mCD8::GFP	#26220	mCD8::GFP (*81*)
GCaMP6s	Primary neuron expression of GCaMP6s	#100843	GCaMP6s (*15*)
Mission shRNA pLKO.1-puro-CMV_TurboGFP	Lentivirus production for transgene delivery into cultured Glioblastoma	Sigma Aldrich #SHC016	TurboGFP
bArrestin2-TEV	expression of beta-Arrestin 2 for PRESTO-Tango assay	#107245	ARRB2 (*23*)
CHRM3-Tango	expression of CHRM3 for PRESTO-Tango assay	#66250	CHRM3 (*23*)
DRD2-Tango	expression of DRD2 for PRESTO-Tango assay	#66269	DRD2 (*23*)
GRM2-Tango	expression of GRM2 for PRESTO-Tango assay	#66388	GRM2 (*23*)
GABBR1-Tango	expression of GABBR1 for PRESTO-Tango assay	#66287	GABBR1 (*23*)
ADRB2-Tango	expression of ADRB2 for PRESTO-Tango assay	#66220	ADRB2 (*23*)
HTR4-Tango	expression of HTR4 for PRESTO-Tango assay	#66412	HTR4 (*23*)
pET51b-His-TEV-HaloTag7	Overexpression of HaloTag7 in *E. coli*	#167266	HaloTag7
This study			
pET-51b(+)-His10_TEVsite_cpHaloTag_141-145	cpHaloTag protein production in *E .coli*	#194660	cpHaloTag_141-145
pET-51b(+)-His10_TEVsite_cpHaloTag_154-156	cpHaloTag protein production in *E .coli*	#194661	cpHaloTag_154-156
pET-51b(+)-His10_TEVsite_cpHaloΔ	cpHaloTag protein production in *E .coli*	#194659	cpHaloTag_141-156_aka_cpHaloDelta
pET-51b(+)_FRB_(GGS)1_Hpep1	Hpep1-FRB fusion protein production in *E .coli*	NA	FRB_(GGS)1_Hpep1
pET-51b(+)_FKBP_(GGS)1_cpHaloDelta	cpHaloDelta-FKBP fusion protein production in *E .coli*	NA	FKBP_(GGS)1_cpHaloDelta
pET-51b(+)_Hpep1_(GGS)3_FRB	Hpep1-FRB fusion protein production in *E .coli*	NA	Hpep1_(GGS)3_FRB
pET-51b(+)_Hpep3_(GGS)3_FRB	Hpep3-FRB fusion protein production in *E .coli*	NA	Hpep3_(GGS)3_FRB
pET-51b(+)_cpHaloDelta_(GGS)9_FKBP	cpHaloDelta-FKBP fusion protein production in *E .coli*	NA	cpHaloDelta_(GGS)9_FKBP
pCDNA5/FRT-Lyn11-mEGFP-FKBP-(GGS)-cpHaloΔ-P2A-FRB-(GGS)-Hpep1-mScarlet	Mammalian cell co-expression of FKBP- and FRB-split-HaloTag fusions	NA	mEGFP-FKBP-cpHaloΔ FRB- Hpep1-mScarlet
pCDNA5/FRT-Lyn11-mEGFP-FKBP-(GGS)-cpHaloΔ-P2A-FRB-(GGS)-Hpep3-mScarlet	Mammalian cell co-expression of FKBP- and FRB-split-HaloTag fusions	NA	mEGFP-FKBP-cpHaloΔ FRB-Hpep3-mScarlet

pCDNA5/FRT-Lyn11-mEGFP-cpHaloΔ-$(GGS)_9$-FKBP-P2A-Hpep1-$(GGS)_3$-FRB-mScarlet	Mammalian cell co-expression of FKBP- and FRB-split-HaloTag fusions	NA	mEGFP-cpHaloΔ-FKBP Hpep1-FRB-mScarlet
pCDNA5/FRT-Lyn11-mEGFP-cpHaloΔ-$(GGS)_9$-FKBP-P2A-Hpep3-$(GGS)_3$-FRB-mScarlet	Mammalian cell co-expression of FKBP- and FRB-split-HaloTag fusions	#194677	mEGFP-cpHaloΔ-FKBP Hpep3-FRB-mScarlet
pcDNA3.1-GABBR1-cpHaloΔ-mEGFP	Mammalian expression of split-HaloTag GPCR fusion	NA	GABBR1-cpHaloΔ
pcDNA3.1-ADRB2-cpHaloΔ-mEGFP	Mammalian expression of split-HaloTag GPCR fusion	NA	ADRB2-cpHaloΔ
pcDNA3.1-HTR4-cpHaloΔ-mEGFP	Mammalian expression of split-HaloTag GPCR fusion	NA	HTR4-cpHaloΔ
pcDNA3.1-Hpep1-betaArrestin2-T2A-mTagBFP2	Mammalian expression of split-HaloTag beta-Arrestin 2 fusion [Hpep1]	#194680	Hpep1-beta-Arrestin 2
pcDNA3.1-Hpep3-betaArrestin2-T2A-mTagBFP2	Mammalian expression of split-HaloTag beta-Arrestin 2 fusion [Hpep3]	NA	Hpep3-beta-Arrestin 2
pcDNA3.1-Hpep7-betaArrestin2-T2A-mTagBFP2	Mammalian expression of split-HaloTag beta-Arrestin 2 fusion [Hpep7]	NA	Hpep7-beta-Arrestin 2
pET-51b(+) $Caprola_1$	Caprola protein production in *E .coli*	#194662	$Caprola_1$
pET-51b(+) $Caprola_2$	Caprola protein production in *E .coli*	#194663	$Caprola_2$
pET-51b(+) $Caprola_3$	Caprola protein production in *E .coli*	#194664	$Caprola_3$
pET-51b(+) $Caprola_4$	Caprola protein production in *E .coli*	#194665	$Caprola_4$
pET-51b(+) $Caprola_5$	Caprola protein production in *E .coli*	#194666	$Caprola_5$
pET-51b(+) $Caprola_6$	Caprola protein production in *E .coli*	#194667	$Caprola_6$
pET-51b(+) $Caprola_7$	Caprola protein production in *E .coli*	#194668	$Caprola_7$
pET-51b(+) $Caprola_8$	Caprola protein production in *E .coli*	#194669	$Caprola_8$
pET-51b(+) $Caprola_9$	Caprola protein production in *E .coli*	#194670	$Caprola_9$
pET-51b(+) $Caprola_{10}$	Caprola protein production in *E .coli*	#194671	$Caprola_{10}$
pET-51b(+) $Caprola_{11}$	Caprola protein production in *E .coli*	#194672	$Caprola_{11}$
pET-51b(+) $Caprola_{12}$	Caprola protein production in *E .coli*	#194673	$Caprola_{12}$
pET-51b(+) $Caprola_{13}$	Caprola protein production in *E .coli*	#194674	$Caprola_{13}$
pET-51b(+) $Caprola_{14}$	Caprola protein production in *E .coli*	#194675	$Caprola_{14}$
pET-51b(+) $Caprola_{15}$	Caprola protein production in *E .coli*	#194676	$Caprola_{15}$
pCDNA5/FRT_CMV_NES-$Caprola_1$-mEGFP[a]	Mammalian cell expression of Caprola in cytosol	#194681	NES-$Caprola_1$-mEGFP
pCDNA5/FRT_CMV_NES-$Caprola_2$-mEGFP[a]	Mammalian cell expression of Caprola in cytosol	NA	NES-$Caprola_2$-mEGFP
pCDNA5/FRT_CMV_NES-$Caprola_3$-mEGFP[a]	Mammalian cell expression of Caprola in cytosol	NA	NES-$Caprola_3$-mEGFP
pCDNA5/FRT_CMV_NES-$Caprola_4$-mEGFP[a]	Mammalian cell expression of Caprola in cytosol	#194682	NES-$Caprola_4$-mEGFP
pCDNA5/FRT_CMV_NES-$Caprola_5$-mEGFP[a]	Mammalian cell expression of Caprola in cytosol	#194683	NES-$Caprola_5$-mEGFP
pCDNA5/FRT_CMV_NES-$Caprola_6$-mEGFP[a]	Mammalian cell expression of Caprola in cytosol	#194684	NES-$Caprola_6$-mEGFP
pCDNA5/FRT_CMV_NES-$Caprola_7$-mEGFP[a]	Mammalian cell expression of Caprola in cytosol	NA	NES-$Caprola_7$-mEGFP
pCDNA5/FRT_CMV_NES-$Caprola_8$-mEGFP[a]	Mammalian cell expression of Caprola in cytosol	NA	NES-$Caprola_8$-mEGFP
pCDNA5/FRT_CMV_NES-$Caprola_9$-mEGFP[a]	Mammalian cell expression of Caprola in cytosol	#194685	NES-$Caprola_9$-mEGFP
pCDNA5/FRT_CMV_NES-$Caprola_{10}$-mEGFP[a]	Mammalian cell expression of Caprola in cytosol	NA	NES-$Caprola_{10}$-mEGFP
pCDNA5/FRT_CMV_NES-$Caprola_{11}$-mEGFP[a]	Mammalian cell expression of Caprola in cytosol	NA	NES-$Caprola_{11}$-mEGFP

pCDNA5/FRT_CMV_NES-Caprola$_{12}$-mEGFP[a]	Mammalian cell expression of Caprola in cytosol	NA	NES-Caprola$_{12}$-mEGFP
pCDNA5/FRT_CMV_NES-Caprola$_{13}$-mEGFP[a]	Mammalian cell expression of Caprola in cytosol	NA	NES-Caprola$_{13}$-mEGFP
pCDNA5/FRT_CMV_NES-Caprola$_{14}$-mEGFP[a]	Mammalian cell expression of Caprola in cytosol	NA	NES-Caprola$_{14}$-mEGFP
pCDNA5/FRT_CMV_NES-Caprola$_{15}$-mEGFP[a]	Mammalian cell expression of Caprola in cytosol	NA	NES-Caprola$_{15}$-mEGFP
pCDNA5/FRT_CMV_NES-Caprola$_{on}$-mEGFP[a]	Mammalian cell expression of Caprola posCTRL in cytosol	#194686	NES-Caprola$_{on}$-mEGFP
pCDNA5/FRT_CMV_NES-Caprola$_{off}$-mEGFP[a]	Mammalian cell expression of Caprola negCTRL in cytosol	#194687	NES-Caprola$_{off}$-mEGFP
pAAV_hSyn_NES-Caprola$_4$-mEGFP_WRPE-SV40	Primary neuron culture expression of Caprola in cytosol	#194688	NES-Caprola$_4$-mEGFP
pAAV_hSyn_NES-Caprola$_5$-mEGFP_WRPE-SV40	Primary neuron culture expression of Caprola in cytosol	#194689	NES-Caprola$_5$-mEGFP
pAAV_hSyn_NES-Caprola$_6$-mEGFP_WRPE-SV40	Primary neuron culture expression of Caprola in cytosol	#194690	NES-Caprola$_6$-mEGFP
pAAV_hSyn_NES-Caprola$_{on}$-mEGFP_WRPE-SV40	Primary neuron culture expression of Caprola posCTRL in cytosol	#194691	NES-Caprola$_{on}$-mEGFP
pAAV_hSyn_NES-Caprola$_{off}$-mEGFP_WRPE-SV40	Primary neuron culture expression of Caprola negCTRL in cytosol	#194692	NES-Caprola$_{off}$-mEGFP
pLKO.1-puro_CMV_NES-Caprola$_6$-mEGFP	Glioblastoma expression of Caprola in cytosol	#194693	NES-Caprola$_6$-mEGFP
pLKO.1-puro_CMV_NES-Caprola$_{on}$-mEGFP	Glioblastoma expression of Caprola posCTRL in cytosol	#194694	NES-Caprola$_{on}$-mEGFP
pLKO.1-puro_CMV_NES-Caprola$_{off}$-mEGFP	Glioblastoma expression of Caprola negCTRL in cytosol	#194695	NES-Caprola$_{off}$-mEGFP
pJFRC7-20XUAS-IVS-NES_Caprola$_5$-mEGFP	*Drosophila* expression of Caprola in cytosol	TBD	NES-CaProLa$_5$_meGFP
pTol2_*elavl3*(HuC)_NES-Caprola$_1$-mEGFP	Zebrafish expression of Caprola in cytosol	#194696	NES-Caprola$_1$-mEGFP
pTol2_*elavl3*(HuC)_NES-Caprola$_6$-mEGFP	Zebrafish expression of Caprola in cytosol	NA	NES-Caprola$_6$-mEGFP
pTol2_*elavl3*(HuC)_NES-Caprola$_{on}$-mEGFP	Zebrafish expression of Caprola posCTRL in cytosol	#194697	NES-Caprola$_{on}$-mEGFP
pTol2_*elavl3*(HuC)_NES-Caprola$_{off}$-mEGFP	Zebrafish expression of Caprola negCTRL in cytosol	#194698	NES-Caprola$_{off}$-mEGFP

[a] stable HeLa Kyoto Flp-In cell line generated.

Table S6. X-ray structure data collection and refinement statistics.

	cpHaloΔ [8B6N]	cpHaloTag154-156 [8B6P]
Data collection		
Space group	$C222_1$	$P2_12_12_1$
Unit-cell parameters		
a, b, c (Å)	45.85, 79.32, 154.18	68.87, 94.66, 100.11
α, β, γ (°)	90.00, 90.00, 90.00	90.00, 90.00, 90.00
Radiation source	PXII-X10SA, SLS	PXII-X10SA, SLS
Wavelength (Å)	0.97797	0.99986
Temperature (K)	100	100
Resolution range (Å)	50-2.30 (2.40-2.30)	50-1.10 (1.20-1.10)
No. of observed reflections	79790 (7342)	1085412 (223098)
No. of unique reflections	12786 (1438)	251839 (54597)
Multiplicity		
Completeness (%)	99.1 (94.6)	95.4 (90.8)
R_{merge} (%)	6.5 (65.1)	4.8 (17.4)
$\langle I/\sigma(I)\rangle$	15.8 (2.2)	17.7 (8.5)
$CC_{1/2}$ (%)[#]	99.9 (76.8)	99.8 (96.5)
Refinement		
Molecules per a.u.	1	2
No. of reflections	12781	251832
No. of reflections in test set	640	12591
Resolution range (Å)	39.70-2.30	42.79-1.10
No. of non-hydrogen atoms		
Protein	2163	4736
Ligand/ion	13	2
Water	13	680
Total	2189	5418
R (%)	21.46	13.70
R_{free} (%)	25.00	14.90
RMS deviations from ideal		
bonds (Å)	0.004	0.010
angles (°)	0.659	1.165
B-factors (Å^2)		
Protein	58.00	10.70
Ligand/ion	41.72	8.66
Water	46.48	20.99
Average	57.84	11.99
Wilson B (Å^2)	52.48	8.62
Ramachandran statistics (%)		
favored regions	96.6	97.1
allowed regions	3.4	2.9
disallowed regions	0	0
Clashscore	4.40	0.96

as implemented in XDS (*50*). Values in parentheses are for the highest resolution shell.

Table S7. Experimental parameters for confocal and widefield fluorescence microscopy.

Figure	Construct	Label	Microscope	Objective	Excitation [nm]	Emission [nm]	Fluorophore conc.
1M	Lyn11-mEGFP-FKBP-cpHaloΔ-P2A-Hpep1-FRB-mScarlet	mEGFP CPY	Confocal	40x/1.10 water	488 610	494-556 618-750	- 100 nM
2B	Hpep1-betaArrestin2-T2A-mTagBFP2 + DRD2-cpHaloΔ-mEGFP	mTagBFP2 mEGFP CPY	Confocal	20x/0.80 dry	405 488 608	430-494 494-590 617-730	- - 200 nM
4A	NES-Caprola$_5$-mEGFP	mEGFP CPY	Confocal	20x/0.80 dry	488 610	505-550 620-660	- 100 nM
4D	NES-Caprola$_5$-mEGFP	mEGFP JF552 CPY JF669	Confocal	20x/0.80 dry	488 525 610 699	505-540 565-600 620-660 680-750	- 300 nM 25 nM 300 nM
4E	NES-Caprola$_4$-mEGFP	mEGFP CPY	Widefield	20x/0.80 dry	470 635	525/50 700/75	- 250 nM
4G	NES-Caprola$_6$-mEGFP	mEGFP CPY	Confocal	20x/0.80 dry	488 610	505-550 620-660	- 100 nM /1 µM
5B	NES-Caprola$_5$-mEGFP	mEGFP CPY	Confocal	20x/0.6 water	488 610	505-550 620-660	- 5 µM
5C/E	NES-Caprola$_1$-mEGFP	mEGFP CPY	Confocal	20x/1.00 water	488 610	505-550 620-660	- 5 µM
5F	NES-Caprola$_1$-mEGFP	mEGFP CPY JF669	Confocal	20x/1.00 water	488 610 669	505-550 620-660 680-750	- 5 µM 5 µM
5G/H	NES-Caprola$_1$-mEGFP	mEGFP CPY	Confocal	20x/1.00 water	488 610	505-550 620-660	- 5 µM
S5A	(**A**) Lyn11-mEGFP-FKBP-(GGS)-cpHaloΔ-P2A-FRB-(GGS)-Hpep1-mScarlet	mEGFP CPY	Confocal	40x/1.10 water	488 610	494-556 618-750	- 100 nM
S5B	Lyn11-mEGFP-FKBP-(GGS)-cpHaloΔ-P2A-FRB-(GGS)-Hpep3-mScarlet	mEGFP CPY	Confocal	40x/1.10 water	488 610	494-556 618-750	- 100 nM
S5C	Lyn11-mEGFP-cpHaloΔ-(GGS)$_9$-FKBP-P2A-Hpep1-(GGS)$_3$-FRB-mScarlet	mEGFP CPY	Confocal	40x/1.10 water	488 610	494-556 618-750	- 100 nM
S5D	Lyn11-mEGFP-cpHaloΔ-(GGS)$_9$-FKBP-P2A-	mEGFP CPY	Confocal	40x/1.10 water	488 610	494-556 618-750	- 100 nM

	Hpep3-$(GGS)_3$-FRB-mScarlet						
S6	HPep1/3/7-betaArrestin2-T2A-mTagBFP2 + DRD2-cpHaloΔ-mEGFP	mTagBFP2 mEGFP CPY	Confocal	20x/0.80 dry	405 488 608	430-494 494-590 617-730	- - 200 nM
S7	HPep1-betaArrestin2-T2A-mTagBFP2 + DRD2/ m3 mAchR/ β2AR/ mGluR2/ GABAβ1R-cpHaloΔ-mEGFP	mTagBFP2 mEGFP CPY	Confocal	20x/0.80 dry	405 488 608	430-494 494-590 617-730	- - 200 nM
S14	NES-$Caprola_5$-mEGFP	mEGFP CPY	Confocal	20x/0.80 dry	488 610	505-550 620-660	- 125 nM
S16	NES-$Caprola_5$-mEGFP	mEGFP JF552 CPY JF669	Confocal	20x/0.80 dry	488 525 610 699	505-540 565-600 620-660 680-750	- 300 nM 25 nM 300 nM
S17 A	NES-$Caprola_5$-mEGFP	mEGFP	Widefield	40x/1.10 water	488	505-560	-
17 C	GCaMP6s	GCaMP	Widefield	20x/0.80 dry	488	505-560	-
S18	NES-$Caprola_4$-mEGFP	mEGFP CPY	Widefield	20x/0.80 dry	470 635	525/50 700/75	- 250 nM
S19	NES-$Caprola_6$-mEGFP	mEGFP CPY	Confocal	20x/0.80 dry	488 610	505-540 620-660	- 100 nM
S20	NES-$Caprola_6$-mEGFP	mEGFP CPY	Confocal	20x/0.80 dry	488 610	505-540 620-660	- 100 nM /1 µM
S21	NES-$Caprola_4$-mEGFP	mEGFP CPY	Confocal	20x/0.80 dry	488 610	505-540 620-660	- 500 nM
S25	NES-$Caprola_5$-mEGFP	mEGFP CPY	Confocal	20x/0.6 water	488 610	505-550 620-660	- 5 µM
S26	NES-$Caprola_1$-mEGFP	mEGFP CPY JF525 JF552 JF669	Confocal	20x/1.00 water	488 610 525 552 669	505-540 620-660 540-580 570-610 680-750	- 5 µM 5 µM 5 µM 5 µM
S27	NES-$Caprola_1$-mEGFP	mEGFP CPY	Confocal	20x/1.00 water	488 610	505-540 620-660	- 5 µM
S28	NES-$Caprola_1$-mEGFP	mEGFP CPY	Confocal	20x/1.00 water	488 610	505-540 620-660	- 5 µM
S29	NES-$Caprola_1$-mEGFP	mEGFP CPY	Confocal	20x/1.00 water	488 610	505-540 620-660	- 5 µM

S30	NES-Caprola$_1$-mEGFP	mEGFP CPY JF669	Confocal	20x/1.00 water	488 610 669	505-550 620-660 680-750	- 5 µM 5 µM
S31	NES-Caprola$_1$-mEGFP	mEGFP CPY	Confocal	20x/1.00 water	488 610	505-540 620-660	- 5 µM

Protein sequences

cpHaloTag and split-HaloTag

cpHaloTag screening

>cp135-137

MASWSHPQFEKGADDDDKVPHTWDEWPEFARETFQAFRTTDVGRKLIIDQNVFIEGTLPMGVVR
PLTEVEMDHYREPFLNPVDREPLWRFPNELPIAGEPANIVALVEEYMDWLHQSPVPKLLFWGTP
GVLIPPAEAARLAKSLPNCKAVDIGPGLNLLQEDNPDLIGSEIARWLSTLEIGGTGGSGGTGGS
GGSIGTGFPFDPHYVEVLGERMHYVDVGPRDGTPVLFLHGNPTSSYVWRNIIPHVAPTHRCIAP
DLIGMGKSDKPDLGYFFDDHVRFMDAFIEALGLEEVVLVIHDWGSALGFHWAKRNPERVKGIAF
MEFIRPIAPGFSSISAHHHHHHHHHH

His-tag; Strep-tag; enterokinase cleavage site, HaloTag, GGS linker

>cp141-144

MASWSHPQFEKGADDDDKVPHFARETFQAFRTTDVGRKLIIDQNVFIEGTLPMGVVRPLTEVEM
DHYREPFLNPVDREPLWRFPNELPIAGEPANIVALVEEYMDWLHQSPVPKLLFWGTPGVLIPPA
EAARLAKSLPNCKAVDIGPGLNLLQEDNPDLIGSEIARWLSTLEIGGTGGSGGTGGSGGSIGTG
FPFDPHYVEVLGERMHYVDVGPRDGTPVLFLHGNPTSSYVWRNIIPHVAPTHRCIAPDLIGMGK
SDKPDLGYFFDDHVRFMDAFIEALGLEEVVLVIHDWGSALGFHWAKRNPERVKGIAFMEFIRPI
PTWDEWAPGFSSISAHHHHHHHHHH

>cp141-145

MASWSHPQFEKGADDDDKVPHARETFQAFRTTDVGRKLIIDQNVFIEGTLPMGVVRPLTEVEMD
HYREPFLNPVDREPLWRFPNELPIAGEPANIVALVEEYMDWLHQSPVPKLLFWGTPGVLIPPAE
AARLAKSLPNCKAVDIGPGLNLLQEDNPDLIGSEIARWLSTLEIGGTGGSGGTGGSGGSIGTGF
PFDPHYVEVLGERMHYVDVGPRDGTPVLFLHGNPTSSYVWRNIIPHVAPTHRCIAPDLIGMGKS
DKPDLGYFFDDHVRFMDAFIEALGLEEVVLVIHDWGSALGFHWAKRNPERVKGIAFMEFIRPIP
TWDEWAPGFSSISAHHHHHHHHHH

>cp141-149

MASWSHPQFEKGADDDDKVPHFQAFRTTDVGRKLIIDQNVFIEGTLPMGVVRPLTEVEMDHYRE
PFLNPVDREPLWRFPNELPIAGEPANIVALVEEYMDWLHQSPVPKLLFWGTPGVLIPPAEAARL
AKSLPNCKAVDIGPGLNLLQEDNPDLIGSEIARWLSTLEIGGTGGSGGTGGSGGSIGTGFPFDP
HYVEVLGERMHYVDVGPRDGTPVLFLHGNPTSSYVWRNIIPHVAPTHRCIAPDLIGMGKSDKPD
LGYFFDDHVRFMDAFIEALGLEEVVLVIHDWGSALGFHWAKRNPERVKGIAFMEFIRPIPTWDE
WAPGFSSISAHHHHHHHHHH

>cp154-156

MASWSHPQFEKGADDDDKVPHDVGRKLIIDQNVFIEGTLPMGVVRPLTEVEMDHYREPFLNPVD
REPLWRFPNELPIAGEPANIVALVEEYMDWLHQSPVPKLLFWGTPGVLIPPAEAARLAKSLPNC
KAVDIGPGLNLLQEDNPDLIGSEIARWLSTLEIGGTGGSGGTGGSGGSIGTGFPFDPHYVEVLG
ERMHYVDVGPRDGTPVLFLHGNPTSSYVWRNIIPHVAPTHRCIAPDLIGMGKSDKPDLGYFFDD
HVRFMDAFIEALGLEEVVLVIHDWGSALGFHWAKRNPERVKGIAFMEFIRPIPTWDEWPEFARE
TFQAFRTAPGFSSISAHHHHHHHHHH

>cp163-165

MASWSHPQFEKGADDDDKVPHQNVFIEGTLPMGVVRPLTEVEMDHYREPFLNPVDREPLWRFPN
ELPIAGEPANIVALVEEYMDWLHQSPVPKLLFWGTPGVLIPPAEAARLAKSLPNCKAVDIGPGL
NLLQEDNPDLIGSEIARWLSTLEIGGTGGSGGTGGSGGSIGTGFPFDPHYVEVLGERMHYVDVG
PRDGTPVLFLHGNPTSSYVWRNIIPHVAPTHRCIAPDLIGMGKSDKPDLGYFFDDHVRFMDAFI
EALGLEEVVLVIHDWGSALGFHWAKRNPERVKGIAFMEFIRPIPTWDEWPEFARETFQAFRTTD
VGRKLIIAPGFSSISAHHHHHHHHHH

>cp177-179
MASWSHPQFEKGADDDDKVPHRPLTEVEMDHYREPFLNPVDREPLWRFPNELPIAGEPANIVAL
VEEYMDWLHQSPVPKLLFWGTPGVLIPPAEAARLAKSLPNCKAVDIGPGLNLLQEDNPDLIGSE
IARWLSTLEIGGTGGSGGTGGSGGSIGTGFPFDPHYVEVLGERMHYVDVGPRDGTPVLFLHGNP
TSSYVWRNIIPHVAPTHRCIAPDLIGMGKSDKPDLGYFFDDHVRFMDAFIEALGLEEVVLVIHD
WGSALGFHWAKRNPERVKGIAFMEFIRPIPTWDEWPEFARETFQAFRTTDVGRKLIIDQNVFIE
GTLPMGVAPGFSSISAHHHHHHHHHH

>cp178-179
MASWSHPQFEKGADDDDKVPHRPLTEVEMDHYREPFLNPVDREPLWRFPNELPIAGEPANIVAL
VEEYMDWLHQSPVPKLLFWGTPGVLIPPAEAARLAKSLPNCKAVDIGPGLNLLQEDNPDLIGSE
IARWLSTLEIGGTGGSGGTGGSGGSIGTGFPFDPHYVEVLGERMHYVDVGPRDGTPVLFLHGNP
TSSYVWRNIIPHVAPTHRCIAPDLIGMGKSDKPDLGYFFDDHVRFMDAFIEALGLEEVVLVIHD
WGSALGFHWAKRNPERVKGIAFMEFIRPIPTWDEWPEFARETFQAFRTTDVGRKLIIDQNVFIE
GTLPMGVVAPGFSSISAHHHHHHHHHH

>cp212-213
MASWSHPQFEKGADDDDKVPHGEPANIVALVEEYMDWLHQSPVPKLLFWGTPGVLIPPAEAARL
AKSLPNCKAVDIGPGLNLLQEDNPDLIGSEIARWLSTLEIGGTGGSGGTGGSGGSIGTGFPFDP
HYVEVLGERMHYVDVGPRDGTPVLFLHGNPTSSYVWRNIIPHVAPTHRCIAPDLIGMGKSDKPD
LGYFFDDHVRFMDAFIEALGLEEVVLVIHDWGSALGFHWAKRNPERVKGIAFMEFIRPIPTWDE
WPEFARETFQAFRTTDVGRKLIIDQNVFIEGTLPMGVVRPLTEVEMDHYREPFLNPVDREPLWR
FPNELPIAAPGFSSISAHHHHHHHHHH

>cp212-214
MASWSHPQFEKGADDDDKVPHEPANIVALVEEYMDWLHQSPVPKLLFWGTPGVLIPPAEAARLA
KSLPNCKAVDIGPGLNLLQEDNPDLIGSEIARWLSTLEIGGTGGSGGTGGSGGSIGTGFPFDPH
YVEVLGERMHYVDVGPRDGTPVLFLHGNPTSSYVWRNIIPHVAPTHRCIAPDLIGMGKSDKPDL
GYFFDDHVRFMDAFIEALGLEEVVLVIHDWGSALGFHWAKRNPERVKGIAFMEFIRPIPTWDEW
PEFARETFQAFRTTDVGRKLIIDQNVFIEGTLPMGVVRPLTEVEMDHYREPFLNPVDREPLWRF
PNELPIAAPGFSSISAHHHHHHHHHH

<u>cpHaloTag characterization</u>
>HaloTag
MHHHHHHHHHHENLYFQGIGTGFPFDPHYVEVLGERMHYVDVGPRDGTPVLFLHGNPTSSYVWR
NIIPHVAPTHRCIAPDLIGMGKSDKPDLGYFFDDHVRFMDAFIEALGLEEVVLVIHDWGSALGF
HWAKRNPERVKGIAFMEFIRPIPTWDEWPEFARETFQAFRTTDVGRKLIIDQNVFIEGTLPMGV
VRPLTEVEMDHYREPFLNPVDREPLWRFPNELPIAGEPANIVALVEEYMDWLHQSPVPKLLFWG
TPGVLIPPAEAARLAKSLPNCKAVDIGPGLNLLQEDNPDLIGSEIARWLSTLEI
His-tag; TEVsite; HaloTag

>cpHaloTag154-156
MHHHHHHHHHHENLYFQGGGDVGRKLIIDQNVFIEGTLPMGVVRPLTEVEMDHYREPFLNPVDR
EPLWRFPNELPIAGEPANIVALVEEYMDWLHQSPVPKLLFWGTPGVLIPPAEAARLAKSLPNCK
AVDIGPGLNLLQEDNPDLIGSEIARWLSTLEIGGTGGSGGTGGSGGSIGTGFPFDPHYVEVLGE
RMHYVDVGPRDGTPVLFLHGNPTSSYVWRNIIPHVAPTHRCIAPDLIGMGKSDKPDLGYFFDDH
VRFMDAFIEALGLEEVVLVIHDWGSALGFHWAKRNPERVKGIAFMEFIRPIPTWDEWPEFARET
FQAFRT
His-tag; TEVsite; cpHaloTag; linker

>cpHaloTag141-145
MHHHHHHHHHHENLYFQGGGARETFQAFRTTDVGRKLIIDQNVFIEGTLPMGVVRPLTEVEMDH
YREPFLNPVDREPLWRFPNELPIAGEPANIVALVEEYMDWLHQSPVPKLLFWGTPGVLIPPAEA
ARLAKSLPNCKAVDIGPGLNLLQEDNPDLIGSEIARWLSTLEIGGTGGSGGTGGSGGSIGTGFP
FDPHYVEVLGERMHYVDVGPRDGTPVLFLHGNPTSSYVWRNIIPHVAPTHRCIAPDLIGMGKSD
KPDLGYFFDDHVRFMDAFIEALGLEEVVLVIHDWGSALGFHWAKRNPERVKGIAFMEFIRPIPT
WDEW
His-tag; TEVsite; cpHaloTag; linker

split-HaloTag characterization
>cpHaloΔ
MHHHHHHHHHHENLYFQGDVGRKLIIDQNVFIEGTLPMGVVRPLTEVEMDHYREPFLNPVDREP
LWRFPNELPIAGEPANIVALVEEYMDWLHQSPVPKLLFWGTPGVLIPPAEAARLAKSLPNCKAV
DIGPGLNLLQEDNPDLIGSEIARWLSTLEIGGTGGSGGTGGSGGSIGTGFPFDPHYVEVLGERM
HYVDVGPRDGTPVLFLHGNPTSSYVWRNIIPHVAPTHRCIAPDLIGMGKSDKPDLGYFFDDHVR
FMDAFIEALGLEEVVLVIHDWGSALGFHWAKRNPERVKGIAFMEFIRPI
His-tag; TEVsite; cpHaloΔ; linker

>Hpep1 ARETFQAFRT
>Hpep2 AREMFQAFRT
>Hpep3 SKRDAREMFQAFRT
>Hpep4 WKEEVIKAFKLFRD
>Hpep5 WREEVRKAFKLFRQ
>Hpep6 WRETFQLFRT
>Hpep7 WREMFRLFRT
>Hpep8 WKRDWREMFRLFRT

FKBP/FRB constructs

>cpHaloΔ-(GGS/T)$_3$-FKBP

MASWSHPQFEKGADDDDKVPHGGDVGRKLIIDQNVFIEGTLPMGVVRPLTEVEMDHYREPFLNP
VDREPLWRFPNELPIAGEPANIVALVEEYMDWLHQSPVPKLLFWGTPGVLIPPAEAARLAKSLP
NCKAVDIGPGLNLLQEDNPDLIGSEIARWLSTLEIGGTGGSGGTGGSGGSIGTGFPFDPHYVEV
LGERMHYVDVGPRDGTPVLFLHGNPTSSYVWRNIIPHVAPTHRCIAPDLIGMGKSDKPDLGYFF
DDHVRFMDAFIEALGLEEVVLVIHDWGSALGFHWAKRNPERVKGIAFMEFIRPIPTWDEWGGSG
GTGGSMGVQVETISPGDGRTFPKRGQTCVVHYTGMLEDGKKFDSSRDRNKPFKFMLGKQEVIRG
WEEGVAQMSVGQRAKLTISPDYAYGATGHPGIIPPHATLVFDVELLKLEAPGFSSISAHHHHHH
HHHH

FKBP; Strep-tag; His-tag; cpHaloΔ; linker

>cpHaloΔ-(GGS/T)$_9$-FKBP

MASWSHPQFEKGADDDDKVPHGGDVGRKLIIDQNVFIEGTLPMGVVRPLTEVEMDHYREPFLNP
VDREPLWRFPNELPIAGEPANIVALVEEYMDWLHQSPVPKLLFWGTPGVLIPPAEAARLAKSLP
NCKAVDIGPGLNLLQEDNPDLIGSEIARWLSTLEIGGTGGSGGTGGSGGSIGTGFPFDPHYVEV
LGERMHYVDVGPRDGTPVLFLHGNPTSSYVWRNIIPHVAPTHRCIAPDLIGMGKSDKPDLGYFF
DDHVRFMDAFIEALGLEEVVLVIHDWGSALGFHWAKRNPERVKGIAFMEFIRPIPTWDEWGSGG
TGGSGGSGGTGGSGGSGGTGGSGMGVQVETISPGDGRTFPKRGQTCVVHYTGMLEDGKKFDSSR
DRNKPFKFMLGKQEVIRGWEEGVAQMSVGQRAKLTISPDYAYGATGHPGIIPPHATLVFDVELL
KLEAPGFSSISAHHHHHHHHHH

FKBP; Strep-tag; His-tag; cpHaloΔ; linker

>Hpep1-(GGS/T)$_3$-FRB

MASWSHPQFEKGADDDDKVPHGGARETFQAFRTGGSGGTGGSAILWHEMWHEGLEEASRLYFGE
RNVKGMFEVLEPLHAMMERGPQTLKETSFNQAYGRDLMEAQEWCRKYMKSGNVKDLLQAWDLYY
HVFRRISKAPGFSSISAHHHHHHHHHH

FRB; Strep-tag; His-tag; Hpep; linker

> Lyn11-mEGFP-FKBP-(GGS)-cpHaloΔ-P2A-FRB-(GGS)-Hpep1-mScarlet

MGCIKSKGKDSAGADSAGSAGMVSKGEELFTGVVPILVELDGDVNGHKFSVSGEGEGDATYGKL
TLKFICTTGKLPVPWPTLVTTLTYGVQCFSRYPDHMKQHDFFKSAMPEGYVQERTIFFKDDGNY
KTRAEVKFEGDTLVNRIELKGIDFKEDGNILGHKLEYNYNSHNVYIMADKQKNGIKVNFKIRHN
IEDGSVQLADHYQQNTPIGDGPVLLPDNHYLSTQSALSKDPNEKRDHMVLLEFVTAAGITLGMD
ELYKGSGMGVQVETISPGDGRTFPKRGQTCVVHYTGMLEDGKKFDSSRDRNKPFKFMLGKQEVI
RGWEEGVAQMSVGQRAKLTISPDYAYGATGHPGIIPPHATLVFDVELLKLEGGSDVGRKLIIDQ
NVFIEGTLPMGVVRPLTEVEMDHYREPFLNPVDREPLWRFPNELPIAGEPANIVALVEEYMDWL
HQSPVPKLLFWGTPGVLIPPAEAARLAKSLPNCKAVDIGPGLNLLQEDNPDLIGSEIARWLSTL
EIGGTGGSGGTGGSGGSIGTGFPFDPHYVEVLGERMHYVDVGPRDGTPVLFLHGNPTSSYVWRN
IIPHVAPTHRCIAPDLIGMGKSDKPDLGYFFDDHVRFMDAFIEALGLEEVVLVIHDWGSALGFH
WAKRNPERVKGIAFMEFIRPIPTWDEWGSGATNFSLLKQAGDVEENPGPGGSAILWHEMWHEGL
EEASRLYFGERNVKGMFEVLEPLHAMMERGPQTLKETSFNQAYGRDLMEAQEWCRKYMKSGNVK
DLLQAWDLYYHVFRRISKGGSARETFQAFRTGSGGSGVSKGEAVIKEFMRFKVHMEGSMNGHEF
EIEGEGEGRPYEGTQTAKLKVTKGGPLPFSWDILSPQFMYGSRAFTKHPADIPDYYKQSFPEGF
KWERVMNFEDGGAVTVTQDTSLEDGTLIYKVKLRGTNFPPDGPVMQKKTMGWEASTERLYPEDG
VLKGDIKMALRLKDGGRYLADFKTTYKAKKPVQMPGAYNVDRKLDITSHNEDYTVVEQYERSEG
RHSTG

FRB; FKBP; Strep-tag; Lyn11; cpHaloΔ; Hpep; mEGFP; mScarlet; P2A; linker

> Lyn11-mEGFP-FKBP-(GGS)-cpHaloΔ-P2A-FRB-(GGS)-Hpep3-mScarlet

MGCIKSKGKDSAGADSAGSAGMVSKGEELFTGVVPILVELDGDVNGHKFSVSGEGEGDATYGKL
TLKFICTTGKLPVPWPTLVTTLTYGVQCFSRYPDHMKQHDFFKSAMPEGYVQERTIFFKDDGNY
KTRAEVKFEGDTLVNRIELKGIDFKEDGNILGHKLEYNYNSHNVYIMADKQKNGIKVNFKIRHN
IEDGSVQLADHYQQNTPIGDGPVLLPDNHYLSTQSALSKDPNEKRDHMVLLEFVTAAGITLGMD
ELYKGSGMGVQVETISPGDGRTFPKRGQTCVVHYTGMLEDGKKFDSSRDRNKPFKFMLGKQEVI
RGWEEGVAQMSVGQRAKLTISPDYAYGATGHPGIIPPHATLVFDVELLKLEGGSDVGRKLIIDQ
NVFIEGTLPMGVVRPLTEVEMDHYREPFLNPVDREPLWRFPNELPIAGEPANIVALVEEYMDWL
HQSPVPKLLFWGTPGVLIPPAEAARLAKSLPNCKAVDIGPGLNLLQEDNPDLIGSEIARWLSTL
EIGGTGGSGGTGGSGGSIGTGFPFDPHYVEVLGERMHYVDVGPRDGTPVLFLHGNPTSSYVWRN
IIPHVAPTHRCIAPDLIGMGKSDKPDLGYFFDDHVRFMDAFIEALGLEEVVLVIHDWGSALGFH
WAKRNPERVKGIAFMEFIRPIPTWDEWGSGATNFSLLKQAGDVEENPGPGGSAILWHEMWHEGL
EEASRLYFGERNVKGMFEVLEPLHAMMERGPQTLKETSFNQAYGRDLMEAQEWCRKYMKSGNVK
DLLQAWDLYYHVFRRISKGGSSKRDAREMFQAFRTGSGGSGVSKGEAVIKEFMRFKVHMEGSMN
GHEFEIEGEGEGRPYEGTQTAKLKVTKGGPLPFSWDILSPQFMYGSRAFTKHPADIPDYYKQSF
PEGFKWERVMNFEDGGAVTVTQDTSLEDGTLIYKVKLRGTNFPPDGPVMQKKTMGWEASTERLY
PEDGVLKGDIKMALRLKDGGRYLADFKTTYKAKKPVQMPGAYNVDRKLDITSHNEDYTVVEQYE
RSEGRHSTG

FRB; FKBP; Strep-tag; Lyn11; cpHaloΔ; Hpep; mEGFP; mScarlet; P2A; linker

> Lyn11-mEGFP-cpHaloΔ-(GGS)9-FKBP-P2A-Hpep1-(GGS)3-FRB-mScarlet

MGCIKSKGKDSAGADSAGSAGMVSKGEELFTGVVPILVELDGDVNGHKFSVSGEGEGDATYGKL
TLKFICTTGKLPVPWPTLVTTLTYGVQCFSRYPDHMKQHDFFKSAMPEGYVQERTIFFKDDGNY
KTRAEVKFEGDTLVNRIELKGIDFKEDGNILGHKLEYNYNSHNVYIMADKQKNGIKVNFKIRHN
IEDGSVQLADHYQQNTPIGDGPVLLPDNHYLSTQSALSKDPNEKRDHMVLLEFVTAAGITLGMD
ELYKGSGGSGDVGRKLIIDQNVFIEGTLPMGVVRPLTEVEMDHYREPFLNPVDREPLWRFPNEL
PIAGEPANIVALVEEYMDWLHQSPVPKLLFWGTPGVLIPPAEAARLAKSLPNCKAVDIGPGLNL
LQEDNPDLIGSEIARWLSTLEIGGTGGSGGTGGSGGSIGTGFPFDPHYVEVLGERMHYVDVGPR
DGTPVLFLHGNPTSSYVWRNIIPHVAPTHRCIAPDLIGMGKSDKPDLGYFFDDHVRFMDAFIEA
LGLEEVVLVIHDWGSALGFHWAKRNPERVKGIAFMEFIRPIPTWDEWGSGGTGGSGGSGGTGGS
GGSGGTGGSGMGVQVETISPGDGRTFPKRGQTCVVHYTGMLEDGKKFDSSRDRNKPFKFMLGKQ
EVIRGWEEGVAQMSVGQRAKLTISPDYAYGATGHPGIIPPHATLVFDVELLKLEGSGATNFSLL
KQAGDVEENPGPGGSARETFQAFRTGGSGGTGGSAILWHEMWHEGLEEASRLYFGERNVKGMFE
VLEPLHAMMERGPQTLKETSFNQAYGRDLMEAQEWCRKYMKSGNVKDLLQAWDLYYHVFRRISK
GSGVSKGEAVIKEFMRFKVHMEGSMNGHEFEIEGEGEGRPYEGTQTAKLKVTKGGPLPFSWDIL
SPQFMYGSRAFTKHPADIPDYYKQSFPEGFKWERVMNFEDGGAVTVTQDTSLEDGTLIYKVKLR
GTNFPPDGPVMQKKTMGWEASTERLYPEDGVLKGDIKMALRLKDGGRYLADFKTTYKAKKPVQM
PGAYNVDRKLDITSHNEDYTVVEQYERSEGRHSTG

FRB; FKBP; Strep-tag; Lyn11; cpHaloΔ; Hpep; mEGFP; mScarlet; P2A; linker

> Lyn11-mEGFP-cpHaloΔ-(GGS)9-FKBP-P2A-Hpep3-(GGS)3-FRB-mScarlet

MGCIKSKGKDSAGADSAGSAGMVSKGEELFTGVVPILVELDGDVNGHKFSVSGEGEGDATYGKL
TLKFICTTGKLPVPWPTLVTTLTYGVQCFSRYPDHMKQHDFFKSAMPEGYVQERTIFFKDDGNY
KTRAEVKFEGDTLVNRIELKGIDFKEDGNILGHKLEYNYNSHNVYIMADKQKNGIKVNFKIRHN
IEDGSVQLADHYQQNTPIGDGPVLLPDNHYLSTQSALSKDPNEKRDHMVLLEFVTAAGITLGMD

ELYKGSGGSGDVGRKLIIDQNVFIEGTLPMGVVRPLTEVEMDHYREPFLNPVDREPLWRFPNEL
PIAGEPANIVALVEEYMDWLHQSPVPKLLFWGTPGVLIPPAEAARLAKSLPNCKAVDIGPGLNL
LQEDNPDLIGSEIARWLSTLEIGGTGGSGGTGGSGGSIGTGFPFDPHYVEVLGERMHYVDVGPR
DGTPVLFLHGNPTSSYVWRNIIPHVAPTHRCIAPDLIGMGKSDKPDLGYFFDDHVRFMDAFIEA
LGLEEVVLVIHDWGSALGFHWAKRNPERVKGIAFMEFIRPIPTWDEWGSGGTGGSGGSGGTGGS
GGSGGTGGSGMGVQVETISPGDGRTFPKRGQTCVVHYTGMLEDGKKFDSSRDRNKPFKFMLGKQ
EVIRGWEEGVAQMSVGQRAKLTISPDYAYGATGHPGIIPPHATLVFDVELLKLEGSGATNFSLL
KQAGDVEENPGPGGSSKRDAREMFQAFRTGGSGGTGGSAILWHEMWHEGLEEASRLYFGERNVK
GMFEVLEPLHAMMERGPQTLKETSFNQAYGRDLMEAQEWCRKYMKSGNVKDLLQAWDLYYHVFR
RISKGSGVSKGEAVIKEFMRFKVHMEGSMNGHEFEIEGEGEGRPYEGTQTAKLKVTKGGPLPFS
WDILSPQFMYGSRAFTKHPADIPDYYKQSFPEGFKWERVMNFEDGGAVTVTQDTSLEDGTLIYK
VKLRGTNFPPDGPVMQKKTMGWEASTERLYPEDGVLKGDIKMALRLKDGGRYLADFKTTYKAKK
PVQMPGAYNVDRKLDITSHNEDYTVVEQYERSEGRHSTG

FRB; FKBP; Strep-tag; Lyn11; cpHaloΔ; Hpep; mEGFP; mScarlet; P2A; linker

GPCR characterizations

>DRD2-V2-GGS/T3-cpHalo-mEGFP (positive control)

MKTIIALSYIFCLVFADYKDDDDASIDMDPLNLSWYDDDLERQNWSRPFNGSDGKADRPHYNYY
ATLLTLLIAVIVFGNVLVCMAVSREKALQTTTNYLIVSLAVADLLVATLVMPWVVYLEVVGEWK
FSRIHCDIFVTLDVMMCTASILNLCAISIDRYTAVAMPMLYNTRYSSKRRVTVMISIVWVLSFT
ISCPLLFGLNNADQNECIIANPAFVVYSSIVSFYVPFIVTLLVYIKIYIVLRRRRKRVNTKRSS
RAFRAHLRAPLKGNCTHPEDMKLCTVIMKSNGSFPVNRRRVEAARRAQELEMEMLSSTSPPERT
RYSPIPPSHHQLTLPDPSHHGLHSTPDSPAKPEKNGHAKDHPKIAKIFEIQTMPNGKTRTSLKT
MSRRKLSQQKEKKATQMLAIVLGVFIICWLPFFITHILNIHCDCNIPPVLYSAFTWLGYVNSAV
NPIIYTTFNIEFRKAFLKILHCGRTPPSLGPQDESCTTASSSLAKDTSSFARETFQAFRTTDVG
RKLIIDQNVFIEGTLPMGVVRPLTEVEMDHYREPFLNPVDREPLWRFPNELPIAGEPANIVALV
EEYMDWLHQSPVPKLLFWGTPGVLIPPAEAARLAKSLPNCKAVDIGPGLNLLQEDNPDLIGSEI
ARWLSTLEIGGTGGSGGTGGSGGSIGTGFPFDPHYVEVLGERMHYVDVGPRDGTPVLFLHGNPT
SSYVWRNIIPHVAPTHRCIAPDLIGMGKSDKPDLGYFFDDHVRFMDAFIEALGLEEVVLVIHDW
GSALGFHWAKRNPERVKGIAFMEFIRPIPTWDEWGGSMVSKGEELFTGVVPILVELDGDVNGHK
FSVSGEGEGDATYGKLTLKFICTTGKLPVPWPTLVTTLTYGVQCFSRYPDHMKQHDFFKSAMPE
GYVQERTIFFKDDGNYKTRAEVKFEGDTLVNRIELKGIDFKEDGNILGHKLEYNYNSHNVYIMA
DKQKNGIKVNFKIRHNIEDGSVQLADHYQQNTPIGDGPVLLPDNHYLSTQSKLSKDPNEKRDHM
VLLEFVTAAGITLGMDELYK

HA-Tag+FLAG-Tag; DRD2-TANGO; His-tag; V2 tail; cpHalo; mEGFP; linker

>Hpep-GGS/T3-betaArrestin2-T2A-mTagBFP2

MARETFQAFRTGGSGGTGGSMGEKPGTRVFKKSSPNCKLTVYLGKRDFVDHLDKVDPVDGVVLV
DPDYLKDRKVFVTLTCAFRYGREDLDVLGLSFRKDLFIATYQAFPPVPNPPRPPTRLQDRLLRK
LGQHAHPFFFTIPQNLPCSVTLQPGPEDTGKACGVDFEIRAFCAKSLEEKSHKRNSVRLVIRKV
QFAPEKPGPQPSAETTRHFLMSDRSLHLEASLDKELYYHGEPLNVNVHVTNNSTKTVKKIKVSV
RQYADICLFSTAQYKCPVAQLEQDDQVSPSSTFCKVYTITPLLSDNREKRGLALDGKLKHEDTN
LASSTIVKEGANKEVLGILVSYRVKVKLVVSRGGDVSVELPFVLMHPKPHDHIPLPRPQSAAPE
TDVPVDTNLIEFDTNYATDDDIVFEDFARLRLKGMKDDDYDDQLCGSGEGRGSLLTCGDVEENP
GPMVSKGEELIKENMHMKLYMEGTVDNHHFKCTSEGEGKPYEGTQTMRIKVVEGGPLPFAFDIL
ATSFLYGSKTFINHTQGIPDFFKQSFPEGFTWERVTTYEDGGVLTATQDTSLQDGCLIYNVKIR
GVNFTSNGPVMQKKTLGWEAFTETLYPADGGLEGRNDMALKLVGGSHLIANAKTTYRSKKPAKN
LKMPGVYYVDYRLERIKEANNETYVEQHEVAVARYCDLPSKLGHKLN

Hpep; β-Arrestin2; T2A; TagBFP2; linker

> DRD2-V2-GGS/T3-cpHaloΔ-mEGFP

MKTIIALSYIFCLVFADYKDDDDASIDMDPLNLSWYDDDLERQNWSRPFNGSDGKADRPHYNYY
ATLLTLLIAVIVFGNVLVCMAVSREKALQTTTNYLIVSLAVADLLVATLVMPWVVYLEVVGEWK
FSRIHCDIFVTLDVMMCTASILNLCAISIDRYTAVAMPMLYNTRYSSKRRVTVMISIVWVLSFT
ISCPLLFGLNNADQNECIIANPAFVVYSSIVSFYVPFIVTLLVYIKIYIVLRRRRKRVNTKRSS
RAFRAHLRAPLKGNCTHPEDMKLCTVIMKSNGSFPVNRRRVEAARRAQELEMEMLSSTSPPERT
RYSPIPPSHHQLTLPDPSHHGLHSTPDSPAKPEKNGHAKDHPKIAKIFEIQTMPNGKTRTSLKT
MSRRKLSQQKEKKATQMLAIVLGVFIICWLPFFITHILNIHCDCNIPPVLYSAFTWLGYVNSAV
NPIIYTTFNIEFRKAFLKILHCGRTPPSLGPQDESCTTASSSLAKDTSSGGDVGRKLIIDQNVF
IEGTLPMGVVRPLTEVEMDHYREPFLNPVDREPLWRFPNELPIAGEPANIVALVEEYMDWLHQS
PVPKLLFWGTPGVLIPPAEAARLAKSLPNCKAVDIGPGLNLLQEDNPDLIGSEIARWLSTLEIG
GTGGSGGTGGSGGSIGTGFPFDPHYVEVLGERMHYVDVGPRDGTPVLFLHGNPTSSYVWRNIIP

HVAPTHRCIAPDLIGMGKSDKPDLGYFFDDHVRFMDAFIEALGLEEVVLVIHDWGSALGFHWAK
RNPERVKGIAFMEFIRPIPTWDEWGGSMVSKGEELFTGVVPILVELDGDVNGHKFSVSGEGEGD
ATYGKLTLKFICTTGKLPVPWPTLVTTLTYGVQCFSRYPDHMKQHDFFKSAMPEGYVQERTIFF
KDDGNYKTRAEVKFEGDTLVNRIELKGIDFKEDGNILGHKLEYNYNSHNVYIMADKQKNGIKVN
FKIRHNIEDGSVQLADHYQQNTPIGDGPVLLPDNHYLSTQSKLSKDPNEKRDHMVLLEFVTAAG
ITLGMDELYK
HA-Tag+FLAG-Tag; DRD2; V2 tail; Hpep; mEGFP; cpHaloΔ; linker

> DRD2-V2 -Hpep-mEGFP
MKTIIALSYIFCLVFADYKDDDDASIDMDPLNLSWYDDDLERQNWSRPFNGSDGKADRPHYNYY
ATLLTLLIAVIVFGNVLVCMAVSREKALQTTTNYLIVSLAVADLLVATLVMPWVVYLEVVGEWK
FSRIHCDIFVTLDVMMCTASILNLCAISIDRYTAVAMPMLYNTRYSSKRRVTVMISIVWVLSFT
ISCPLLFGLNNADQNECIIANPAFVVYSSIVSFYVPFIVTLLVYIKIYIVLRRRRKRVNTKRSS
RAFRAHLRAPLKGNCTHPEDMKLCTVIMKSNGSFPVNRRRVEAARRAQELEMEMLSSTSPPERT
RYSPIPPSHHQLTLPDPSHHGLHSTPDSPAKPEKNGHAKDHPKIAKIFEIQTMPNGKTRTSLKT
MSRRKLSQQKEKKATQMLAIVLGVFIICWLPFFITHILNIHCDCNIPPVLYSAFTWLGYVNSAV
NPIIYTTFNIEFRKAFLKILHCGRTPPSLGPQDESCTTASSSLAKDTSSGGARETFQAFRTGGS
MVSKGEELFTGVVPILVELDGDVNGHKFSVSGEGEGDATYGKLTLKFICTTGKLPVPWPTLVTT
LTYGVQCFSRYPDHMKQHDFFKSAMPEGYVQERTIFFKDDGNYKTRAEVKFEGDTLVNRIELKG
IDFKEDGNILGHKLEYNYNSHNVYIMADKQKNGIKVNFKIRHNIEDGSVQLADHYQQNTPIGDG
PVLLPDNHYLSTQSKLSKDPNEKRDHMVLLEFVTAAGITLGMDELYK
HA-Tag+FLAG-Tag; DRD2-TANGO; V2 tail; Hpep; mEGFP; linker

> CHRM3-V2-GGS/T3-cpHaloΔ-mEGFP
MKTIIALSYIFCLVFADYKDDDDASIDMTLHNNSTTSPLFPNISSSWIHSPSDAGLPPGTVTHF
GSYNVSRAAGNFSSPDGTTDDPLGGHTVWQVVFIAFLTGILALVTIIGNILVIVSFKVNKQLKT
VNNYFLLSLACADLIIGVISMNLFTTYIIMNRWALGNLACDLWLAIDYVASNASVMNLLVISFD
RYFSITRPLTYRAKRTTKRAGVMIGLAWVISFVLWAPAILFWQYFVGKRTVPPGECFIQFLSEP
TITFGTAIAAFYMPVTIMTILYWRIYKETEKRTKELAGLQASGTEAETENFVHPTGSSRSCSSY
ELQQQSMKRSNRRKYGRCHFWFTTKSWKPSSEQMDQDHSSSDSWNNNDAAASLENSASSDEEDI
GSETRAIYSIVLKLPGHSTILNSTKLPSSDNLQVPEEELGMVDLERKADKLQAQKSVDDGGSFP
KSFSKLPIQLESAVDTAKTSDVNSSVGKSTATLPLSFKEATLAKRFALKTRSQITKRKRMSLVK
EKKAAQTLSAILLAFIITWTPYNIMVLVNTFCDSCIPKTFWNLGYWLCYINSTVNPVCYALCNK
TFRTTFKMLLLCQCDKKKRRKQQYQQRQSVIFHKRAPEQALGRTPPSLGPQDESCTTASSSLAK
DTSSGGDVGRKLIIDQNVFIEGTLPMGVVRPLTEVEMDHYREPFLNPVDREPLWRFPNELPIAG
EPANIVALVEEYMDWLHQSPVPKLLFWGTPGVLIPPAEAARLAKSLPNCKAVDIGPGLNLLQED
NPDLIGSEIARWLSTLEIGGTGGSGGTGGSGGSIGTGFPFDPHYVEVLGERMHYVDVGPRDGTP
VLFLHGNPTSSYVWRNIIPHVAPTHRCIAPDLIGMGKSDKPDLGYFFDDHVRFMDAFIEALGLE
EVVLVIHDWGSALGFHWAKRNPERVKGIAFMEFIRPIPTWDEWGGSMVSKGEELFTGVVPILVE
LDGDVNGHKFSVSGEGEGDATYGKLTLKFICTTGKLPVPWPTLVTTLTYGVQCFSRYPDHMKQH
DFFKSAMPEGYVQERTIFFKDDGNYKTRAEVKFEGDTLVNRIELKGIDFKEDGNILGHKLEYNY
NSHNVYIMADKQKNGIKVNFKIRHNIEDGSVQLADHYQQNTPIGDGPVLLPDNHYLSTQSKLSK
DPNEKRDHMVLLEFVTAAGITLGMDELYK
HA-Tag+FLAG-Tag; CHRM3; V2 tail; Hpep; mEGFP; cpHaloΔ; linker

> GRM2-V2-GGS/T3-cpHaloΔ-mEGFP

MKTIIALSYIFCLVFADYKDDDDASIDSLLALLALLLLWGAVAEGPAKKVLTLEGDLVLGGLFP
VHQKGGPAEDCGPVNEHRGIQRLEAMLFALDRINRDPHLLPGVRLGAHILDSCSKDTHALEQAL
DFVRASLSRGADGSRHICPDGSYATHGDAPTAITGVIGGSYSDVSIQVANLLRLFQIPQISYAS
TSAKLSDKSRYDYFARTVPPDFFQAKAMAEILRFFNWTYVSTVASEGDYGETGIEAFELEARAR
NICVATSEKVGRAMSRAAFEGVVRALLQKPSARVAVLFTRSEDARELLAASQRLNASFTWVASD
GWGALESVVAGSEGAAEGAITIELASYPISDFASYFQSLDPWNNSRNPWFREFWEQRFRCSFRQ
RDCAAHSLRAVPFEQESKIMFVVNAVYAMAHALHNMHRALCPNTTRLCDAMRPVNGRRLYKDFV
LNVKFDAPFRPADTHNEVRFDRFGDGIGRYNIFTYLRAGSGRYRYQKVGYWAEGLTLDTSLIPW
ASPSAGPLPASRCSEPCLQNEVKSVQPGEVCCWLCIPCQPYEYRLDEFTCADCGLGYWPNASLT
GCFELPQEYIRWGDAWAVGPVTIACLGALATLFVLGVFVRHNATPVVKASGRELCYILLGGVFL
CYCMTFIFIAKPSTAVCTLRRLGLGTAFSVCYSALLTKTNRIARIFGGAREGAQRPRFISPASQ
VAICLALISGQLLIVVAWLVVEAPGTGKETAPERREVVTLRCNHRDASMLGSLAYNVLLIALCT
LYAFKTRKCPENFNEAKFIGFTMYTTCIIWLAFLPIFYVTSSDYRVQTTTMCVSVSLSGSVVLG
CLFAPKLHIILFQPQKNVVSHRAPTSRFGSAAARASSSLGQGSGSQFVPTVCNGREVVDSTTSS
GRTPPSLGPQDESCTTASSSLAKDTSSGGDVGRKLIIDQNVFIEGTLPMGVVRPLTEVEMDHYR
EPFLNPVDREPLWRFPNELPIAGEPANIVALVEEYMDWLHQSPVPKLLFWGTPGVLIPPAEAAR
LAKSLPNCKAVDIGPGLNLLQEDNPDLIGSEIARWLSTLEIGGTGGSGGTGGSGGSIGTGFPFD
PHYVEVLGERMHYVDVGPRDGTPVLFLHGNPTSSYVWRNIIPHVAPTHRCIAPDLIGMGKSDKP
DLGYFFDDHVRFMDAFIEALGLEEVVLVIHDWGSALGFHWAKRNPERVKGIAFMEFIRPIPTWD
EWGGSMVSKGEELFTGVVPILVELDGDVNGHKFSVSGEGEGDATYGKLTLKFICTTGKLPVPWP
TLVTTLTYGVQCFSRYPDHMKQHDFFKSAMPEGYVQERTIFFKDDGNYKTRAEVKFEGDTLVNR
IELKGIDFKEDGNILGHKLEYNYNSHNVYIMADKQKNGIKVNFKIRHNIEDGSVQLADHYQQNT
PIGDGPVLLPDNHYLSTQSKLSKDPNEKRDHMVLLEFVTAAGITLGMDELYK
HA-Tag+FLAG-Tag; GRM2; V2 tail; Hpep; mEGFP; cpHaloΔ; linker

> GABBR1-V2-GGS/T3-cpHaloΔ-mEGFP
MKTIIALSYIFCLVFADYKDDDDASIDLLLLLLAPLFLRPPGAGGAQTPNATSEGCQIIHPPWE
GGIRYRGLTRDQVKAINFLPVDYEIEYVCRGEREVVGPKVRKCLANGSWTDMDTPSRCVRICSK
SYLTLENGKVFLTGGDLPALDGARVDFRCDPDFHLVGSSRSICSQGQWSTPKPHCQVNRTPHSE
RRAVYIGALFPMSGGWPGGQACQPAVEMALEDVNSRRDILPDYELKLIHHDSKCDPGQATKYLY
ELLYNDPIKIILMPGCSSVSTLVAEAARMWNLIVLSYGSSSPALSNRQRFPTFFRTHPSATLHN
PTRVKLFEKWGWKKIATIQQTTEVFTSTLDDLEERVKEAGIEITFRQSFFSDPAVPVKNLKRQD
ARIIVGLFYETEARKVFCEVYKERLFGKKYVWFLIGWYADNWFKIYDPSINCTVDEMTEAVEGH
ITTEIVMLNPANTRSISNMTSQEFVEKLTKRLKRHPEETGGFQEAPLAYDAIWALALALNKTSG
GGGRSGVRLEDFNYNNQTITDQIYRAMNSSSFEGVSGHVVFDASGSRMAWTLIEQLQGGSYKKI
GYYDSTKDDLSWSKTDKWIGGSPPADQTLVIKTFRFLSQKLFISVSVLSSLGIVLAVVCLSFNI
YNSHVRYIQNSQPNLNNLTAVGCSLALAAVFPLGLDGYHIGRNQFPFVCQARLWLLGLGFSLGY
GSMFTKIWWVHTVFTKKEEKKEWRKTLEPWKLYATVGLLVGMDVLTLAIWQIVDPLHRTIETFA
KEEPKEDIDVSILPQLEHCSSRKMNTWLGIFYGYKGLLLLLGIFLAYETKSVSTEKINDHRAVG
MAIYNVAVLCLITAPVTMILSSQQDAAFAFASLAIVFSSYITLVVLFVPKMRRLITRGEWQSEA
QDTMKTGSSTNNNEEEKSRLLEKENRELEKIIAEKEERVSELRHQLQSRQQLRSRRHPPTPPEP
SGGLPRGPPEPPDRLSCDGSRVHLLYKGRTPPSLGPQDESCTTASSSLAKDTSSGGDVGRKLII
DQNVFIEGTLPMGVVRPLTEVEMDHYREPFLNPVDREPLWRFPNELPIAGEPANIVALVEEYMD
WLHQSPVPKLLFWGTPGVLIPPAEAARLAKSLPNCKAVDIGPGLNLLQEDNPDLIGSEIARWLS
TLEIGGTGGSGGTGGSGGSIGTGFPFDPHYVEVLGERMHYVDVGPRDGTPVLFLHGNPTSSYVW
RNIIPHVAPTHRCIAPDLIGMGKSDKPDLGYFFDDHVRFMDAFIEALGLEEVVLVIHDWGSALG
FHWAKRNPERVKGIAFMEFIRPIPTWDEWGGSMVSKGEELFTGVVPILVELDGDVNGHKFSVSG

EGEGDATYGKLTLKFICTTGKLPVPWPTLVTTLTYGVQCFSRYPDHMKQHDFFKSAMPEGYVQE
RTIFFKDDGNYKTRAEVKFEGDTLVNRIELKGIDFKEDGNILGHKLEYNYNSHNVYIMADKQKN
GIKVNFKIRHNIEDGSVQLADHYQQNTPIGDGPVLLPDNHYLSTQSKLSKDPNEKRDHMVLLEF
VTAAGITLGMDELYK

HA-Tag+FLAG-Tag; GRM2; V2 tail; Hpep; mEGFP; cpHaloΔ; linker

Caprola

>Caprola$_1$

(M)ARETFQAFRTGSDQLTEEQIAEFKEAFSLFDKDGDGTITTKELGTVMRSLGQNPTEAELQD
MINEVDADGDGTIDFPEFLTMMARKMKDTDSEEEIREAFRVFDKDGNGYISAAELRHVMTNLGE
KLTDEEVDEMIREADIDGDGQVNYEEFVVMMTAKEFPPPPPPPPPPPPPPPPPPPPPPPPPPP
PPGGSRVDSSRRKMNKTGHALRAIGRLSSLEGGSDVGRKLIIDQNVFIEGTLPMGVVRPLTEVE
MDHYREPFLNPVDREPLWRFPNELPIAGEPANIVALVEEYMDWLHQSPVPKLLFWGTPGVLIPP
AEAARLAKSLPNCKAVDIGPGLNLLQEDNPDLIGSEIARWLSTLEIGGTGGSGGTGGSGGSIGT
GFPFDPHYVEVLGERMHYVDVGPRDGTPVLFLHGNPTSSYVWRNIIPHVAPTHRCIAPDLIGMG
KSDKPDLGYFFDDHVRFMDAFIEALGLEEVVLVIHDWGSALGFHWAKRNPERVKGIAFMEFIRP
IPTWDEW

>Caprola$_{off}$

(M)DQLTEEQIAEFKEAFSLFDKDGDGTITTKELGTVMRSLGQNPTEAELQDMINEVDADGDGT
IDFPEFLTMMARKMKDTDSEEEIREAFRVFDKDGNGYISAAELRHVMTNLGEKLTDEEVDEMIR
EADIDGDGQVNYEEFVVMMTAKEFPPPPPPPPPPPPPPPPPPPPPPPPPPPPGGSRVDSSRR
KMNKTGHALRAIGRLSSLEGGSDVGRKLIIDQNVFIEGTLPMGVVRPLTEVEMDHYREPFLNPV
DREPLWRFPNELPIAGEPANIVALVEEYMDWLHQSPVPKLLFWGTPGVLIPPAEAARLAKSLPN
CKAVDIGPGLNLLQEDNPDLIGSEIARWLSTLEIGGTGGSGGTGGSGGSIGTGFPFDPHYVEVL
GERMHYVDVGPRDGTPVLFLHGNPTSSYVWRNIIPHVAPTHRCIAPDLIGMGKSDKPDLGYFFD
DHVRFMDAFIEALGLEEVVLVIHDWGSALGFHWAKRNPERVKGIAFMEFIRPIPTWDEW

>Caprola$_{on}$

(M)ARETFQAFRTGSDQLTEEQIAEFKEAFSLFDKDGDGTITTKELGTVMRSLGQNPTEAELQD
MINEVDADGDGTIDFPEFLTMMARKMKDTDSEEEIREAFRVFDKDGNGYISAAELRHVMTNLGE
KLTDEEVDEMIREADIDGDGQVNYEEFVVMMTAKEFPPPPPPPPPPPPPPPPPPPPPPPPPPP
PPGGSRVDSSRRKLNKTGHALRAIGRLSSLEGGSFARETFQAFRTTDVGRKLIIDQNVFIEGTL
PMGVVRPLTEVEMDHYREPFLNPVDREPLWRFPNELPIAGEPANIVALVEEYMDWLHQSPVPKL
LFWGTPGVLIPPAEAARLAKSLPNCKAVDIGPGLNLLQEDNPDLIGSEIARWLSTLEIGGTGGS
GGTGGSGGSIGTGFPFDPHYVEVLGERMHYVDVGPRDGTPVLFLHGNPTSSYVWRNIIPHVAPT
HRCIAPDLIGMGKSDKPDLGYFFDDHVRFMDAFIEALGLEEVVLVIHDWGSALGFHWAKRNPER
VKGIAFMEFIRPIPTWDEW

Hpep; Calmodulin; M13; cpHalo; cpHaloΔ; linker

M13 sequences

Caprola$_1$ RVDSSRRKWNKTGHALRAIGRLSSLE
Caprola$_2$ RVDSSRRKWNKTGHAVRAIGRLSSLE
Caprola$_3$ RVDSSRRKFNKAGHALRAIGRLSSLE
Caprola$_4$ RVDSSRRKFNKTGHAVRAIGRLSSLE
Caprola$_5$ RVDSSRRKFNKTAHALRAIGRLSSLE
Caprola$_6$ RVDSSRRKFNKTGHALRAIGRLSSLE
Caprola$_7$ RVDSSRRKLNKTGHALRAIGRLSSLE
Caprola$_8$ RVDSSRRKWNKTGHATRAIGRLSSLE
Caprola$_9$ RVDSSRRKMNKTGHALRAIGRLSSLE
Caprola$_{10}$ RVDSSRRKVNKTGHALRAIGRLSSLE
Caprola$_{11}$ RVDSSRRKWNKTDHALRAIGRLSSLE
Caprola$_{12}$ RVDSSRRKYNKTGHALRAIGRLSSLE
Caprola$_{13}$ RVDSSRRKFNKTGKALRAIGRLSSLE
Caprola$_{14}$ RVDSSRRKFNKTGHATRAIGRLSSLE
Caprola$_{15}$ RVDSSRRKFNKDGHALRAIGRLSSLE

>mEGFP (C-terminally, monomeric)
[…]GGSMVSKGEELFTGVVPILVELDGDVNGHKFSVSGEGEGDATYGKLTLKFICTTGKLPVPW
PTLVTTLTYGVQCFSRYPDHMKQHDFFKSAMPEGYVQERTIFFKDDGNYKTRAEVKFEGDTLVN
RIELKGIDFKEDGNILGHKLEYNYNSHNVYIMADKQKNGIKVNFKIRHNIEDGSVQLADHYQQN
TPIGDGPVLLPDNHYLSTQSALSKDPNEKRDHMVLLEFVTAAGITLGMDELYK

Localization sequences (N-terminally fused)

>Nuclear export sequence (NES, N-terminally)
(M) LQNELALKLAGLDINKT

Purification sequences

>pET-51b(+) N-term (Strep-tag)
MASWSHPQFEKGADDDDKVPHGGS
Strep-tag; linker
>pET-51b(+) C-term (His-tag)
APGFSSISAHHHHHHHHHH
His-tag; linker

Data S1:

Contains source data for main and supplementary figures.

References and Notes

1. C. J. Guenthner, K. Miyamichi, H. H. Yang, H. C. Heller, L. Luo, Permanent genetic access to transiently active neurons via TRAP: Targeted recombination in active populations. *Neuron* **78**, 773–784 (2013). doi:10.1016/j.neuron.2013.03.025 Medline

2. X. J. Gao, O. Riabinina, J. Li, C. J. Potter, T. R. Clandinin, L. Luo, A transcriptional reporter of intracellular Ca^{2+} in *Drosophila*. *Nat. Neurosci.* **18**, 917–925 (2015). doi:10.1038/nn.4016 Medline

3. H. K. Inagaki, S. Ben-Tabou de-Leon, A. M. Wong, S. Jagadish, H. Ishimoto, G. Barnea, T. Kitamoto, R. Axel, D. J. Anderson, Visualizing neuromodulation in vivo: TANGO-mapping of dopamine signaling reveals appetite control of sugar sensing. *Cell* **148**, 583–595 (2012). doi:10.1016/j.cell.2011.12.022 Medline

4. M. Sheng, M. E. Greenberg, The regulation and function of c-fos and other immediate early genes in the nervous system. *Neuron* **4**, 477–485 (1990). doi:10.1016/0896-6273(90)90106-P Medline

5. L. G. Reijmers, B. L. Perkins, N. Matsuo, M. Mayford, Localization of a stable neural correlate of associative memory. *Science* **317**, 1230–1233 (2007). doi:10.1126/science.1143839 Medline

6. D. Lin, X. Li, E. Moult, P. Park, B. Tang, H. Shen, J. B. Grimm, N. Falco, B. Z. Jia, D. Baker, L. D. Lavis, A. E. Cohen, Time-tagged ticker tapes for intracellular recordings. *Nat. Biotechnol.* **41**, 631–639 (2023). doi:10.1038/s41587-022-01524-7 Medline

7. C. Linghu, B. An, M. Shpokayte, O. T. Celiker, N. Shmoel, R. Zhang, C. Zhang, D. Park, W. M. Park, S. Ramirez, E. S. Boyden, Recording of cellular physiological histories along optically readable self-assembling protein chains. *Nat. Biotechnol.* **41**, 640–651 (2023). doi:10.1038/s41587-022-01586-7 Medline

8. R. Y. Tsien, Very long-term memories may be stored in the pattern of holes in the perineuronal net. *Proc. Natl. Acad. Sci. U.S.A.* **110**, 12456–12461 (2013). doi:10.1073/pnas.1310158110 Medline

9. F. Schmidt, J. Zimmermann, T. Tanna, R. Farouni, T. Conway, A. J. Macpherson, R. J. Platt, Noninvasive assessment of gut function using transcriptional recording sentinel cells. *Science* **376**, eabm6038 (2022). doi:10.1126/science.abm6038 Medline

10. F. Farzadfard, N. Gharaei, Y. Higashikuni, G. Jung, J. Cao, T. K. Lu, Single-nucleotide-resolution computing and memory in living cells. *Mol. Cell* **75**, 769–780.e4 (2019). doi:10.1016/j.molcel.2019.07.011 Medline

11. B. F. Fosque, Y. Sun, H. Dana, C.-T. Yang, T. Ohyama, M. R. Tadross, R. Patel, M. Zlatic, D. S. Kim, M. B. Ahrens, V. Jayaraman, L. L. Looger, E. R. Schreiter, Labeling of active neural circuits in vivo with designed calcium integrators. *Science* **347**, 755–760 (2015). doi:10.1126/science.1260922 Medline

12. A. Das, S. Holden, J. Borovicka, J. Icardi, A. O'Niel, A. Chaklai, D. Patel, R. Patel, S. Kaech Petrie, J. Raber, H. Dana, Large-scale recording of neuronal activity in freely-moving mice at cellular resolution. *Nat. Commun.* **14**, 6399 (2023). doi:10.1038/s41467-023-42083-y Medline

13. D. Lee, J. H. Hyun, K. Jung, P. Hannan, H. B. Kwon, A calcium- and light-gated switch to induce gene expression in activated neurons. *Nat. Biotechnol.* **35**, 858–863 (2017). doi:10.1038/nbt.3902 Medline

14. W. Wang, C. P. Wildes, T. Pattarabanjird, M. I. Sanchez, G. F. Glober, G. A. Matthews, K. M. Tye, A. Y. Ting, A light- and calcium-gated transcription factor for imaging and manipulating activated neurons. *Nat. Biotechnol.* **35**, 864–871 (2017). doi:10.1038/nbt.3909 Medline

15. T. W. Chen, T. J. Wardill, Y. Sun, S. R. Pulver, S. L. Renninger, A. Baohan, E. R. Schreiter, R. A. Kerr, M. B. Orger, V. Jayaraman, L. L. Looger, K. Svoboda, D. S. Kim, Ultrasensitive fluorescent proteins for imaging neuronal activity. *Nature* **499**, 295–300 (2013). doi:10.1038/nature12354 Medline

16. A. S. Abdelfattah, T. Kawashima, A. Singh, O. Novak, H. Liu, Y. Shuai, Y.-C. Huang, L. Campagnola, S. C. Seeman, J. Yu, J. Zheng, J. B. Grimm, R. Patel, J. Friedrich, B. D. Mensh, L. Paninski, J. J. Macklin, G. J. Murphy, K. Podgorski, B.-J. Lin, T.-W. Chen, G. C. Turner, Z. Liu, M. Koyama, K. Svoboda, M. B. Ahrens, L. D. Lavis, E. R. Schreiter, Bright and photostable chemigenetic indicators for extended in vivo voltage imaging. *Science* **365**, 699–704 (2019). doi:10.1126/science.aav6416 Medline

17. J. Ohata, L. Krishnamoorthy, M. A. Gonzalez, T. Xiao, D. A. Iovan, F. D. Toste, E. W. Miller, C. J. Chang, An activity-based methionine bioconjugation approach to developing proximity-activated imaging reporters. *ACS Cent. Sci.* **6**, 32–40 (2020). doi:10.1021/acscentsci.9b01038 Medline

18. G. V. Los, L. P. Encell, M. G. McDougall, D. D. Hartzell, N. Karassina, C. Zimprich, M. G. Wood, R. Learish, R. F. Ohana, M. Urh, D. Simpson, J. Mendez, K. Zimmerman, P. Otto, G. Vidugiris, J. Zhu, A. Darzins, D. H. Klaubert, R. F. Bulleit, K. V. Wood, HaloTag: A novel protein labeling technology for cell imaging and protein analysis. *ACS Chem. Biol.* **3**, 373–382 (2008). doi:10.1021/cb800025k Medline

19. E. Bulovaite, Z. Qiu, M. Kratschke, A. Zgraj, D. G. Fricker, E. J. Tuck, R. Gokhale, B. Koniaris, S. A. Jami, P. Merino-Serrais, E. Husi, L. Mendive-Tapia, M. Vendrell, T. J. O'Dell, J. DeFelipe, N. H. Komiyama, A. Holtmaat, E. Fransén, S. G. N. Grant, A brain atlas of synapse protein lifetime across the mouse lifespan. *Neuron* **110**, 4057–4073.e8 (2022). doi:10.1016/j.neuron.2022.09.009 Medline

20. J. B. Grimm, A. K. Muthusamy, Y. Liang, T. A. Brown, W. C. Lemon, R. Patel, R. Lu, J. J. Macklin, P. J. Keller, N. Ji, L. D. Lavis, A general method to fine-tune fluorophores for live-cell and in vivo imaging. *Nat. Methods* **14**, 987–994 (2017). doi:10.1038/nmeth.4403 Medline

21. J. Wilhelm, S. Kühn, M. Tarnawski, G. Gotthard, J. Tünnermann, T. Tänzer, J. Karpenko, N. Mertes, L. Xue, U. Uhrig, J. Reinstein, J. Hiblot, K. Johnsson, Kinetic and structural characterization of the self-labeling protein tags HaloTag7, SNAP-tag, and CLIP-tag. *Biochemistry* **60**, 2560–2575 (2021). doi:10.1021/acs.biochem.1c00258 Medline

22. L. A. Banaszynski, C. W. Liu, T. J. Wandless, Characterization of the FKBP.rapamycin.FRB ternary complex. *J. Am. Chem. Soc.* **127**, 4715–4721 (2005). doi:10.1021/ja043277y Medline

23. W. K. Kroeze, M. F. Sassano, X.-P. Huang, K. Lansu, J. D. McCorvy, P. M. Giguère, N. Sciaky, B. L. Roth, PRESTO-Tango as an open-source resource for interrogation of the druggable human GPCRome. *Nat. Struct. Mol. Biol.* **22**, 362–369 (2015). doi:10.1038/nsmb.3014 Medline

24. D. Lee, M. Creed, K. Jung, T. Stefanelli, D. J. Wendler, W. C. Oh, N. L. Mignocchi, C. Lüscher, H.-B. Kwon, Temporally precise labeling and control of neuromodulatory

circuits in the mammalian brain. *Nat. Methods* **14**, 495–503 (2017). doi:10.1038/nmeth.4234 Medline

25. Q. Zheng, A. X. Ayala, I. Chung, A. V. Weigel, A. Ranjan, N. Falco, J. B. Grimm, A. N. Tkachuk, C. Wu, J. Lippincott-Schwartz, R. H. Singer, L. D. Lavis, Rational design of fluorogenic and spontaneously blinking labels for super-resolution imaging. *ACS Cent. Sci.* **5**, 1602–1613 (2019). doi:10.1021/acscentsci.9b00676 Medline

26. J. B. Grimm, A. N. Tkachuk, L. Xie, H. Choi, B. Mohar, N. Falco, K. Schaefer, R. Patel, Q. Zheng, Z. Liu, J. Lippincott-Schwartz, T. A. Brown, L. D. Lavis, A general method to optimize and functionalize red-shifted rhodamine dyes. *Nat. Methods* **17**, 815–821 (2020). doi:10.1038/s41592-020-0909-6 Medline

27. M. Weller, W. Wick, K. Aldape, M. Brada, M. Berger, S. M. Pfister, R. Nishikawa, M. Rosenthal, P. Y. Wen, R. Stupp, G. Reifenberger, Glioma. *Nat. Rev. Dis. Primers* **1**, 15017 (2015). doi:10.1038/nrdp.2015.17 Medline

28. K. D. Miller, Q. T. Ostrom, C. Kruchko, N. Patil, T. Tihan, G. Cioffi, H. E. Fuchs, K. A. Waite, A. Jemal, R. L. Siegel, J. S. Barnholtz-Sloan, Brain and other central nervous system tumor statistics, 2021. *CA Cancer J. Clin.* **71**, 381–406 (2021). doi:10.3322/caac.21693 Medline

29. M. Osswald, E. Jung, F. Sahm, G. Solecki, V. Venkataramani, J. Blaes, S. Weil, H. Horstmann, B. Wiestler, M. Syed, L. Huang, M. Ratliff, K. Karimian Jazi, F. T. Kurz, T. Schmenger, D. Lemke, M. Gömmel, M. Pauli, Y. Liao, P. Häring, S. Pusch, V. Herl, C. Steinhäuser, D. Krunic, M. Jarahian, H. Miletic, A. S. Berghoff, O. Griesbeck, G. Kalamakis, O. Garaschuk, M. Preusser, S. Weiss, H. Liu, S. Heiland, M. Platten, P. E. Huber, T. Kuner, A. von Deimling, W. Wick, F. Winkler, Brain tumour cells interconnect to a functional and resistant network. *Nature* **528**, 93–98 (2015). doi:10.1038/nature16071 Medline

30. V. Venkataramani, D. I. Tanev, C. Strahle, A. Studier-Fischer, L. Fankhauser, T. Kessler, C. Körber, M. Kardorff, M. Ratliff, R. Xie, H. Horstmann, M. Messer, S. P. Paik, J. Knabbe, F. Sahm, F. T. Kurz, A. A. Acikgöz, F. Herrmannsdörfer, A. Agarwal, D. E. Bergles, A. Chalmers, H. Miletic, S. Turcan, C. Mawrin, D. Hänggi, H.-K. Liu, W. Wick, F. Winkler, T. Kuner, Glutamatergic synaptic input to glioma cells drives brain tumour progression. *Nature* **573**, 532–538 (2019). doi:10.1038/s41586-019-1564-x Medline

31. H. S. Venkatesh, W. Morishita, A. C. Geraghty, D. Silverbush, S. M. Gillespie, M. Arzt, L. T. Tam, C. Espenel, A. Ponnuswami, L. Ni, P. J. Woo, K. R. Taylor, A. Agarwal, A. Regev, D. Brang, H. Vogel, S. Hervey-Jumper, D. E. Bergles, M. L. Suvà, R. C. Malenka, M. Monje, Electrical and synaptic integration of glioma into neural circuits. *Nature* **573**, 539–545 (2019). doi:10.1038/s41586-019-1563-y Medline

32. P. G. Gritsenko, N. Atlasy, C. E. J. Dieteren, A. C. Navis, J.-H. Venhuizen, C. Veelken, D. Schubert, A. Acker-Palmer, B. A. Westerman, T. Wurdinger, W. Leenders, P. Wesseling, H. G. Stunnenberg, P. Friedl, p120-catenin-dependent collective brain infiltration by glioma cell networks. *Nat. Cell Biol.* **22**, 97–107 (2020). doi:10.1038/s41556-019-0443-x Medline

33. F. Winkler, W. Wick, Harmful networks in the brain and beyond. *Science* **359**, 1100–1101 (2018). doi:10.1126/science.aar5555 Medline

34. J. Lee, S. Kotliarova, Y. Kotliarov, A. Li, Q. Su, N. M. Donin, S. Pastorino, B. W. Purow, N. Christopher, W. Zhang, J. K. Park, H. A. Fine, Tumor stem cells derived from

glioblastomas cultured in bFGF and EGF more closely mirror the phenotype and genotype of primary tumors than do serum-cultured cell lines. *Cancer Cell* **9**, 391–403 (2006). doi:10.1016/j.ccr.2006.03.030 Medline

35. J. N. Weinstein, E. A. Collisson, G. B. Mills, K. R. M. Shaw, B. A. Ozenberger, K. Ellrott, I. Shmulevich, C. Sander, J. M. Stuart; Cancer Genome Atlas Research Network, The Cancer Genome Atlas Pan-Cancer analysis project. *Nat. Genet.* **45**, 1113–1120 (2013). doi:10.1038/ng.2764 Medline

36. M. S. Maisak, J. Haag, G. Ammer, E. Serbe, M. Meier, A. Leonhardt, T. Schilling, A. Bahl, G. M. Rubin, A. Nern, B. J. Dickson, D. F. Reiff, E. Hopp, A. Borst, A directional tuning map of *Drosophila* elementary motion detectors. *Nature* **500**, 212–216 (2013). doi:10.1038/nature12320 Medline

37. K. F. Fischbach, A. P. M. Dittrich, The optic lobe of *Drosophila melanogaster*. I. A Golgi analysis of wild-type structure. *Cell Tissue Res.* **258**, 441–475 (1989). doi:10.1007/BF00218858

38. Y. Wu, M. Dal Maschio, F. Kubo, H. Baier, An optical illusion pinpoints an essential circuit node for global motion processing. *Neuron* **108**, 722–734.e5 (2020). doi:10.1016/j.neuron.2020.08.027 Medline

39. E. Robles, E. Laurell, H. Baier, The retinal projectome reveals brain-area-specific visual representations generated by ganglion cell diversity. *Curr. Biol.* **24**, 2085–2096 (2014). doi:10.1016/j.cub.2014.07.080 Medline

40. J. L. Semmelhack, J. C. Donovan, T. R. Thiele, E. Kuehn, E. Laurell, H. Baier, A dedicated visual pathway for prey detection in larval zebrafish. *eLife* **3**, e04878 (2014). doi:10.7554/eLife.04878 Medline

41. D. S. Mearns, J. C. Donovan, A. M. Fernandes, J. L. Semmelhack, H. Baier, Deconstructing hunting behavior reveals a tightly coupled stimulus-response loop. *Curr. Biol.* **30**, 54–69.e9 (2020). doi:10.1016/j.cub.2019.11.022 Medline

42. P. Antinucci, M. Folgueira, I. H. Bianco, Pretectal neurons control hunting behaviour. *eLife* **8**, e48114 (2019). doi:10.7554/eLife.48114 Medline

43. J. Wilhelm, johnsson-lab/splitHaloTag_Hpep_design. Zenodo (2024); https://doi.org/10.5281/zenodo.8113621.

44. A. N. Butkevich, G. Y. Mitronova, S. C. Sidenstein, J. L. Klocke, D. Kamin, D. N. H. Meineke, E. D'Este, P.-T. Kraemer, J. G. Danzl, V. N. Belov, S. W. Hell, Fluorescent rhodamines and fluorogenic carbopyronines for super-resolution STED microscopy in living cells. *Angew. Chem. Int. Ed.* **55**, 3290–3294 (2016). doi:10.1002/anie.201511018 Medline

45. J. B. Grimm, T. A. Brown, A. N. Tkachuk, L. D. Lavis, General synthetic method for Si-fluoresceins and Si-rhodamines. *ACS Cent. Sci.* **3**, 975–985 (2017). doi:10.1021/acscentsci.7b00247 Medline

46. H. Wickham, M. Averick, J. Bryan, W. Chang, L. McGowan, R. François, G. Grolemund, A. Hayes, L. Henry, J. Hester, M. Kuhn, T. Pedersen, E. Miller, S. Bache, K. Müller, J. Ooms, D. Robinson, D. Seidel, V. Spinu, K. Takahashi, D. Vaughan, C. Wilke, K. Woo, H. Yutani, Welcome to the Tidyverse. *J. Open Source Softw.* **4**, 1686 (2019). doi:10.21105/joss.01686

47. R Core Team, R version 4.1.2 (2021-11-01) (R Foundation for Statistical Computing, Vienna, 2022); https://www.R-project.org/.

48. D. G. Gibson, L. Young, R.-Y. Chuang, J. C. Venter, C. A. Hutchison III, H. O. Smith, Enzymatic assembly of DNA molecules up to several hundred kilobases. *Nat. Methods* **6**, 343–345 (2009). doi:10.1038/nmeth.1318 Medline

49. L. D. Cabrita, D. Gilis, A. L. Robertson, Y. Dehouck, M. Rooman, S. P. Bottomley, Enhancing the stability and solubility of TEV protease using in silico design. *Protein Sci.* **16**, 2360–2367 (2007). doi:10.1110/ps.072822507 Medline

50. W. Kabsch, Xds. *Acta Crystallogr. D Biol. Crystallogr.* **66**, 125–132 (2010). doi:10.1107/S0907444909047337 Medline

51. A. J. McCoy, R. W. Grosse-Kunstleve, P. D. Adams, M. D. Winn, L. C. Storoni, R. J. Read, Phaser crystallographic software. *J. Appl. Crystallogr.* **40**, 658–674 (2007). doi:10.1107/S0021889807021206 Medline

52. P. Emsley, B. Lohkamp, W. G. Scott, K. Cowtan, Features and development of Coot. *Acta Crystallogr. D Biol. Crystallogr.* **66**, 486–501 (2010). doi:10.1107/S0907444910007493 Medline

53. G. N. Murshudov, P. Skubák, A. A. Lebedev, N. S. Pannu, R. A. Steiner, R. A. Nicholls, M. D. Winn, F. Long, A. A. Vagin, REFMAC5 for the refinement of macromolecular crystal structures. *Acta Crystallogr. D Biol. Crystallogr.* **67**, 355–367 (2011). doi:10.1107/S0907444911001314 Medline

54. P. D. Adams, P. V. Afonine, G. Bunkóczi, V. B. Chen, I. W. Davis, N. Echols, J. J. Headd, L.-W. Hung, G. J. Kapral, R. W. Grosse-Kunstleve, A. J. McCoy, N. W. Moriarty, R. Oeffner, R. J. Read, D. C. Richardson, J. S. Richardson, T. C. Terwilliger, P. H. Zwart, PHENIX: A comprehensive Python-based system for macromolecular structure solution. *Acta Crystallogr. D Biol. Crystallogr.* **66**, 213–221 (2010). doi:10.1107/S0907444909052925 Medline

55. V. B. Chen, W. B. Arendall III, J. J. Headd, D. A. Keedy, R. M. Immormino, G. J. Kapral, L. W. Murray, J. S. Richardson, D. C. Richardson, MolProbity: All-atom structure validation for macromolecular crystallography. *Acta Crystallogr. D Biol. Crystallogr.* **66**, 12–21 (2010). doi:10.1107/S0907444909042073 Medline

56. P. Kuzmič, Program DYNAFIT for the analysis of enzyme kinetic data: Application to HIV proteinase. *Anal. Biochem.* **237**, 260–273 (1996). doi:10.1006/abio.1996.0238 Medline

57. M. Straume, M. L. Johnson in *Essential Numerical Computer Methods*, M. L. Johnson, Ed. (Academic Press, 1992), pp. 117–129.

58. P. S. Huang, Y. E. Ban, F. Richter, I. Andre, R. Vernon, W. R. Schief, D. Baker, RosettaRemodel: A generalized framework for flexible backbone protein design. *PLOS ONE* **6**, e24109 (2011). Medline

59. D. Lemke, M. Weiler, J. Blaes, B. Wiestler, L. Jestaedt, A.-C. Klein, S. Löw, G. Eisele, B. Radlwimmer, D. Capper, K. Schmieder, M. Mittelbronn, S. E. Combs, M. Bendszus, M. Weller, M. Platten, W. Wick, Primary glioblastoma cultures: Can profiling of stem cell markers predict radiotherapy sensitivity? *J. Neurochem.* **131**, 251–264 (2014). doi:10.1111/jnc.12802 Medline

60. J. Schindelin, I. Arganda-Carreras, E. Frise, V. Kaynig, M. Longair, T. Pietzsch, S. Preibisch, C. Rueden, S. Saalfeld, B. Schmid, J.-Y. Tinevez, D. J. White, V. Hartenstein, K. Eliceiri, P. Tomancak, A. Cardona, Fiji: An open-source platform for biological-image analysis. *Nat. Methods* **9**, 676–682 (2012). doi:10.1038/nmeth.2019 Medline

61. C. McClure, K. L. H. Cole, P. Wulff, M. Klugmann, A. J. Murray, Production and titering of recombinant adeno-associated viral vectors. *J. Vis. Exp.* **2011**, e3348 (2011). doi:10.3791/3348-v Medline

62. C. Aurnhammer, M. Haase, N. Muether, M. Hausl, C. Rauschhuber, I. Huber, H. Nitschko, U. Busch, A. Sing, A. Ehrhardt, A. Baiker, Universal real-time PCR for the detection and quantification of adeno-associated virus serotype 2-derived inverted terminal repeat sequences. *Hum. Gene Ther. Methods* **23**, 18–28 (2012). doi:10.1089/hgtb.2011.034 Medline

63. T. J. Wardill, T. W. Chen, E. R. Schreiter, J. P. Hasseman, G. Tsegaye, B. F. Fosque, R. Behnam, B. C. Shields, M. Ramirez, B. E. Kimmel, R. A. Kerr, V. Jayaraman, L. L. Looger, K. Svoboda, D. S. Kim, A neuron-based screening platform for optimizing genetically-encoded calcium indicators. *PLOS ONE* **8**, e77728 (2013). Medline

64. Y. Chastagnier, E. Moutin, A.-L. Hemonnot, J. Perroy, Image processing for bioluminescence resonance energy transfer measurement—*BRET-Analyzer*. *Front. Comput. Neurosci.* **11**, 118 (2018). doi:10.3389/fncom.2017.00118 Medline

65. A. Dobin, C. A. Davis, F. Schlesinger, J. Drenkow, C. Zaleski, S. Jha, P. Batut, M. Chaisson, T. R. Gingeras, STAR: Ultrafast universal RNA-seq aligner. *Bioinformatics* **29**, 15–21 (2013). doi:10.1093/bioinformatics/bts635 Medline

66. Y. Liao, G. K. Smyth, W. Shi, featureCounts: An efficient general purpose program for assigning sequence reads to genomic features. *Bioinformatics* **30**, 923–930 (2014). doi:10.1093/bioinformatics/btt656 Medline

67. A. Frankish, M. Diekhans, I. Jungreis, J. Lagarde, J. E. Loveland, J. M. Mudge, C. Sisu, J. C. Wright, J. Armstrong, I. Barnes, A. Berry, A. Bignell, C. Boix, S. Carbonell Sala, F. Cunningham, T. Di Domenico, S. Donaldson, I. T. Fiddes, C. García Girón, J. M. Gonzalez, T. Grego, M. Hardy, T. Hourlier, K. L. Howe, T. Hunt, O. G. Izuogu, R. Johnson, F. J. Martin, L. Martínez, S. Mohanan, P. Muir, F. C. P. Navarro, A. Parker, B. Pei, F. Pozo, F. C. Riera, M. Ruffier, B. M. Schmitt, E. Stapleton, M.-M. Suner, I. Sycheva, B. Uszczynska-Ratajczak, M. Y. Wolf, J. Xu, Y. T. Yang, A. Yates, D. Zerbino, Y. Zhang, J. S. Choudhary, M. Gerstein, R. Guigó, T. J. P. Hubbard, M. Kellis, B. Paten, M. L. Tress, P. Flicek, Gencode 2021. *Nucleic Acids Res.* **49**, D916–D923 (2021). doi:10.1093/nar/gkaa1087 Medline

68. M. D. Robinson, D. J. McCarthy, G. K. Smyth, edgeR: A Bioconductor package for differential expression analysis of digital gene expression data. *Bioinformatics* **26**, 139–140 (2010). doi:10.1093/bioinformatics/btp616 Medline

69. Z. Gu, L. Gu, R. Eils, M. Schlesner, B. Brors, circlize Implements and enhances circular visualization in R. *Bioinformatics* **30**, 2811–2812 (2014). doi:10.1093/bioinformatics/btu393 Medline

70. S. X. Ge, D. Jung, R. Yao, ShinyGO: A graphical gene-set enrichment tool for animals and plants. *Bioinformatics* **36**, 2628–2629 (2020). doi:10.1093/bioinformatics/btz931 Medline

71. M. Uhlen, C. Zhang, S. Lee, E. Sjöstedt, L. Fagerberg, G. Bidkhori, R. Benfeitas, M. Arif, Z. Liu, F. Edfors, K. Sanli, K. von Feilitzen, P. Oksvold, E. Lundberg, S. Hober, P. Nilsson, J. Mattsson, J. M. Schwenk, H. Brunnström, B. Glimelius, T. Sjöblom, P.-H. Edqvist, D. Djureinovic, P. Micke, C. Lindskog, A. Mardinoglu, F. Ponten, A pathology atlas of the human cancer transcriptome. *Science* **357**, eaan2507 (2017). doi:10.1126/science.aan2507 Medline

72. M. Markstein, C. Pitsouli, C. Villalta, S. E. Celniker, N. Perrimon, Exploiting position effects and the gypsy retrovirus insulator to engineer precisely expressed transgenes. *Nat. Genet.* **40**, 476–483 (2008). doi:10.1038/ng.101 Medline

73. J. Bischof, R. K. Maeda, M. Hediger, F. Karch, K. Basler, An optimized transgenesis system for *Drosophila* using germ-line-specific φC31 integrases. *Proc. Natl. Acad. Sci. U.S.A.* **104**, 3312–3317 (2007). doi:10.1073/pnas.0611511104 Medline

74. G. Maimon, A. D. Straw, M. H. Dickinson, Active flight increases the gain of visual motion processing in *Drosophila*. *Nat. Neurosci.* **13**, 393–399 (2010). doi:10.1038/nn.2492 Medline

75. R. I. Wilson, G. Laurent, Role of GABAergic inhibition in shaping odor-evoked spatiotemporal patterns in the *Drosophila* antennal lobe. *J. Neurosci.* **25**, 9069–9079 (2005). doi:10.1523/JNEUROSCI.2070-05.2005 Medline

76. J. Peirce, J. R. Gray, S. Simpson, M. MacAskill, R. Höchenberger, H. Sogo, E. Kastman, J. K. Lindeløv, PsychoPy2: Experiments in behavior made easy. *Behav. Res. Methods* **51**, 195–203 (2019). doi:10.3758/s13428-018-01193-y Medline

77. C. B. Kimmel, W. W. Ballard, S. R. Kimmel, B. Ullmann, T. F. Schilling, Stages of embryonic development of the zebrafish. *Dev. Dyn.* **203**, 253–310 (1995). doi:10.1002/aja.1002030302 Medline

78. J. A. Lister, C. P. Robertson, T. Lepage, S. L. Johnson, D. W. Raible, *nacre* encodes a zebrafish microphthalmia-related protein that regulates neural-crest-derived pigment cell fate. *Development* **126**, 3757–3767 (1999). doi:10.1242/dev.126.17.3757 Medline

79. M. L. Suster, G. Abe, A. Schouw, K. Kawakami, Transposon-mediated BAC transgenesis in zebrafish. *Nat. Protoc.* **6**, 1998–2021 (2011). doi:10.1038/nprot.2011.416 Medline

80. B. Moeyaert, G. Holt, R. Madangopal, A. Perez-Alvarez, B. C. Fearey, N. F. Trojanowski, J. Ledderose, T. A. Zolnik, A. Das, D. Patel, T. A. Brown, R. N. S. Sachdev, B. J. Eickholt, M. E. Larkum, G. G. Turrigiano, H. Dana, C. E. Gee, T. G. Oertner, B. T. Hope, E. R. Schreiter, Improved methods for marking active neuron populations. *Nat. Commun.* **9**, 4440 (2018). doi:10.1038/s41467-018-06935-2 Medline

81. B. D. Pfeiffer, T.-T. B. Ngo, K. L. Hibbard, C. Murphy, A. Jenett, J. W. Truman, G. M. Rubin, Refinement of tools for targeted gene expression in *Drosophila*. *Genetics* **186**, 735–755 (2010). doi:10.1534/genetics.110.119917 Medline